INFORMATION TO USERS

This manuscript has been reproduced from the microfilm master. UMI films the text directly from the original or copy submitted. Thus, some thesis and dissertation copies are in typewriter face, while others may be from any type of computer printer.

The quality of this reproduction is dependent upon the quality of the copy submitted. Broken or indistinct print, colored or poor quality illustrations and photographs, print bleedthrough, substandard margins, and improper alignment can adversely affect reproduction.

In the unlikely event that the author did not send UMI a complete manuscript and there are missing pages, these will be noted. Also, if unauthorized copyright material had to be removed, a note will indicate the deletion.

Oversize materials (e.g., maps, drawings, charts) are reproduced by sectioning the original, beginning at the upper left-hand corner and continuing from left to right in equal sections with small overlaps.

Photographs included in the original manuscript have been reproduced xerographically in this copy. Higher quality 6" x 9" black and white photographic prints are available for any photographs or illustrations appearing in this copy for an additional charge. Contact UMI directly to order.

Bell & Howell Information and Learning
300 North Zeeb Road, Ann Arbor, MI 48106-1346 USA
800-521-0600

Physical Modelling of Two Phase Flows in Ladle-Shroud Systems

By

Hyoungbae, Kim

A thesis submitted to the Faculty of Graduate Studies and Research in Partial Fulfillment of the Requirement s for the Degree of Master of Engineering.

Department of Mining and Metallurgical Engineering
McGill University
Montreal, Quebec, Canada
December, 1998

ABSTRACT

The onset of a 'late' rotating vortex over an off-centre drain nozzle at 2/3 radius was studied in an 1160-mm diameter tank. It was found that using a sloped bottom ladle could be beneficial in terms of steel yield, provided the exit nozzle is located 'centrically'.

Miner modification of the nozzle (skewed nozzle) to impart a radial component of velocity to the spinning vortex core was found to be effective in making AMEPA system sensitive to early slag entrainment phenomena by diverting the core away from the central vertical axis of the nozzle.

A 0.75 scale water model was constructed to simulate the flow of liquid steel through a ladle shroud in the presence of gas infiltration. It was found that the ladle shroud slag detector could be temporarily 'blinded' by gas bubbles or permanently blinded by a standing submerged gas jet.

RÉSUMÉ

L'apparition d'un vortex rotatif 'à retard' au-dessus d'un tuyau de vidange décentré à deux tiers du rayon du réservoir a été étudié dans un réservoir de 1160mm de diamètre. Il a été montré que l'utilisation d'un fond incliné et en forme de louche améliore le rendement de l'acier. Néanmoins, le tuyau d'évacuation doit être centré.

Des modifications mineures du tuyau (filtrage) pour donner à la vitesse une composante radiale dans le cœur du vortex ont amélioré la sensibilité du système AMEPA aux phénomènes d'entraînement des premières crasses en éloignant le cœur du vortex de l'axe du drain.

Le flux d'acier liquide à travers une 'louche filtrante' en présence d'infiltration de gaz a été modélisé à l'échelle 0,75 avec de l'eau. Il a été montré que le détecteur de crasse de la louche peut être momentanément obstrué par des bulles de gaz ou de façon permanente par un filet de gaz.

ACKNOWLEDGEMENTS

I am greatly indebted to my thesis supervisor, Professor R.I.L. Guthrie, for his encouragement, academic and financial support during the course of study. I would like to thank to Ramani Sankaranarayanan for his valuable knowledge of vortex formation that I learned from him.

My special thanks are due to members of the machine shop staff, Csaba Szalacsi and Harold Ward in particular, for fabricating various components of the experimental apparatus, and also for their enthusiastic suggestions that made for better design.

I would like to express my gratitude to Arnaud Tronche for his efforts in translating the abstract into French. I will cherish the warm memories of time well-spent with friends and colleagues, Chris Carozza, Hiroshi Nogami, Hussein Abuluwefa, Jinsoo Kim, Ji-Young Byun, Mei Li, Pedro Netto, Yong-Bum Park, and all those that I have forgotten to mention.

Lastly, but most importantly, I would like to express my gratitude to my loving parents, and wife, for all the encouragement and support.

TABLE OF CONTENTS

LIST OF FIGURES

CHAPTER 3. EXPERIMENTAL APPARATUS AND PROCEDURES

CHAPTER 4. EXPERIMENTAL OBSERVATIONS

LIST OF TABLES

LIST OF SYMBOLS

A	Radial Reynolds number; Einstein and Li[29]
A	Radius of the drainage nozzle, *m*
A	Constant defined in Eq. (2.19)
A_{ladle}	Area of cross-section of the ladle, m^2
a, a_o	Radius of liquid stream at z and nozzle exit, *mm*
C, C_1	Constant
C_D	Discharge coefficient of the drainage nozzle
C_θ	Constant of proportionality in Eq. (3.2)
d	Diameter of the drainage nozzle, *mm*
D_J	Diameter of the liquid metal jet, *mm*
D_N	Diameter of the drainage nozzle, *mm*
D^*	Envelope diameter of high velocity jet, *mm*
Fr	Froude number
g	Acceleration due to gravity, m/s^2
H_{cr}	Critical liquid height for the formation of a vortexing funnel, *cm*
H_{init}	Initial liquid height, *cm*
H_m	Height of metal (see Figure 2.11)
$H_{ref.}$	Referential Height for water flowrate calculation, *cm*
H_s	Height of slag (see Figure 2.11)
h	Liquid metal height, *m*
h_1, h_2, h_3, h_4	Height (see Figure 2.11)
K	Strength of a potential vortex, m^2/s
K_{gas}	Constant defined in Eq. (4.5)
L	Length, *m*

m	Mass, *kg, ton (1000 kg)*
m	Strength of a line sink, m^2/s
N	Radial Reynolds number; Toyokura and Akaike[27]
n	Constant defined in Eq. 3.2
P	Pressure, *Pa* ($kg/m/s^2$), *atm*
P_J	Atmospheric pressure, *Pa, atm*
P_{act}	Pressure at flow conditions, *Pa*
P_o	Pressure at standard conditions, *Pa*
Q	Liquid metal flowrate, m^3/s
Q_{air}	Equivalent air flow capacity at standard conditions, m^3/s
$Q_{calculation}$	Calculated flowrate of water, m^3/s
Q_{helium}	Equivalent helium flow capacity at standard conditions, m^3/s
$Q_{measured}$	Measured flowrate of water, m^3/s
$Q_{std.}$	Maximum flow of metered gas, m^3/s
Q_{water}	Water flowrate, m^3/s
Re	Reynolds number
R_c	Radius of cavity, *mm*
r	Radial coordinate, *mm*
S_1,, S_2,, S_3	Cross-sectional area, (see Figure 2.11)
T_{act}	Absolute temperature at flow conditions, K
T_o	Absolute temperature at standard conditions, K
t_{init}	Initial drainage time, *sec*
$t_{ref.}$	Time when liquid height reaches to referential height, *sec*
V	Volume of water remained in the ladle defined in the Eq. (4.2)
V_J	Liquid metal jet velocity, *m/s*
V_r	Radial velocity, *m/s*
$V_{r,sink}$	Radial velocity of a sink, *m/s*
V_1, V_2, V_3	Flow rate (see Figure 2.11)
V_θ	Tangential velocity, *m/s, mm/s*
$V_{\theta,cr}$	Critical tangential velocity, *mm/s*
$V_{\theta,i}$	Initial tangential velocity, *mm/s*

$V_{\theta,r}$	Tangential velocity at radial position *r*, *mm/s*
$V_{\theta,R}$	Tangential velocity in the free vortex region far from the nozzle, *mm/s*
$V_{\theta,t}$	Tangential velocity at a holding time of *t seconds*, *mm/s*
$V_{\theta,vortex}$	Tangential velocity of a free vortex, *mm/s*
We	Weber number
Z	Depth of water above the tank floor, *mm*
z	Axial position, *mm*
α	Constant defined in Eq. (2.14)
α	Inclined angle of The ladle, *degree*
Φ_A	Air flowrate, m^3/s
Φ_J	Liquid metal jet flowrate, m^3/s
Γ	Circulation, m^2/s
Γ_f	Circulation in the free vortex region, m^2/s
Γ_r	Relative circulation
ϕ	Scalar velocity potential, m^2/s
φ	Diameter of drainage nozzle, (see Figure 3.6)
η_w	Dynamic viscosity of water, Ns/m^2
ν	Kinematic viscosity, m^2/s
ν_g	Kinematic viscosity of gas, m^2/s
ρ	Density, kg/m^3
ρ_A	Density of air, kg/m^3
ρ_m	Density of metal, kg/m^3
ρ_s	Density of slag, kg/m^3
ρ_w	Density of water, kg/m^3
τ	Surface tension, *N/m*
Ψ	Stream function, m^2/s

CHAPTER
1

INTRODUCTION

1.1 INTRODUCTION

The emptying of ladles of liquid steel into tundishes represents a critical operation in terms of maintaining steel quality and optimizing steel yield versus steel quality. Tests have shown that steel quality of the last part to be emptied from a ladle is poorer than the average teemed, owing to increased amounts of slag entrainment. Whether this decrease in quality is due to an increasing number of micro-droplets of slag entrained within the steel melt that have not yet been re-absorbed into the upper layer of ladle slag, or is due to late rotational vortices setting in towards the end of teeming, is not yet clear. Certainly the last few inches of steel to be drained from a ladle will always contain entrained slag which will originate from a vortex in the presence of weak rotational flows.

The minimization of slag entrainment during the drainage of various metallurgical vessels used in the continuous casting of steel has become increasingly important due to market demands for higher quality. The advantages of complete slag separation are an improvement in purity of steel, better yield, and reduced nozzle clogging and longer life of refractory materials through reduced contact with corrosive slag.

In this chapter, the phenomenon of vortex will be introduced, along with its impact on the continuous casting process. Moreover, introductions to three different subjects namely, (i) slag entrainment in late rotating vortices, (ii) detection of early slag vortexing phenomena using AMEPA (Angewandte Meβtechnik und Prozeβautomatisierung) system and (iii) shroud gas/steel flow interaction will be given.

1.2 SLAG ENTRAINING VORTEXING FUNNEL

1.2.1 What is the Vortexing Funnel

The premature entrainment of any supernatant slag layer, that arises from the formation of what is commonly referred to as the vortex, is known to occur well before the vessel is empty of liquid steel. An essential pre-requisite to the formation of a funnel-shaped vortex is that the liquid being drained out of a holding vessel possesses some rotational motion, whatever the source of such rotation. Haindl[1] concluded that the entrainment due to the vortex is not dependent on Froude number but on Reynolds number.

Vortexing Funnel can be defined as a funnel-shaped vortex formed from rotational motion in the liquid.

1.2.2 Stages in the Formation of a Vortexing Funnel

A general consensus among researchers is that a vortexing funnel goes through four stages of development. These are sketched in Figure 1.1. In the first stage, where the liquid head is very large and/or any residual tangential velocity is low, a tiny dimple is formed on the surface (Figure 1.1(a)), usually centered on the axis of rotation of the tangential motion. Then, the dimple starts extending down towards the drainage nozzle as the liquid head decreases, or as the residual tangential velocity increases. It develops first into a tiny surface vortex (Figure 1.1(b)), and then a deeper vortex funnel whose tip shows rapid rotation (Figure 1.1(c)), as required by the law of conservation of angular momentum. Finally a fully developed vortexing funnel (Figure 1.1(d)) that entrains the supernatant air (slag) into the drainage nozzle forms. Often, a discrete stream of air (slag) bubbles would detach from the tail of the tall funnel (Figure 1.1(c)), and exit through the nozzle, much before the vortexing funnel became fully developed as in Figures 1.1(d). In this Figure, H_{cr} means critical liquid height for the formation of a vortexing funnel.

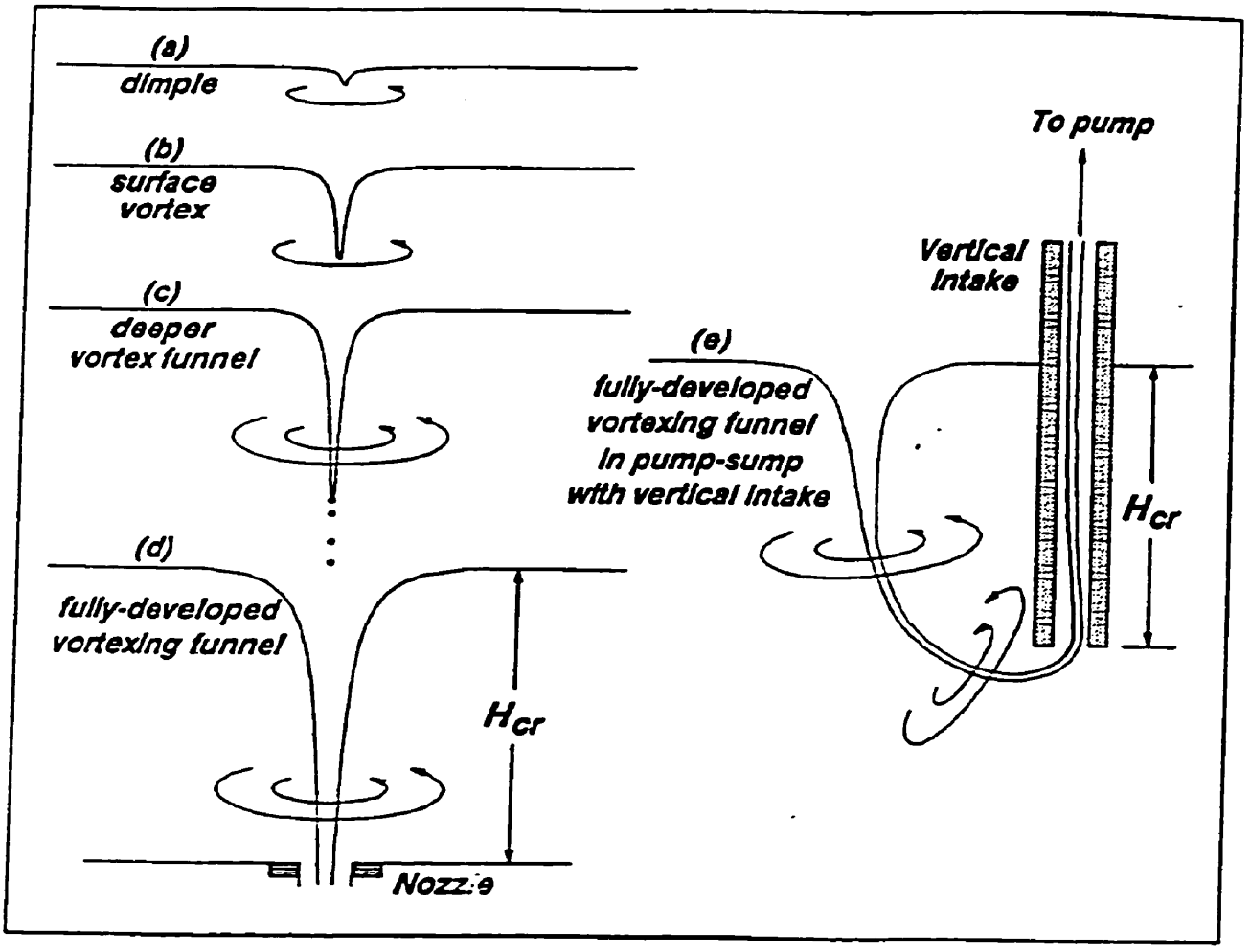

Fig. 1.1 Stages in the development of a vortexing funnel, as summarized from the published literature

In the case of a pump-sump, the fully developed vortexing funnel would bend upwards into the vertical intake (Figure 1.1 (e)), the first three stages being the same as in Figure 1.1 (a)-(c). Likewise, the tail of a vortexing funnel could easily bend into the mouth of a vertical intake tube with a hockey stick shaped into a drainage nozzle located on the side wall of the holding vessel.

It could be seen from the different results of various authors that the rate of progress through the four stages of vortexing funnel development itself is dependent on the residual tangential velocity, and its spatial distribution in the holding vessel. The presence of strong tangential velocity leads to an almost instantaneous progress from the dimple to the fully developed vortexing funnel, while the residual tangential velocities are weaker, the dimple would take longer to grow into a fully developed vortexing funnel, and the diameter of the funnel would be much smaller as well. After becoming a fully developed vortexing funnel, further decrease in the liquid head is usually accompanied by an increase in the diameter of the vortexing funnel, and consequently, an increase in the amount of supernatant air (slag) entrained.[1]

It must be noted that the sketches shown in Figure 1.1 are simplifications of reality. Vortexing funnels are rarely as symmetrical as sketched, except in the case of very weak residual tangential velocities. In the presence of stronger tangential velocities, a helical spiral-like surface is superimposed on the funnel shape; the funnel also moves laterally and spatially with time. Finally, the direction of rotation of a vortexing funnel is always the same as the direction of any residual tangential motion in the vessel.

1.2.3 Characteristic Features of a Vortexing Funnel

With air on top of the liquid as a supernatant fluid, Characteristics of a vortexing funnel formed in a holding vessel drained through the nozzle on the bottom are sketched in Figure 1.2. The critical liquid height at which the vortexing funnel becomes fully developed, H_{cr}, can be much larger than the drainage nozzle diameter d. However, the prediction of H_{cr} for given set of vessel and initial conditions is not possible with present knowledge. Thus, the minimum residual tangential velocity value, $V_{\theta,cr}$, sketched in Figure 1.2 as necessary for the initiation of a dimple as a pre-cursor to a fully developed vortexing funnel is merely an as-yet-unproven hypothesis. By the same token, the existence of unique values of $V_{\theta,cr}$ for various liquids is open to question.

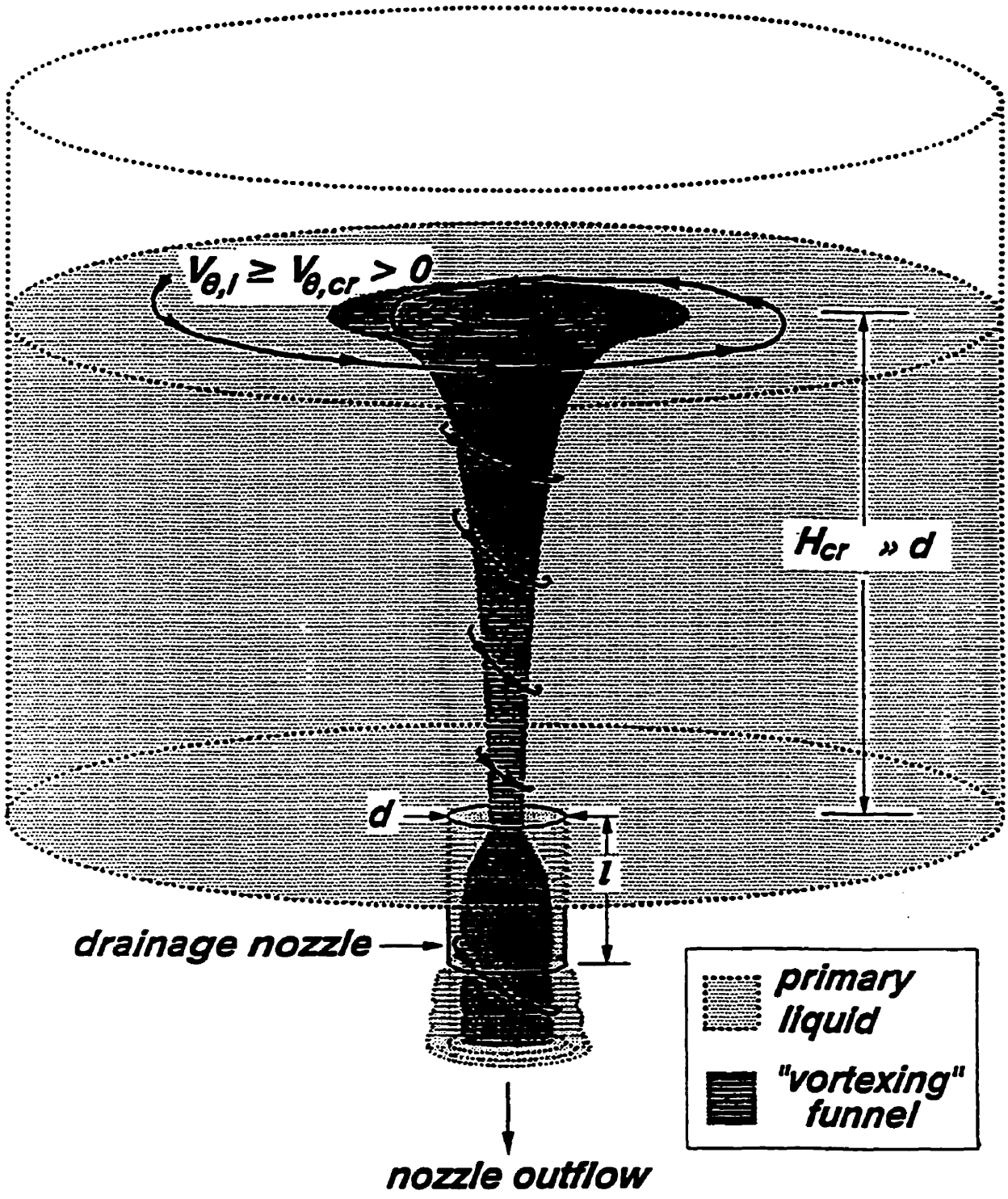

Fig. 1.2 General characteristics of a vortexing funnel[2]

As mentioned earlier, the presence of rotational motion in the liquid is a necessary condition for the formation of a vortexing funnel during the drainage of a holding vessel. Therefore, the pathline followed by hypothetical particles of primary liquid, lying on the primary liquid-supernatant fluid interface, en route to the nozzle, is sketched as a helical spiral.

The most important two properties of vortexing funnel formation might be the discharge coefficient, C_D, of drainage nozzles based on dimensional analysis and the critical liquid height, H_{cr}, for its formation from the point of view of avoiding the entrainment of any supernatant fluid during the drainage of a holding vessel.

The stronger the rotational motion in the vessel, the larger is the size of the vortexing funnel formed; the larger the vortexing funnel, the greater is the volume of air entrained; and the greater the air entrainment, the lower is the flow rate of liquid flowing through the drainage orifice. Hammerschmid *et al*[3] found that H_{cr} decreased as the holding time increased; i.e., it was implicitly understood that H_{cr} was directly proportional to the intensity of the rotational motion possessed by the liquid at the beginning of drainage. The study of the effect of nozzle size and position on H_{cr} revealed that H_{cr} varied inversely with the diameter of the nozzle and decreased with increasing eccentricity.[4]

An interesting result from a comparison of the results of Haindl[1] and Daggett and Keulegan[5] is that the initiation of a vortexing funnel from a given residual tangential velocity distribution is time dependent; H_{cr} itself is only a secondary parameter in the process. The presence of a critical tangential velocity in the liquid as a pre-cursor to vortexing funnel formation is thus a likelihood that has yet to be well understood.

1.3 HAMFUL EFFECTS OF SLAG ENTRAINMENT

1.3.1 Metal Cleanness

Oxides of Al, Ca, Mg, and Si with traces of Mn, Na, S, P, *etc.* are essential inclusions in continuously cast steel. In order to reflect the dependence of their origins on both physical and chemical events inherent to various steel processing operations, inclusions are often classified as being indigenous or exogenous.

Inclusions formed from reoxidation, deoxidization, and desulphurization reactions are usually considered indigenous to steelmaking while entrained slag inclusions are not. Considerable knowledge about the prevention of indigenous inclusion formation is available; for instances, reoxidation of liquid steel streams from the ladle and tundish can be prevented to a large extent by effective inert gas shrouding, argon bubbling in the ladle is effective in floating out a large portion of the deoxidization and desulphurization products; inclusion floatation can be improved by increasing the residence time of steel in the tundish. Modification of flow behavior using dams, weirs and baffles inside of tundish, with the objective of increasing residence times and inclusion flotation efficiency, continues to be an active research area among tundish metallurgists.

Given that there is not much time for inclusion floatation by the continuous nature of the casting process, slag entrainment caused by vortexing funnel formation during tundish-to mould or mould-to-solidifying-steel-strand flow would appear to be the major source of exogenous inclusions.[6] Slag entrained from ladles and converters does have a greater chance of being floated out, and until recently was not expected to contribute to exogenous inclusion formation. However, considerable evidence to the contrary is available in recently published literature. Carry-over of oxidized ladle slag into the tundish was identified as a source of casting defects at the Cleveland, OH, Works of LTV Steel Co.[7,8]

Slag entrainment is also known to cause reoxidation of the metal, the removal of which is bound to result in the generation of additional indigenous inclusion. Entrainment of ladle slag has been observed to result in a steady increase in the volume of slag in the tundish, as sequence casting progresses, and it is reported that the inclusion content of the cast slabs is directly proportional to the tundish slag thickness.[9] Moreover, slag entrainment from a tundish to a mold can be caused by vortex formation, whenever the steel level in the tundish drops below a critical value, and such slag entrainment from tundish levels as high as 500-1000 mm[10] have been reported.

Clearly, the formation of slag entraining funnels contributes directly, as well as indirectly, to an increase in the number of exogenous, as well as indigenous, inclusions in cast products, and must be avoided during all stages of liquid steel transfer.

1.3.2 Liquid Metal Chemistry

The most important of the refining reactions involved in steelmaking are probably dephosphorization and desulphurization, apart from the removal of carbon and silicon. The detrimental effects of P and S have been known from the early days of steelmaking.[11] An embrittling effect on steel is related to P contents in excess of 0.005-0.02%, while poor toughness and ductility are associated with S concentrations greater than 0.005%. Hence it is extremely important to produce steel within required P and S specifications. The bare minimum of O, H and N contents is also needed to keep. Carry-over of converter slag has negative consequences on the P, S and O contents of ladle steel, while entrainment of ladle slag to a tundish promotes reoxidization.

Being rich in FeO, MnO, SiO_2 and P_2O_5 which are easily reduced by deoxidants and desulphurizing agent[12,13] added during ladle refining, converter slag carry-over into the ladle is known to result in poor desulphurization kinetics,[12,13] rephosphorization of steel,[14,15] poor yield of alloying additions,[16,17] increase in the oxygen content of ladle slag and metal, Al loss,[18] etc. The magnitude of these negative influences is directly proportional to the amount of converter slag carried over. Dephosphorization in ladles can

be expensive and requires specialized secondary steelmaking facilities.[19] Mechanical deslagging devices are sometimes used to remove excess converter slag in the ladle; however the benefits of deslagging are offset by temperature losses[14] and increased processing time. Reducing the increase of the oxygen content with attendant losses of dissolved aluminum [7,14] caused by entrainment of ladle and tundish slags invariably lead to temperature losses.

1.3.3 Productivity and Yield of Liquid Metal

It is a well known fact that slag carry-over also causes refractory erosion and thus reduces the life of refractories. This reduction in the life of refractories results in decrease of productivity because of increased production costs. Oxidizing converter slags are known to attack ladle refractories.[17,20] In order to minimize attack on the tundish refractory inserts like dams, weirs, etc., less basic tundish slags than ladle slags are preferable. Entrainment of ladle slag reduces the life of tundish refractories. Entrainment of tundish slag into the mould can lead to mould powder deterioration, [21] which in the worst case can rupture the solidifying shell (mould or strand break out), cause liquid steel spillage and disrupt casting operations.

100 percent clean separation of steel from slag is not theoretically possible. In order to avoid having to deal with the problems likely to be caused by potential slag entrainment, ten to twenty percent early closures with most of the remainder being late to some degree would not be unusual. The amount of liquid steel left behind in each vessel varies from plant to plant depending on specific slag practices, and the grade of steel that is being cast, *etc*. It was reported that yield loss on 290 ton heats could be as high as 20 percent if a full tundish (60 tons) was left after a single heat cast.[22] From the conflicting objectives of no slag carryover and complete liquid steel recovery, increased yield would not nowadays be sought at the expense of quality (metal cleanness). However, the minimization of yield losses has always been, and will continue to be, of importance to steelmaker.

1.4 PURPOSE OF THESIS

1.4.1 Slag Entrainment in Late Rotating Vortices

The minimization of slag entrainment without sacrificing yield of liquid metal is a primary concern of every quality-conscious steelmaker today. Teeming a ladle can be improved considerably if slag can be prevented from flowing with the molten metal. The advantages of complete slag separation are an improvement in purity of steel, better yield, reduced nozzle clogging, higher sequence lengths and a longer life of refractory materials through reduced contact with corrosive slags.

The critical height, H_{cr}, is the most important property of vortexing funnel formation from the point of yield of liquid metal. Many researchers studied parameters effecting on the critical height: holding time, nozzle and ladle size, drainage coefficient, nozzle position in the ladle, *etc.* Holding time is usually kept as low as possible in practice, because holding time is inversely proportional to the critical height. The nozzle size is fixed depending on the productivity of liquid metal in continuous casting. Based on the observation taken by Suker, *et al*[4], higher eccentricity of nozzle position led to lower critical height.

Given that the synergistic interaction between downward axial velocities in the ladle and the tangential velocities present was the motive force for vortexing funnel formation, the objective was to suppress axial velocities along the nozzle axis so as to reduce the critical height.

Sloping a ladle bottom surface can be one of the ways to obstruct the downward axial velocities. In the present work under the title of 'slag entrainment in late rotating vortices', the influence of a sloping bottom surface, with the drain set near the bottom of incline in order to help maximize steel yield prior to slag entrainment, without changing any other parameters, was studied.

1.4.2 Detection of Early Slag Vortexing Phenomena using AMEPA System

The reliable and early detection of slag in the melt has become increasingly important due to market demands for higher quality. Successful prevention of slag entrainment depends on the timing of the decision to stop ladle drainage. For higher quality and yield of liquid metal, AMEPA system, one of the electromagnetic slag detection methods in the category of detection-based end of drainage methods, is currently being used.

The AMEPA slag sensor consists of primary and secondary coil system, which are placed together, concentric to each other (Figure 1.3). An alternating current is fed into these concentrically arranged coils of the sensor, thereby inducing eddy currents within the melt flowing through the nozzle just upstream of the slide gate nozzle and ladle shroud (Figure 1.4.a). If there is any slag in the melt, the conductivity of the melt changes

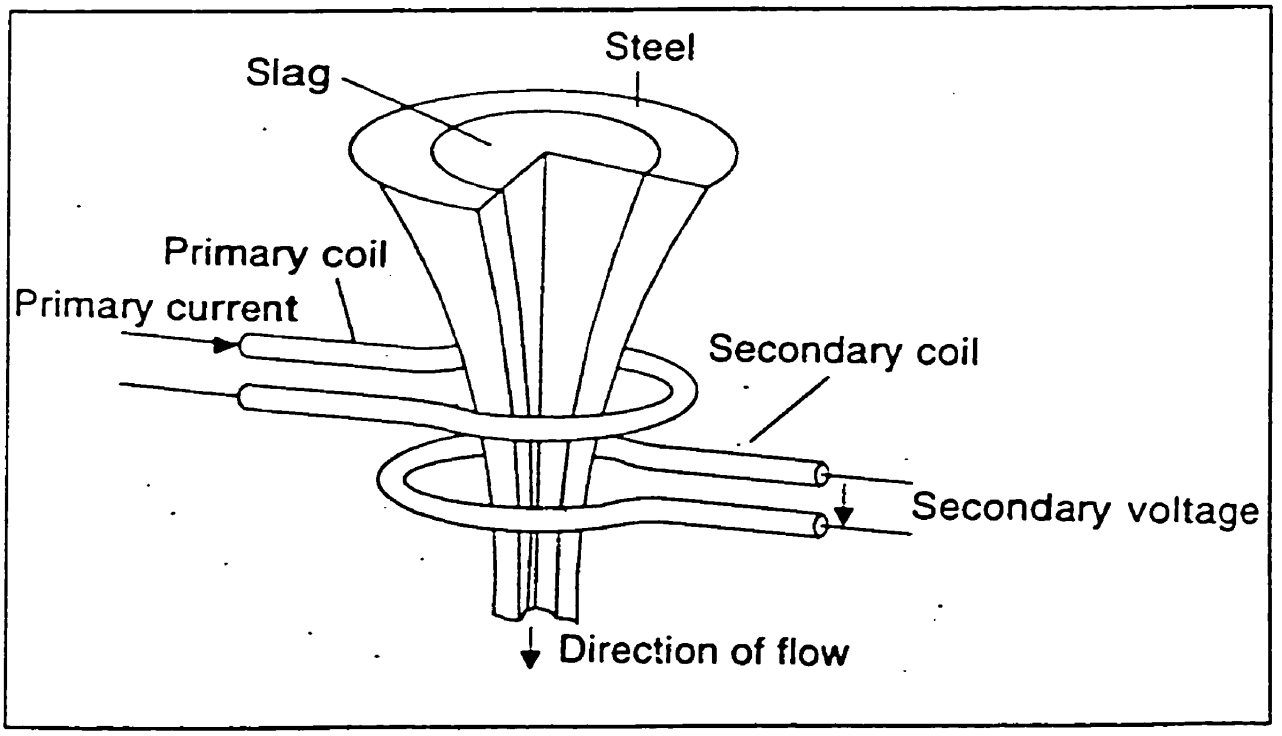

Fig. 1.3 Schematic diagram of the AMEPA measuring system; Julius *et al.*[23]

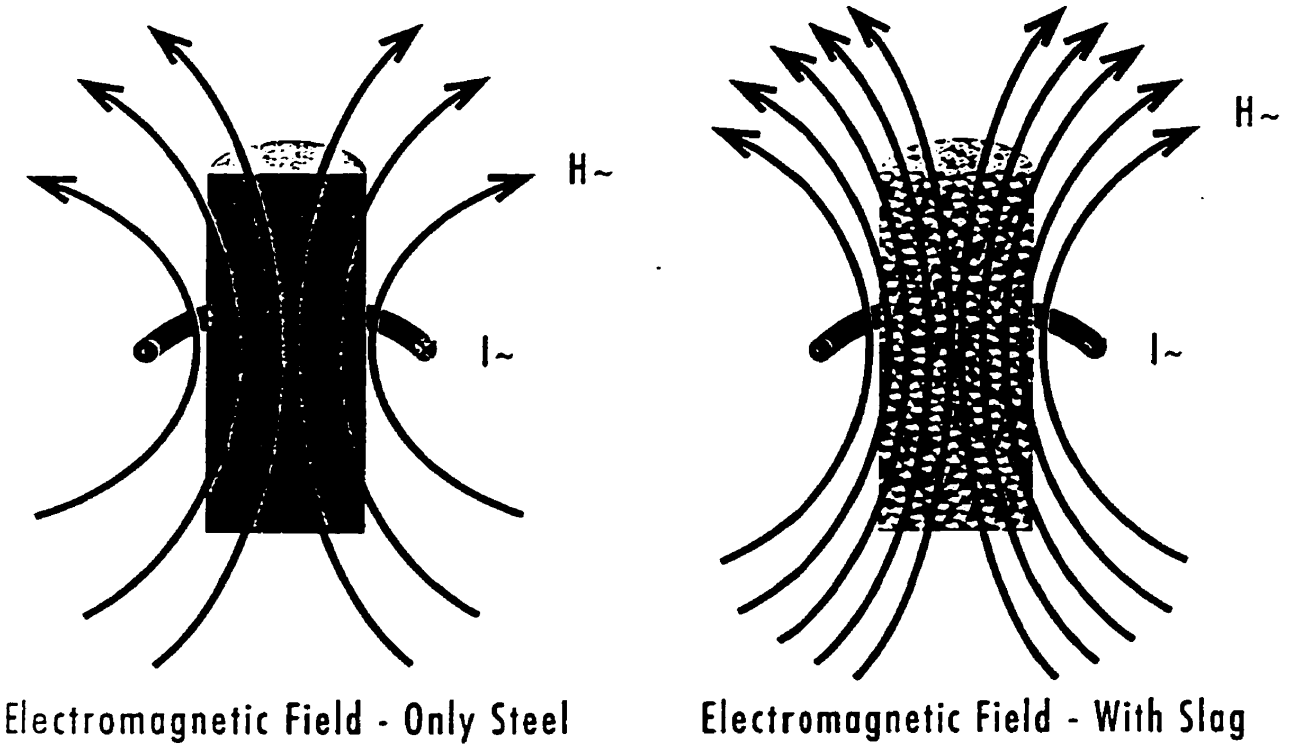

Fig. 1.4 Measuring and sensor principle of AMEPA system, (a) electromagnetic field - only steel (b) electromagnetic filed – with slag

and the electromagnetic field increases slightly (Figure 1.4.b). This change is measured by a secondary coil system. While these electromagnetic sensors offer a remarkable amount of accuracy, consistency, and reliability in the detection and control of slag entrainment, they are not yet capable of detection slag unless, and until, the steel stream contains a significant proportion of slag (at present, the figure is 10% slag).[40] The AMEPA system can be insensitive, if the slag goes through as a thin concentric continuous stream, which happens at the early stage of slag entrainment phenomena. Such phenomena can occur when residual rotational flows within a ladle generate slag entrainment vortices. This implies that a certain minimum of slag entrainment is inevitable, and that it is very difficult to detect the entrainment of discrete emulsified slag droplets that may be produced during the impingement of a metal stream on a pool of

liquid slag in the pouring box of the tundish or precede the onset of a fully-developed vortexing funnel formation.

As the concentric continuous stream of slag can cause AMEPA's insensitivity, the purpose of the present work is to determine how the rotational core of a slag-entraining vortex can be displaced off the central, vertical axis of the nozzle in a simple practicable way, so as to render the AMEPA system sensitive to early slag entrainment phenomena. It will be a preferred method if it doesn't change any other important parameters in process metallurgy, such as H_{cr} and Q (liquid metal flowrate), because flowrate of liquid metal is directly related to the productivity of liquid metal and critical height is directly related to the yield of liquid metal.

1.4.3 Shroud Gas/Steel Flow Interaction

As reoxidation of liquid steel during various processing stages of continuous casting has a well-known negative effect on metal cleanliness and steel chemistry, another part of maintaining steel quality is to use ladle shrouds to protect the killed steel from reoxidation during transfer into the tundish.

Nozzle shrouds are used and these fit snugly over the collector nozzles. Nonetheless, aspiration of gas into the joint is difficult to prevent, since the static pressure at the joint is almost zero for a 1.15 m long shroud nozzle filled with liquid steel. It is common therefore, to protect the liquid steel from air aspiration and consequent reoxidation, by flooding the joint with argon, or by actually injecting argon, under pressure, into a porous refractory surrounding the joint, so as to force some argon into the steel jet in favor of air. This practice can lead to an exposed 'eye' of steel around the entry point of steel from the ladle shroud into the tundish, which in turn, can entrain micro-droplets of tundish slag into the steel within the tundish, that may subsequently report to the final cast product.

In order to detect slag carry-over from the ladle into the tundish, Vesuvius is developing a simple slag detection device that consists of a steel electrode wire in direct electrical contact with the teeming stream. The onset of slag entrainment leads to a positive voltage signal of about 0.2 V at the steel electrode due to ionization of the slag at the slag/steel electrode interface through formation of an electrical "double-layer".[24] By contrast, if the steel electrode is contacted with gas, no current will flow through the system. Field tests with the Vesuvius ladle shroud slag detector have shown this to occur, on occasion, leading one to speculate that the detector can become 'blinded' when gas bubbles pass by.

A fundamental investigation of air entrainment phenomena associated with teeming nozzle/ladle shroud assemblies had therefore been studied as part of on-going research into slag entrainment phenomena in liquid metal transfer operation under the title of 'Shroud gas/steel flow interaction'.

1.5 STRUCTURE OF THE REMAINDER OF THESIS

Chapter 2 is devoted to a discussion of available hydrodynamic theory for vortex formation, prevention of slag entraining funnel formation and air entrainment and shrouding of liquid steel.

As there are three main objects, i.e., (i) slag entrainment in late rotating vortices, (ii) detection of early stage of slag entrainment applying AMEPA system and (iii) shroud gas/steel flow interactions, the experimental apparatus, and the experimental procedures, used in the present study, will be described under each title in Chapter 3.

Chapter 4 is devoted to the experimental observation and discussion, again under three different titles. Observations from flow visualization experiments are presented.

A summary and significant conclusions from the study are presented in Chapter 5.

CHAPTER
2

LITERATURE REVIEW

2.1 INTRODUCTION

An overview of potential flow theory to explain vortexing funnel formation based on the conservation of angular momentum is provided in this chapter. A large number of slag control systems developed will be reviewed also, along with air entrainment and covered shrouding of liquid metal.

2.2 VORTEX FORMATION DURING LADLE DRAINAGE

2.2.1 Potential Theory

The principle of conservation of angular momentum was taken into account for the origins of the vortex since 1936. Andrade[25] hypothesized that "when a particle of water circulating around an axis alters its distance from that axis, it must change speed so that the product of distance and speed remains the same – the closer to center it comes the faster it must move, and, still more, the greater must be the number of revolutions per second, since, the distance being less, the angular velocity would have to increase if the velocity had to remain the same." The principle of conservation of angular momentum can be written as follows:

$$mV_{\theta,r} = \text{constant} \tag{2.1}$$

where m, V_θ and r are the mass, tangential velocity and radial position of the particle rotating about the axis at $r = 0$. Therefore, the tangential velocity distribution of a free vortex can be written as follows:[26,27]

$$V_\theta = \frac{K}{r} \tag{2.2}$$

where K is the strength of the vortex. K can be specified from known value of V and r. The circulation, Γ, usually defined as $2\pi r V_\theta$ for flow around circular paths, is constant, as long as the path over which it is measured encompasses the vortex centre. However, as V_θ is undefined at $r = 0$, the circulation at the center can be shown to be zero. In other words, the vortex is everywhere irrotational except at the center.

Assuming incompressible and inviscid liquid for two-dimensional steady flow, the line vortex and the line sink can be superposed, based on potential theory. This superposition result in the potential vortex, the surface streamlines of which are logarithmic spirals, and the free surface of which is hyperboloidal in shape. The liquid head in the infinitely large vessel is assumed to be constant. A line vortex and a line sink are graphically shown in Figure 2.1.

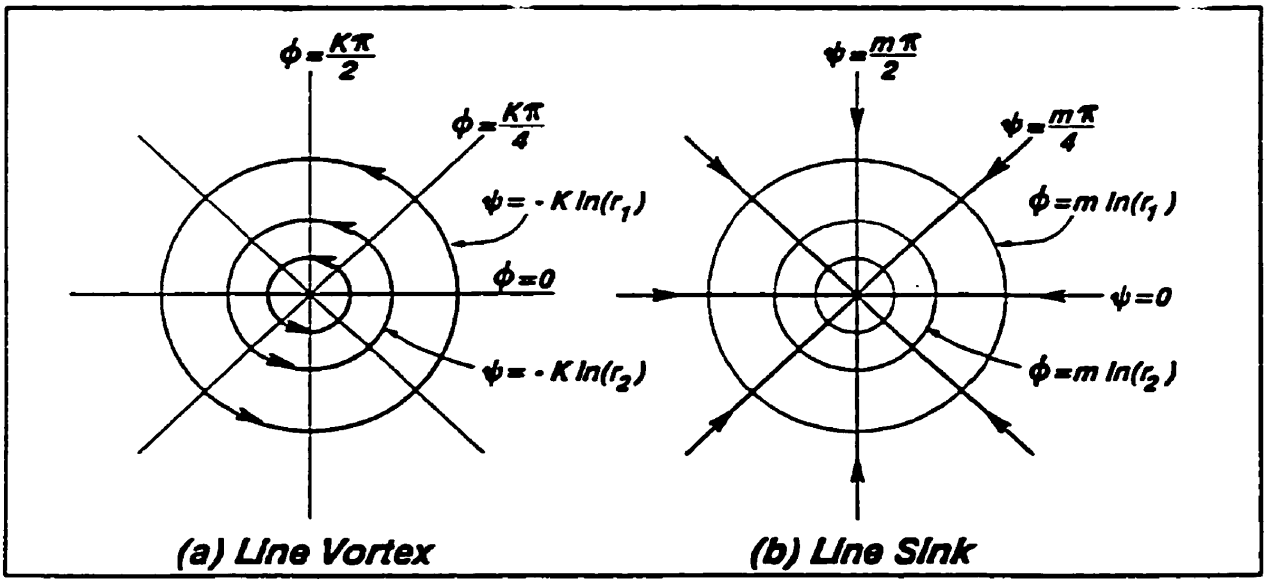

Fig. 2.1 Graphical representation of a line vortex and a line sink.

The radial and tangential velocity distributions for a line sink and a line vortex are given by

$$V_{r,sink} = \frac{m}{r}, \qquad V_{\theta,sink} = 0 \tag{2.3}$$

$$V_{r,vortex} = 0, \qquad V_{\theta,vortex} = \frac{K}{r} \tag{2.4}$$

where the sink strength m has a negative value and the vortex strength K has the same units as m. The sink streamlines flow in towards the central axis. The stream function Ψ and the velocity potential ϕ for the line sink and the line vortex are given by

$$\Psi = m\theta, \qquad \phi = m \ln r \tag{2.5}$$

$$\Psi = -K \ln r, \qquad \phi = K\theta \tag{2.6}$$

Both the sink and the vortex having singularities at the center, the velocities (V_r in the case of the sink and V_θ in the case of the vortex) are infinite. The velocity distributions for the line sink and the line vortex are both incompressible and irrotational.

Being a linear property, the solutions for stream functions and velocity potentials of superposed plane flow solutions can be added. In other words, the stream function and the velocity potential of the combined vortex-plus-sink can be obtained by adding together the individual stream functions of the vortex and the sink. Thus, the stream function and velocity potential of the vortex-plus-sink are given by

$$\Psi = m\theta - K \ln r, \qquad \phi = m \ln r + K\theta \tag{2.7}$$

and the streamlines for the vortex-plus-sink are logarithmic, or equiangular, spirals of the form

$$r = C_1 e^{m\theta/K}, \qquad C_1 = e^{\Psi/K} = \text{constant} \tag{2.8}$$

These streamlines are plotted graphically[26] in Figure 2.2, the stream functions of the vortex-plus-sink lying at the intersection of the individual stream functions of the vortex and of the sink. Such streamlines, with large m/K ratios, have been observed in the laboratory as well as in the vicinity of large turbine intakes located in lakes.

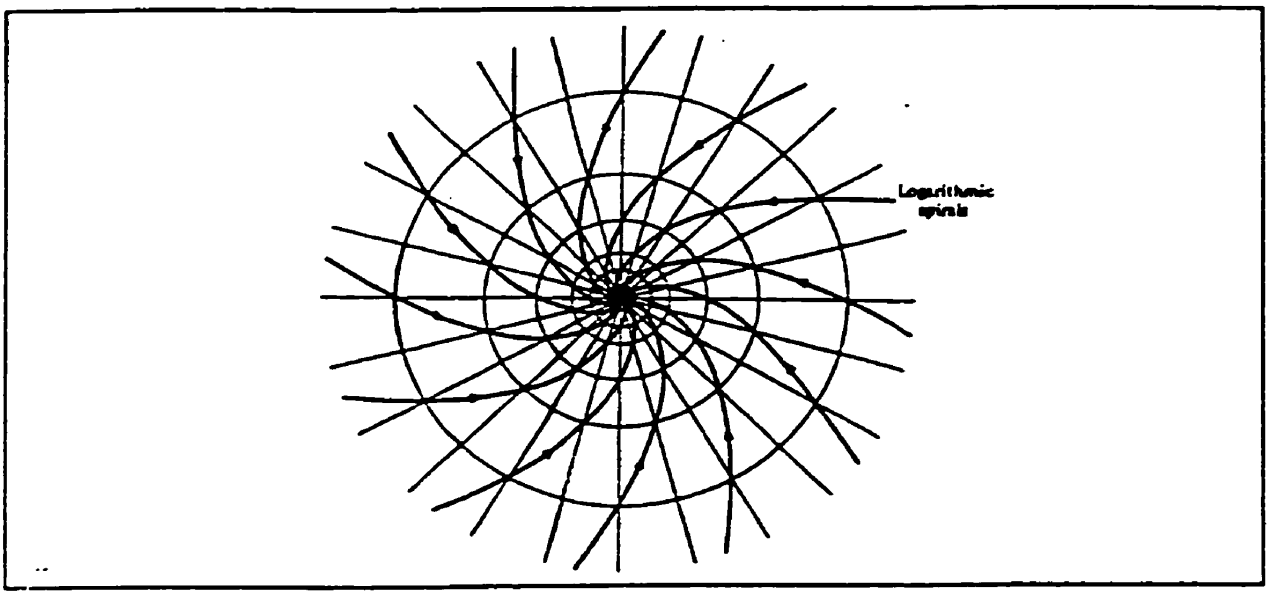

Fig. 2.2 Streamlines for a vortex plus sink constructed by the graphical method[26]

2.2.2 Velocity Distribution and Surface Profile of the Potential Vortex

2.2.2.1 Relative Circulation

Toyokura and Akaike[28] observed the variation of the relative circulation, Γ_r, defined as the ratio of the local circulation at radius r to the circulation in the free vortex region far away from the drainage nozzle, with relative radial position in an inner viscous vortex core at radii similar to that of the drain where the tangential velocity decreased to zero (Figure. 2.3).

$$\Gamma_r = \frac{rV_\theta}{\Gamma_f} = \frac{rV_{\theta.r}}{RV_{\theta.R}} \tag{2.9}$$

Figure 2.3 shows that the relative circulation decreased rapidly with decreasing radius in the viscous vortex core and the outer radius of the viscous vortex core was always greater than the radius of the nozzle itself, often reaching a value nearly 1.5 times the nozzle diameter, depending on the nozzle diameter, d, and the radial Reynolds number, $N = rV_r / \nu$.

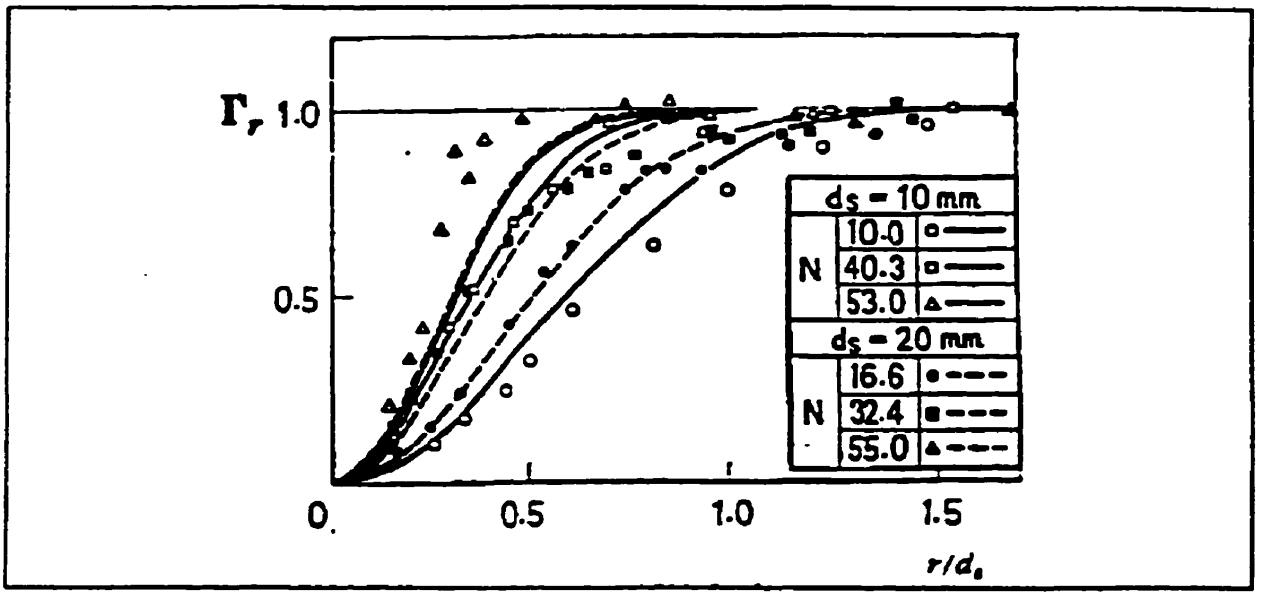

Fig. 2.3 Variation of Γ_r in the vortex core; Toyokura and Akaike.[28]

Figure 2.4 shows that Γ_r was constant in the outer free vortex region,[29] and thus the tangential velocity distribution was more or less identical to that of the inviscid potential vortex.

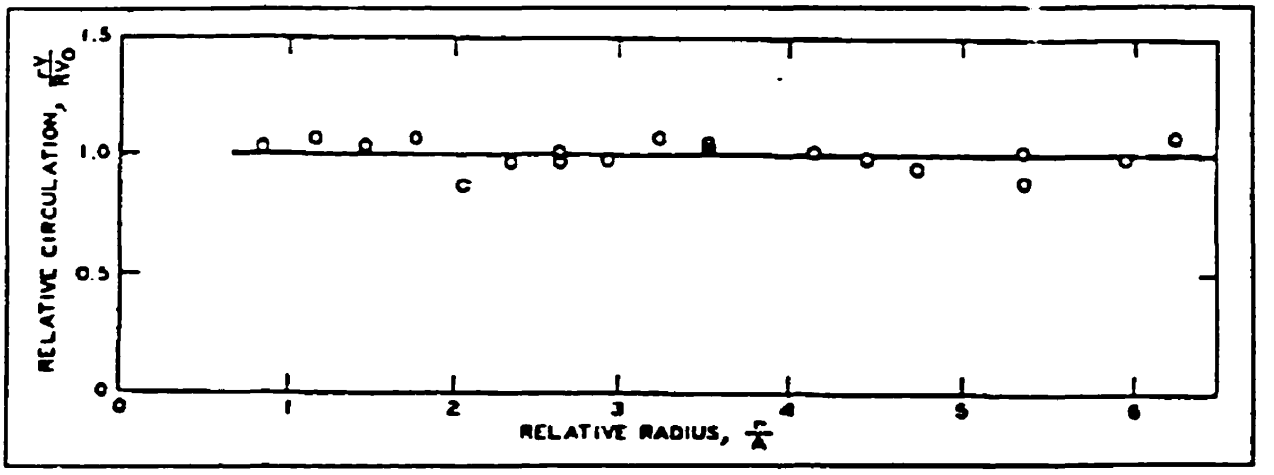

Fig. 2.4 Variation of Γ_r in an outer free vortex region; Daggett and Keulegan.[29]

A similar dependence of Γ_r on radial Reynolds number for viscous liquids was predicted theoretically by Einstein and Li.[30] Figure 2.5 shows the predicted variation of Γ_r with the radial Reynolds number, A, which, by definition, was identical to Toyokura and Akaike's[28] radial Reynolds number N. Γ_r for viscous liquids was shown to lie between the two extremes of rigid body rotation (A = 0) and potential vortex (A = ∞). It was found that measured values of Γ_r could be matched with the predictions from theory if, and only if, the liquid viscosity was assumed to be higher than the laminar viscosity (effective turbulent viscosity); thus, turbulent momentum transfer in the viscous vortex core was indicated.

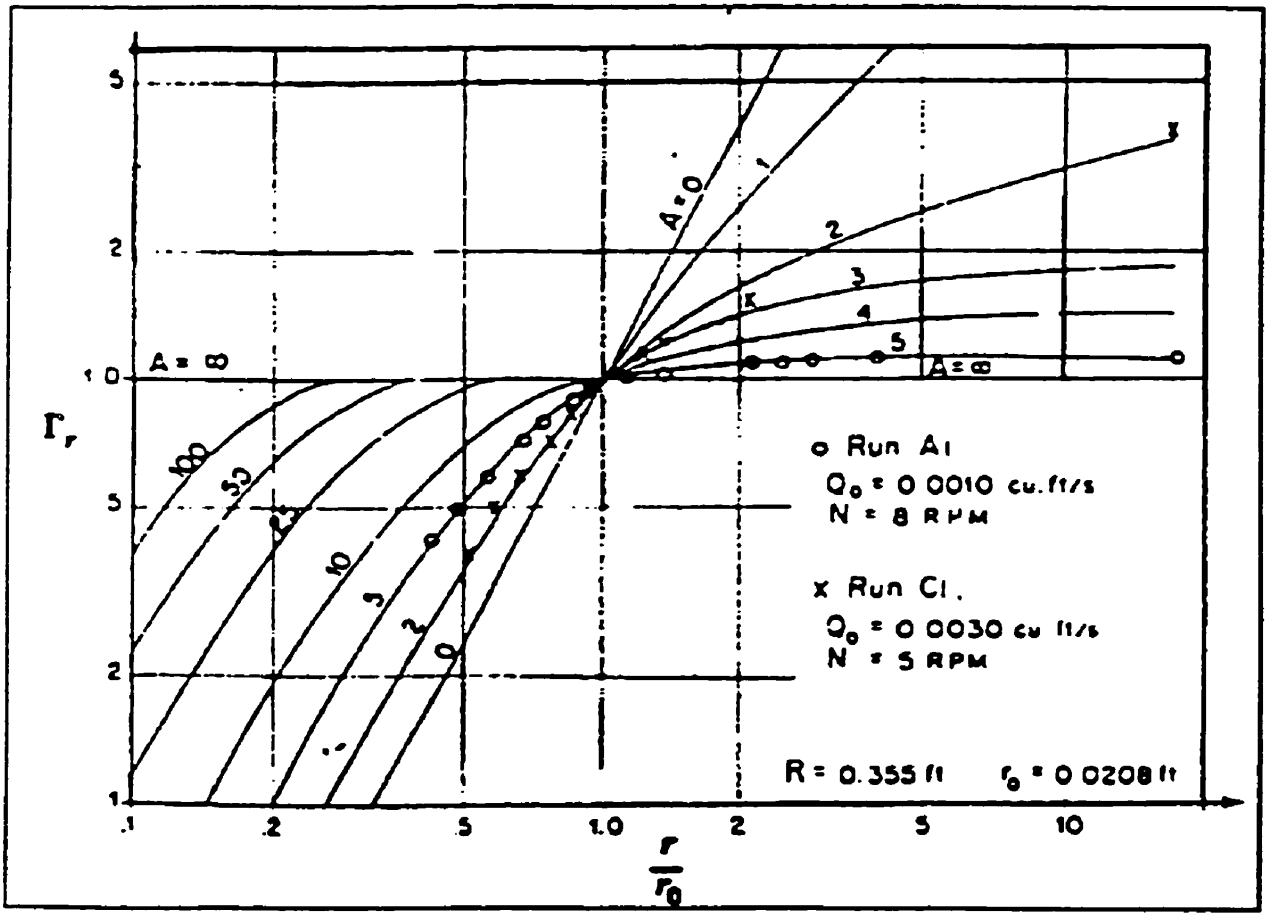

Fig. 2.5 Variation of Γ_r; Einstein and Li.[30]

2.2.2.2 Tangential Velocity Distribution

Daggett and Keulegan[29] studied the tangential velocity in the outer free vortex region. Figure 2.6 shows the tangential velocities in the outer free vortex region at various depths and radii. It shows that the tangential velocity in the outer free vortex region varied with radial position alone, with very little dependence on the axial position. Tangential velocities did not vary with depth, Z, except very close to the floor of the vessel. Anwar[31] compared between calculated and measured tangential velocities in the free vortex region as well as near the vortex core and found reasonable agreement with the tangential velocity distribution of a potential vortex up to the specific point, from which, to air core, significant deviations were observed. Kimura and Hasimoto[32] measured the tangential velocity distribution with radial position, with no drainage, and found its dependency on the radial position and the time period over which measurements were made as well.

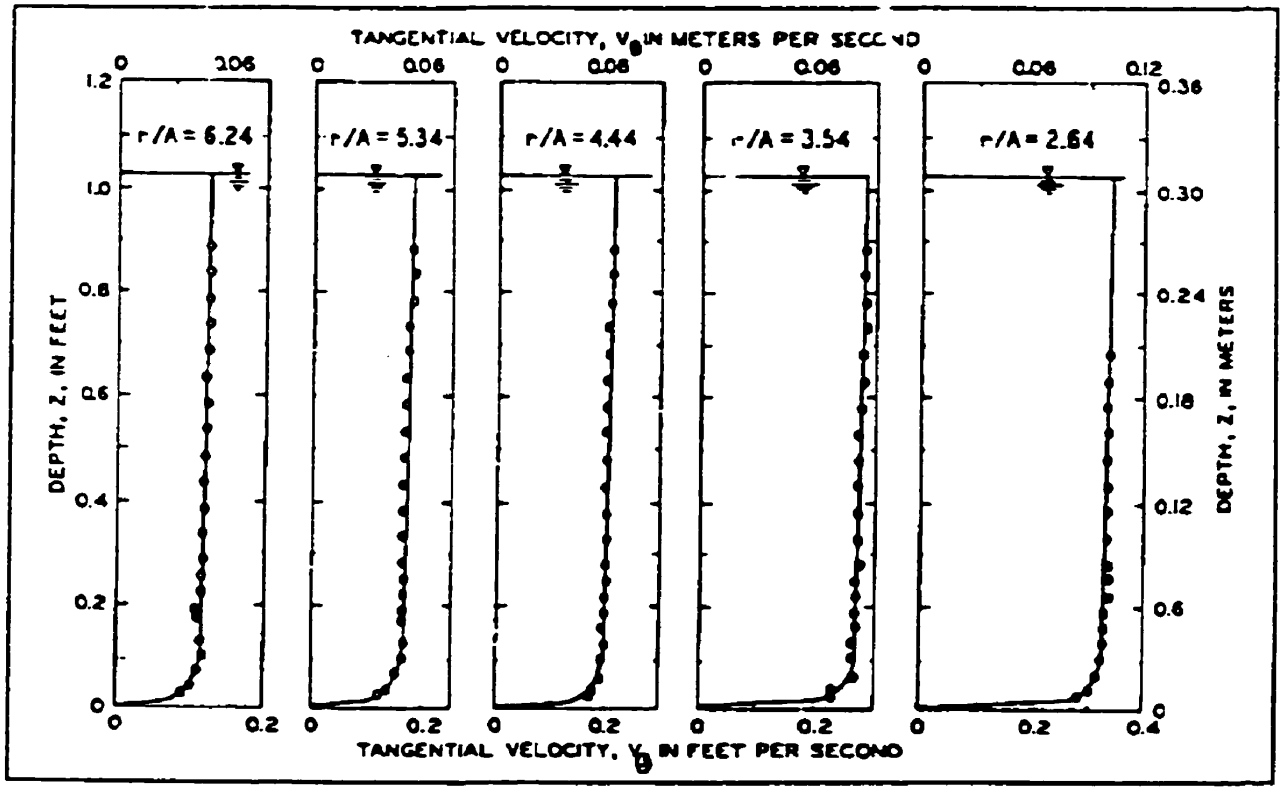

Fig. 2.6 Tangential velocities in the outer free vortex region at various depths and radii (A = nozzle radius); Daggett & Keulegan.[29]

2.2.2.3 Radial Velocity Distribution

Figure 2.7 shows the radial velocities in the outer free vortex region at different depths and radii observed by Daggett and Keulegan.[29] They found the presence of significant radial velocities that are known to increase at smaller radii, and also at lower depths. As can be seen from Figure 2.7, the dependence of radial velocities on the depth was stronger at smaller radius than at larger radius. Similar results were obtained by Toyokura and Akaike.[28]

However, radial velocities in the inner viscous region are lower at smaller radial position. This decrease at radii smaller than the nozzle radius was driven mainly by the predominance of downward axial velocities. Anwar[33] showed that the radial velocity had a maximum at $r/d = 0.375$; the theoretical explanation developed to account for this maximum in the radial velocity also indicated that the radial velocity at the axis would be zero. Daggett and Keulegan[29] reported a maximum in the radial velocity at $r/d = 0.75$.

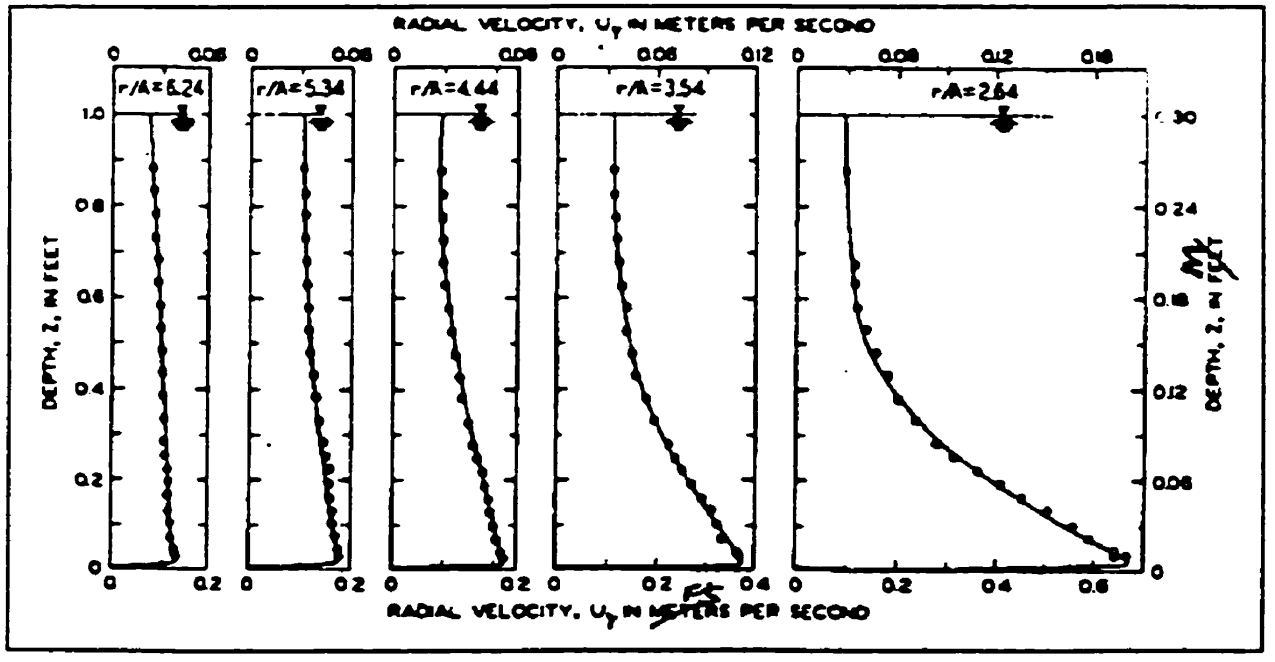

Fig. 2.7 Radial velocities in the outer free vortex region at different depths and radii (A = nozzle radius); Daggett and Keulegan.[29]

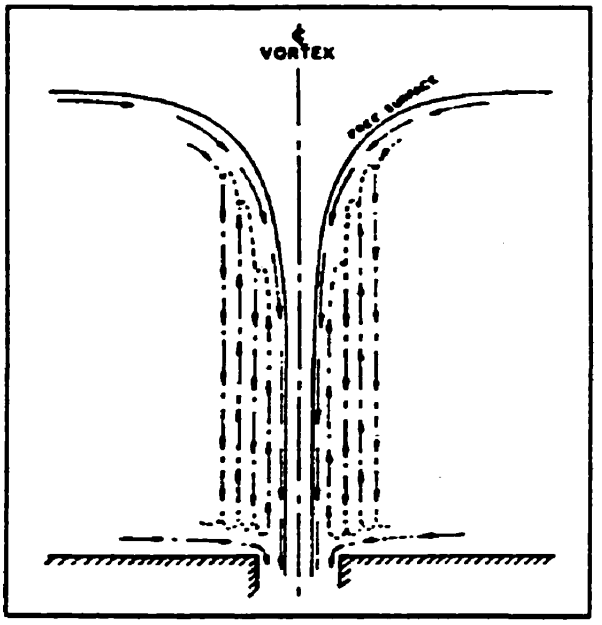

Fig.2.8 Sketch of upward and downward axial velocities near the vortex core; Quick[34]

2.2.2.4 Axial Velocity Distribution

Measurements have shown the presence of significant axial velocities in the vicinity of the vortex core,[34,35] often in excess of 10% of the tangential velocities as required by the conservation of angular momentum. Quick[34] observed downward as well as upward axial velocities. Figure 2.8 shows upward and downward axial velocities near the vortex core. Daggett and Keulegan[29] also suggested the presence of such upward as well as downward velocities by doing numerical computations of the axial velocity distribution, on the basis of measured tangential and radial velocities. Kamel[36] showed that upward axial velocities were inevitable when the flow through the boundary layer close to the vessel floor exceeded the discharge capacity of the drainage nozzle.

2.2.2.5 Surface Profile of the Potential Vortex

The surface profile of the potential vortex when the sink strength m is negligibly small can be determined easily by applying standard Bernoulli analysis. If we substitute the radial and tangential velocity distribution for the line vortex, Eq. (2.4) in the Bernoulli equation, we obtain

$$p + \frac{\rho K^2}{2r^2} + \rho g z = C \tag{2.9}$$

where C is a constant. It can be shown that a surface of constant pressure must therefore have the shape

$$z\big|_{p=p_1} = C_1 - \frac{K^2}{2gr^2} \qquad C_1 = \frac{C - p_1}{\rho g} \tag{2.10}$$

Thus, all constant-pressure surfaces, including the free surface where the pressure is equal to the atmospheric pressure, have the form of a second order hyperboloid; *i.e.* z varies inversely with r^2. Figure 2.9 shows a comparison of measured and calculated free surface profiles carried out by Stevens and Kolf.[37] It can be seen from Figure 2.9 that measured and calculated free surface profiles were in good agreement in the free vortex regions, while the diameter of the vortex was smaller than predicted by theory at all depths in the core region. Similar results were also reported by Anwar,[31] however, it was found that at some point close to the vessel floor, the measured profile became wider than the theoretical profile.

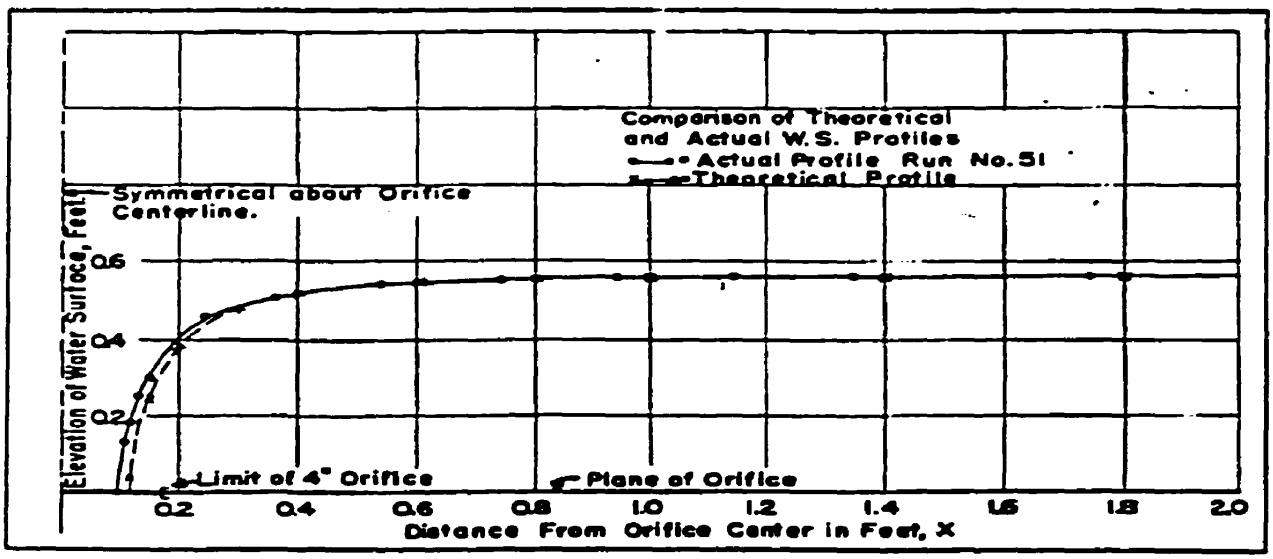

Fig. 2.9 A comparison of calculated and measured free surface profile; Stevens and Kolf[37]

2.3 PREVENTION OF SLAG ENTRAINMENT

2.3.1 Introduction

A large number of slag control systems developed and tested can be grouped in the following four categories, based on analysis of their governing principles.

(1) 'slag-cut' methods,

(2) 'metal-level-control' methods,

(3) 'detection-based end of drainage' methods, and

(4) 'vortex suppression' methods.

The principle of each of these categories is briefly described here, with proper examples, so as to illustrate as well as evaluate methodologies. It should be stated that only one of the slag control methods listed above, vortex suppression methods, addresses the cause of slag entrainment. It is necessary to highlight the fact that a certain minimum of slag entrainment cannot be avoided even with the best of existing technology, and that it is yet impossible to detect, let alone prevent, the entrainment of discrete emulsified droplets of slag.

2.3.2 Slag-Cut methods

Methods under this category of 'slag-cut' take advantage of the density differences between slag and liquid steel to physically interrupt, or cut, slag entrainment as soon as it begins. For the case of BOF converter tapping, slag-cut methods have been largely used. The principle of using slag-cut balls[17] and siphon tapping holes[20,38] will be addressed hereunder.

Figure 2.10 shows a slag-cut ball method. With intermediate density between slag's and metal's, a slag-cut ball would remain at the slag-metal interface, descend into, and block, the tapping hole when slag flow starts. The effectiveness of the slag-cut action is limited by the ability to position the ball close to the tapping hole axis, and by the extent to which the mating contours of the ball and the tapping hole match one another.

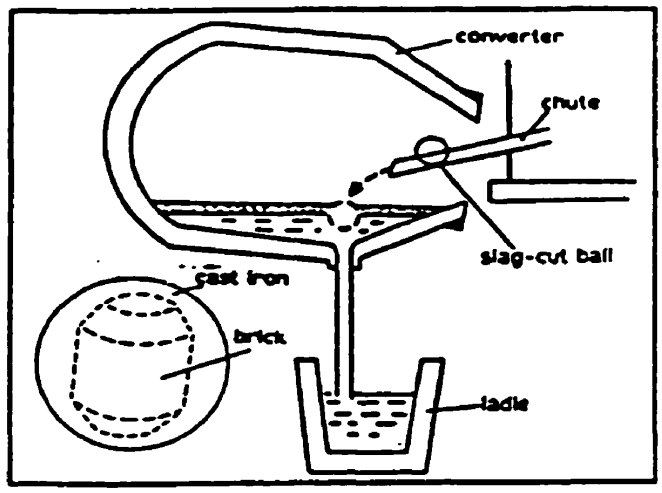

Fig. 2.10 Slag-cut ball method; Saigusa *et al.*[17]

Using a siphon tube attached to the conventional tapping hole (siphon tapping hole) was found to be effective on reducing slag entrainment.[20,38] The basic assumptions used in the siphon tapping hole development are that (1) slag flow begins only after all metal has been tapped, and (2) the ferro-static pressure of the last of the steel could be used to overcome the head of slag remaining in the converter, thereby preventing slag flow. Figure 2.11 illustrates the siphon tapping hole's principle.

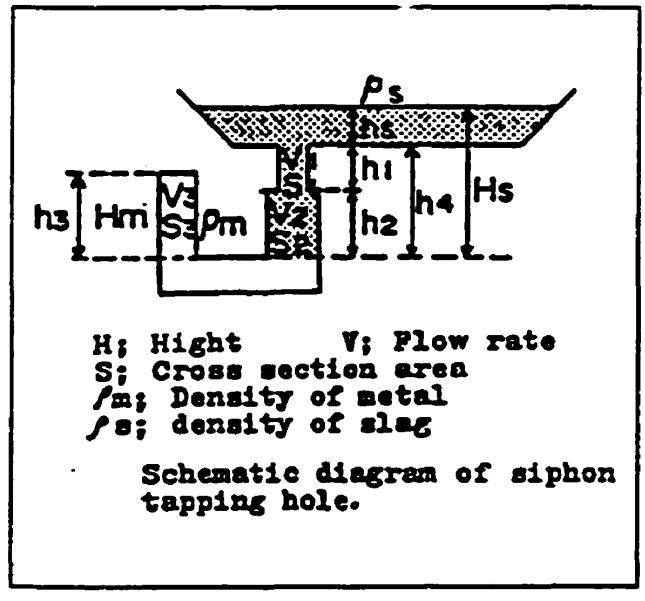

Fig. 2.11 Schematic diagram of siphon tapping hole; Ohmori *et al.*[20]

Slag flow stopped when the ferrostatic pressure in the free arm of the siphon tube could no longer be overcome by the static pressure of the slag, *i.e.*

$$H_s\rho_s < H_m\rho_m \tag{2.11}$$

The necessary dynamic condition that ensured the prevention of slag flow was that the slag-metal interface did not reach the zero datum shown in the Figure 2.12, *i.e.*

$$\rho_m g h_3 - \rho_s g(h_4 + h_s) > \frac{1}{2}(\rho_m V_3^2 + \rho_s V_2^2) \tag{2.12}$$

which, with due consideration to the equation of continuity, was rewritten as,

$$\frac{H_m}{H_s} > \frac{\rho_s}{\rho_m}(1+\alpha) \tag{2.13}$$

where α represented a constant containing various slag and metal heads, cross-sectional areas, and the densities of the slag and steel, as follows:

$$\alpha = \frac{(h_4 - h_3 + \frac{\rho_s}{\rho_m}h_s)(\rho_m \frac{S_1^2}{S_3^2} + \rho_s \frac{S_1^2}{S_2^2})}{\rho_m\rho_s(h_4 + h_3)} \tag{2.14}$$

2.3.3 Metal-Level-Control Methods

Using sensors and appropriate control systems makes it possible to maintain liquid metal level above a pre-set minimum value. Being the simplest metal-level sensor, the weighing scale cannot differentiate between slag and steel. This disadvantage is also shared by other techniques that use infrared, microwave, or laser optic radiations for level detection. However, the Electromagnetic Metal Level Indication (EMLI) system, an electromagnetic measurement technique, has shown its capability of giving an accurate indication of the actual metal level, that is independent of slag volume.[39,40,41]

Figure 2.12 shows the measuring principle of EMLI and schematic of EMLI tundish level sensor. AC-current is fed into a transmitter coil so as to generate an electromagnetic filed, thereby inducing an AC-voltage in a second coil used as a receiver.

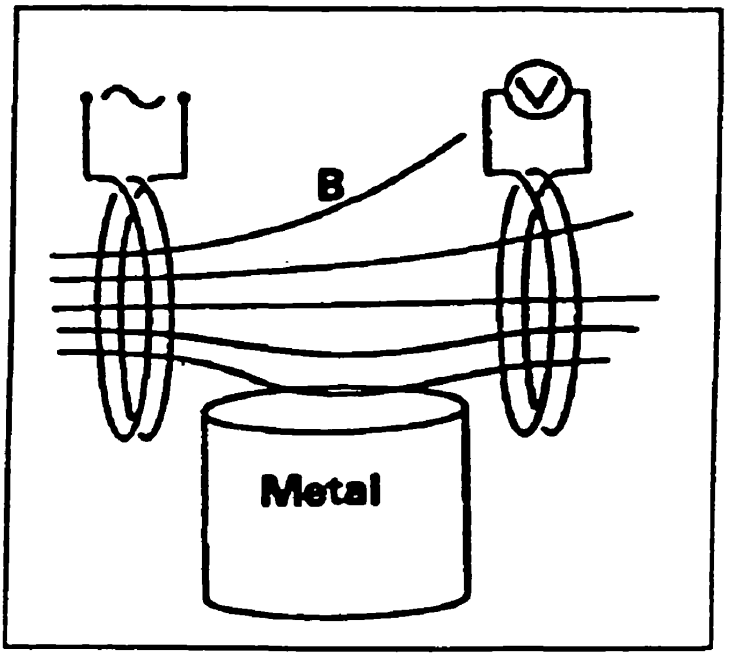

Fig. 2.12 The measuring principle of EMLI systems; Mellberg and Linder.[39]

Slag responds differently from liquid steel to the electromagnetic field generated by the transmitter, which makes it possible to accurately determine the actual metal level. Another metal-level-control method could be to use ultrasonics, the penetration depth of which has been reported as 500 mm.[42,43]

2.3.4 Detection-Based End of Drainage Methods

Since there are various manifestations of slag entrainment, for example, the different spark characteristics of slag from those of steel, **visual sighting of slag** is the simplest of all detection methodologies. In order to get visual access, however, liquid steel has to be poured without any shroud during the last stages of drainage, which results in the reoxidation of liquid steel.

On the basis of the slag-steel stream possessing lower impact energy than a volumetrically equivalent stream of liquid steel, **vibration sensors** mounted on tundishes,

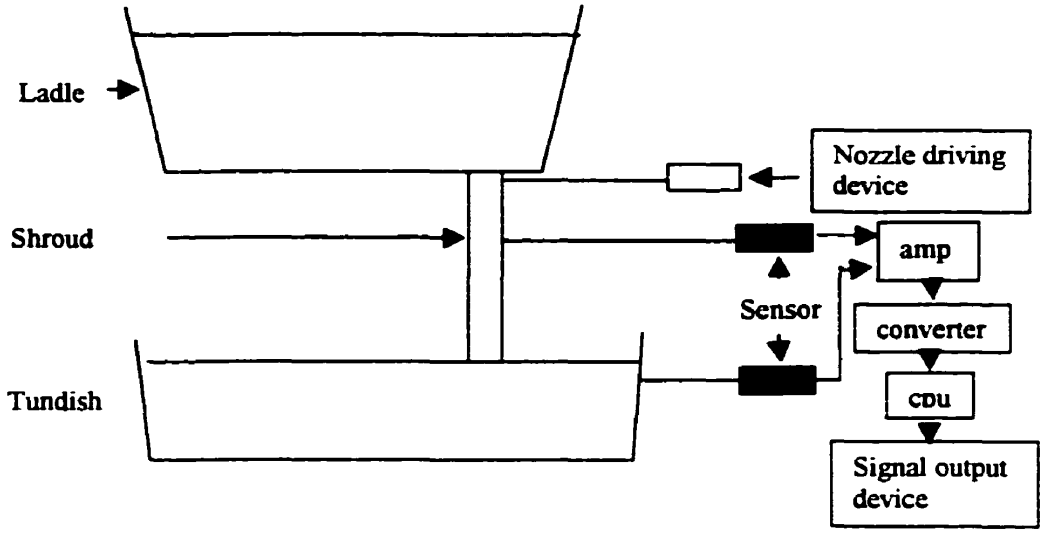

Fig. 2.13 Schematic illustration of a vibration sensor-based automatic slag detection system; Itoh *et al.*[44]

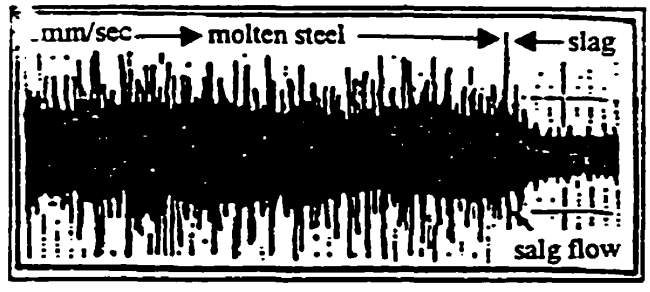

Fig. 2.14 Change in the tundish vibration signal at the onset of slag flow; Itoh *et al.*[44]

and on ladle shrouds, have been used to detect slag entrainment.[44,45] Schematic illustration of a vibration sensor is shown in Figure 2.13 and the change of the tundish vibration signal at the onset of slag flow is shown in Figure 2.14. Even thought the use of the vibration sensor rests on empirical observations, the fact that the sensor allows completely shrouded pouring, to the exclusion of reoxidation, is a definite advantage.

Gravimetric detection of slag entrainment continuously monitors ladle weight during drainage, the signal of which is continually fed to a computer which performs real-time computation of the first and second temporal derivatives of ladle weight, *viz.* Casting

(teeming) rate and rate of change of casting (teeming) rate, respectively.[46,47] With no change in the volumetric flow rate, the onset of slag entrainment results in decrease in the mass flow rate, then the casting rate curve and dramatic increase in the rate of change of casting rate curve (see Figure 2.15 and 2.16). A slag alarm is usually set up go off when the gradient in the rate of change of casting rate exceeds a pre-selected value.

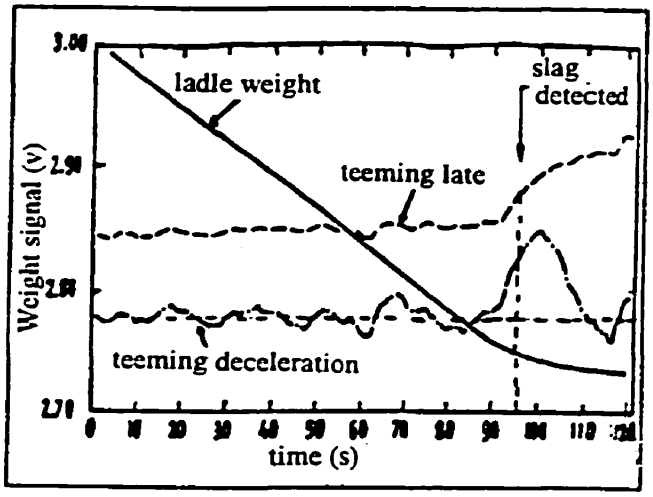

Fig. 2.15 Change in the ladle wt. signal, and its derivatives, during the drainage of a 180 ton ladle; Andrzejewski *et al.*[48]

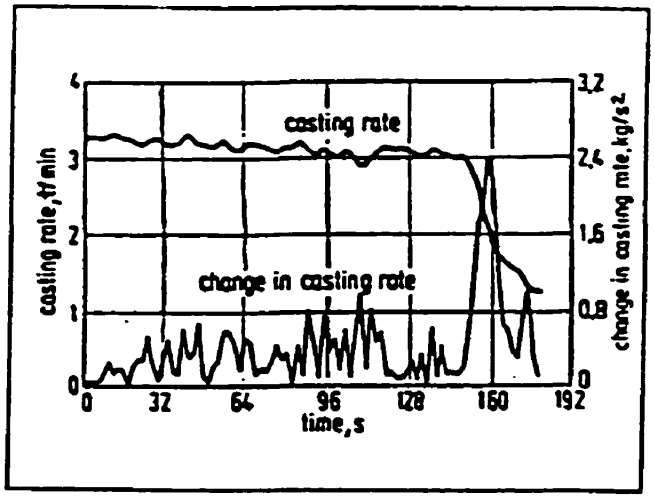

Fig. 2.16 Change in the casting rate and its derivative during the drainage of a ladle; Gruner et al.[49]

Electromagnetic slag detection offers far greater accuracy and reliability than any other detection method. Electromagnetic Metal Level Indication system (EMLI), and Angewandte Meβtechnik und Prozeβautomatisierung (AMEPA) will be briefly treated here. Installation of both of these sensors is so easy that those sensors are quite suitable for use on converters, ladles, and tundishes. EMLI slag detection sensors are based on the same measuring principle as the EMLI metal-level-detection sensors. Figure 2.17 shows schematic implementation of an EMLI sensor on a converter-tapping hole. Variations in the EMLI signal as a function of the relative amounts of steel and slag in the drainage nozzle, and in response to the closure of the ladle slide-gate are shown in Figure 2.18.

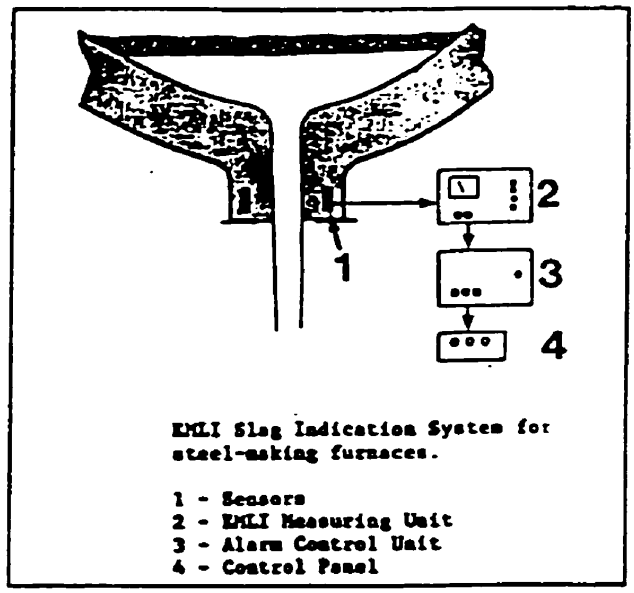

Fig. 2.17 EMLI slag indication system for a BOF converter; Mellberg and Linder.[39]

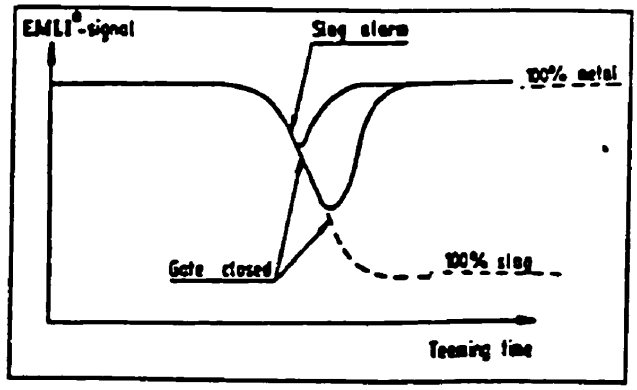

Fig. 2.18 Change in the EMLI signal as the slide-gate is closed; Mellberg.[41]

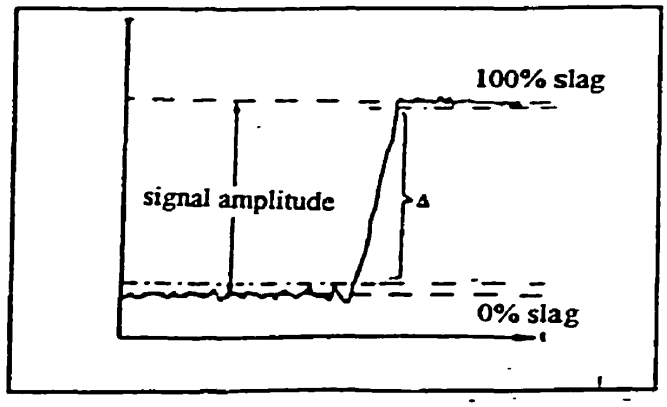

Fig. 2.19 AMEPA signal change at the onset of slag flow in proportion with typical noise levels; Julius *et al.*[23]

As mentioned earlier in chapter one, the AMEPA slag sensor,[23,50] based on the same measuring principle as the EMLI, also has a primary and a secondary coil that are placed together, concentric to one another. Variations in the AMEPA signal with the slag content of the outflow are shown in Figure 2.19, which also shows that the jump in the AMEPA signal at the onset of slag flow is significantly higher in amplitude in comparison with typical signal noise variations.

2.3.5 Vortex Suppression Methods

Stopper rods were found to have roles of vortex suppression as well as tundish nozzle closure and metering of steel flow. However, the use of stopper-rods is often accompanied by air-core penetration from beneath the ladle, severe flaring of the outflow stream, and in the case of less than optimum sized stopper-rods, eccentrically disposed vortexing funnels too. When stopper rods were ineffective at vortex suppression, one or three different forms of funnel shaped entrainment core were observed,[51] which were shown in Figure 2.20, *viz.* an air core extending from the top surface of the liquid into the drainage nozzle and either (a) centered on and enveloping the stopper rod or (b) eccentric to the stopper rod axis, and (c) an air core rising up from below the ladle through the drainage nozzle on to the lower tip of the stopper rod. Jewasinski *et al.*[52] found that stopper-rod can effectively suppress a vortex, especially when the diameter of the stopper

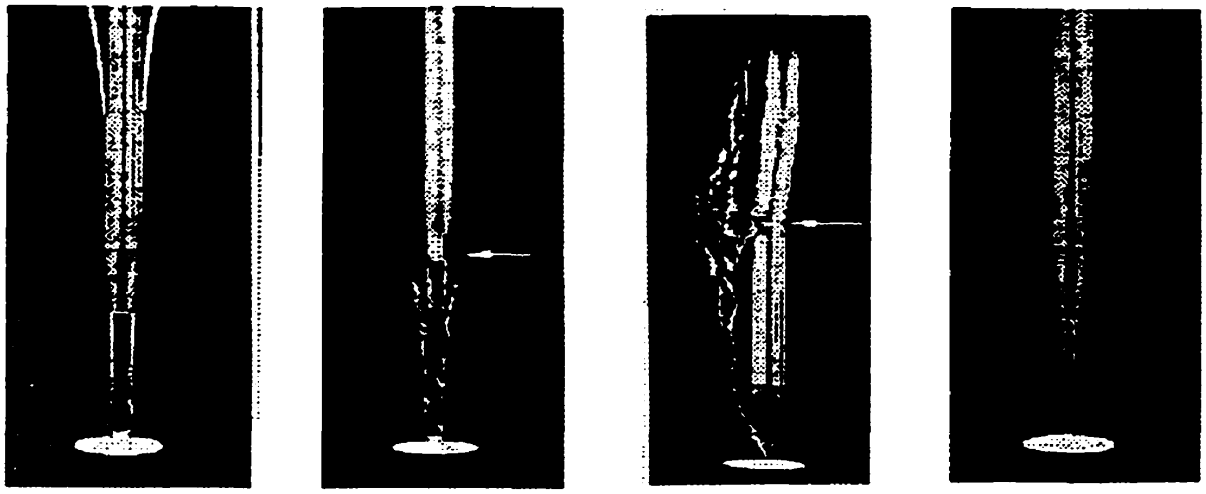

(a) (a) (b) (c)

Fig. 2.20 Vortices that form in the presence of a stopper rod above the drainage nozzle; Dubke and Schwerdtfeger.[51]

rod is at least three times larger than that of the nozzle. A floating donut centred on the stopper-rod was found to be effective in suppressing the eccentric surface vortex (Figure 2.20 (b)), in a full-scale water model of a Stelco tundish.[21]

A "**vortex buster**"[2] was designed to interrupt downward axial flow and rotational flow that are the main two component of the potential vortex, based on the critical tangential velocity hypothesis and the conditions favorable to vortexing funnel formation, *i.e.* the downward axial velocities in the vessel and the tangential velocities present was the motive force for vortexing funnel formation. The horizontal baffle plate that is a physical barrier to downward axial velocities, and vanes as the essential components of the vortex suppression device is schematically shown in Figure 2.21. Vanes and baffles were so fabricated that different dimensions of the horizontal baffle and the vanes could be mixed and matched easily. Sankaranarayanan[2] evaluated the ability of each combination of the baffle and vanes to suppress vortexing funnel formation as a function of initial tangential velocity. The necessary vane height was found to be at least equal to ,if not greater than, half the nozzle's diameter. Moreover, vortexing funnel suppression performance improved with increasing baffle plate diameter, as expected.

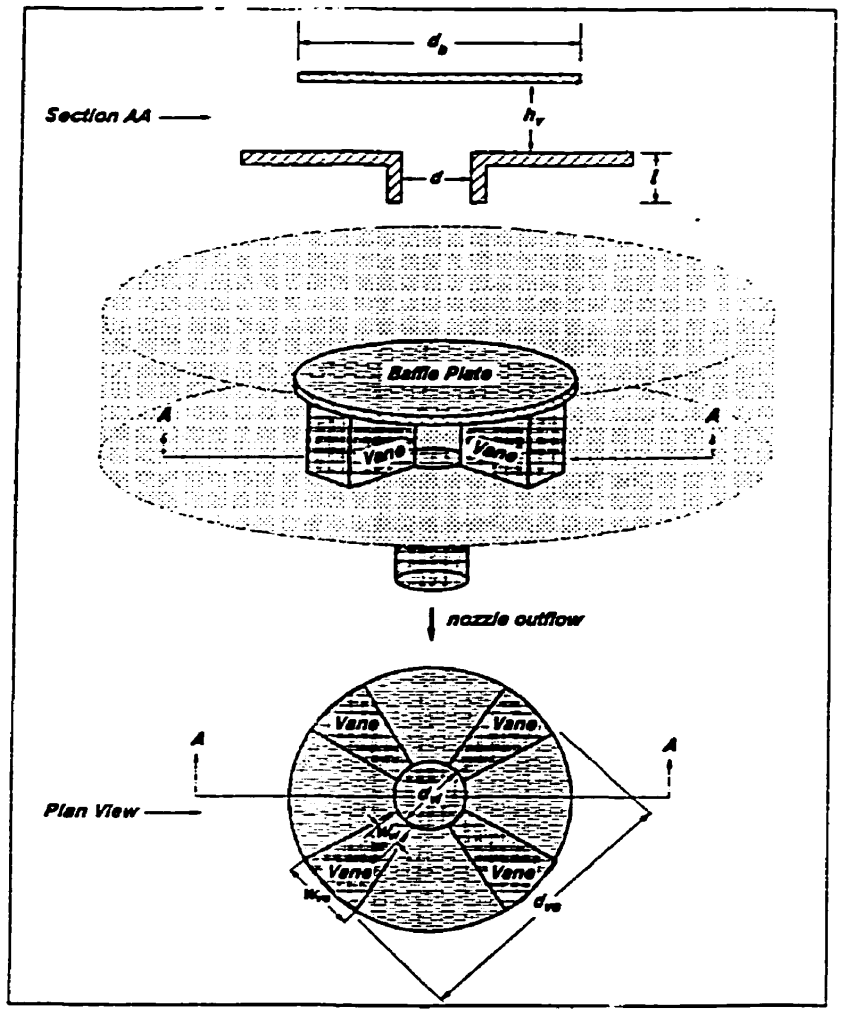

Fig. 2.21 A schematic diagram showing the horizontal baffle plate and vanes as the essential components of the vortex suppression device; Sankaranarayanan[2]

Figure 2.22 shows critical height versus initial tangential velocity for the "vortex buster". By promoting radial flows along the vessel floor, at the expense of downward axial flows along the nozzle axis that are inevitably formed in the presence of strong initial tangential velocities, the "vortex buster" effectively removes the root cause for vortexing funnel formation.[2]

Even though the vortex buster was successfully tested in water model of a steelmaking ladle with a incredible results (no vortex at all!), this was not implemented in steel making ladles yet.

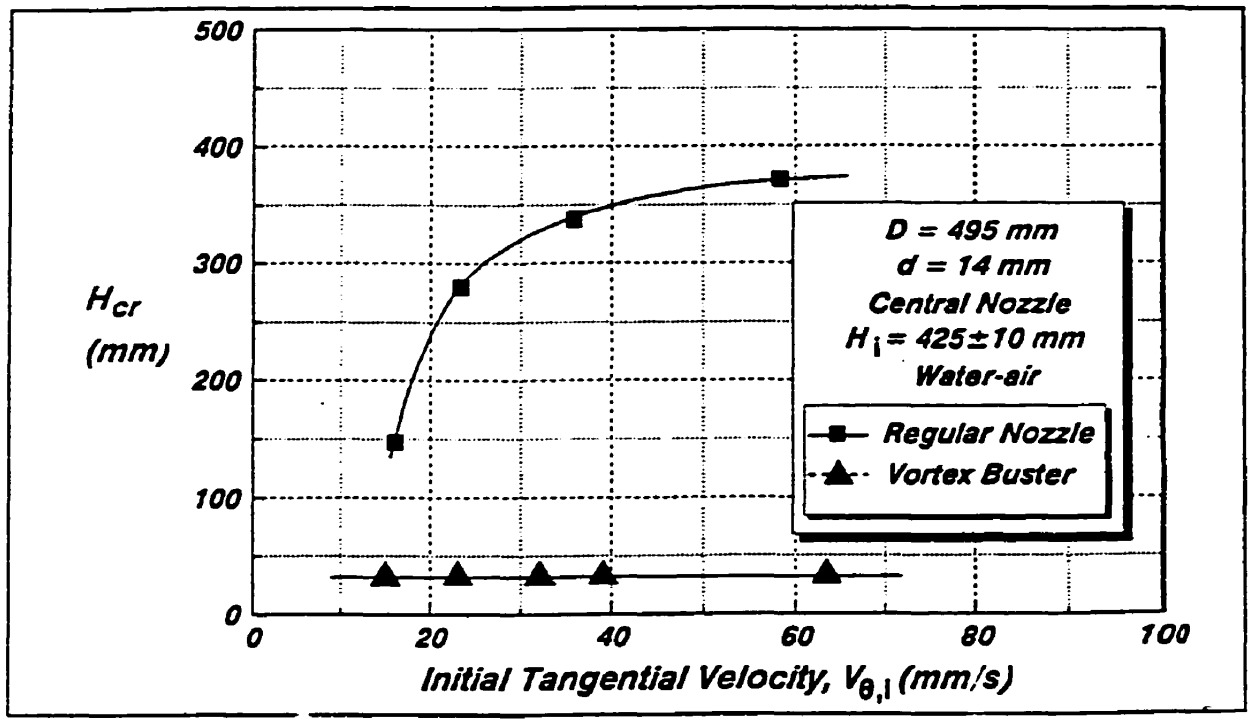

Fig. 2.22 H_{cr} versus $V_{\theta,i}$ for the "vortex buster"; Sankaranarayanan[2]

Gas injection stirring, based on the limit of formation of vortexing funnel : directly proportional to the intensity of residual tangential motion, have long been used to destroy residual tangential velocities in the bulk of the liquid.[3,6,53] The most popular method of injection gas has been through a porous plug built into the drainage nozzle. It was observed that air injection into a water-liquid paraffin model of a tundish considerably reduced liquid paraffin entrainment (Figure 2.23).[6] Considerable improvements in slag quality were obtained when the porous plug was installed in the tundish. Based on experiments about gas injection to suppress slag entrainment with water models of a steelmaking ladle, Hammerschmid *et al.*[3] concluded that (1) the shape of the gas plume was important and (2) suppression of the paraffin oil vortex improved as the gas flow rate was increased. Subsequent adoption of the porous plug to the tapping hole of a 120 ton and a 300 ton converter resulted in significantly lower slag thicknesses in the ladle at the end of converter tapping.

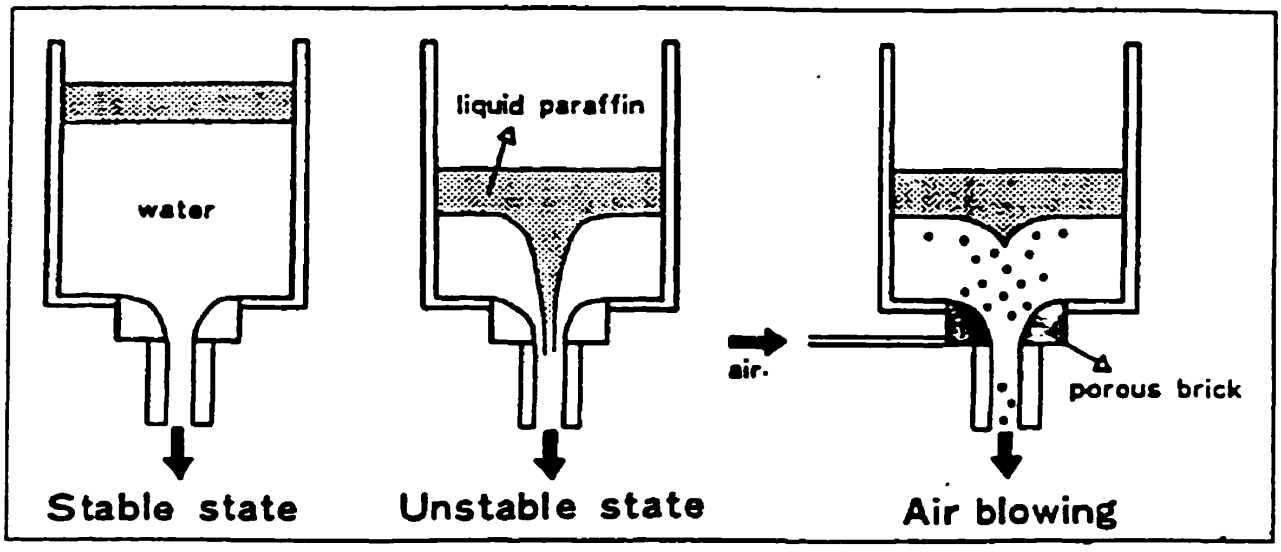

Fig. 2.23 Gas injection into tundish water model; Ichikawa *et al.*[5]

2.4 AIR ENTRAINMENT AND SHROUDING OF LIQUI D STEEL

2.4.1 Air Entrainment

The entrainment of gas by liquid jets plunging into pools has been of interest to chemical and mechanical engineers as well as process metallurgists. Lin and Donnely[54] observed that there is a minimum critical velocity for a given jet diameter at the plunging point over which entrainment occurs. Van de Sande and Smith[55] also observe the minimum critical velocity. Noting that as the jet velocity is increased, there are three regimes for entrainment, they suggested two equations, one for short jets and the other for long vertical jets. Burley and Kennedy[56] used a continuous moving plane tape to measure air entrainment into a fluid bath. They observed that the velocity of air entrainment is a function of surface tension and viscosity. The air entrainment velocity tended to be a constant value of 9.5 cm/s independent of surface tension when viscosity is over a certain critical value (4.65 poise). Several equations describing the volumetric ratio of entrained gas to liquid, Φ_A / Φ_J, have been proposed by different researchers who used a variety of experimental conditions. For instance:

Ohyama *et al.*[57] gives

$$\frac{\Phi_A}{\Phi_J} = 0.75\left(\frac{V_J}{gL}\right)^{-0.447}\left(\frac{D_J V_J \rho_W}{\eta_W}\right)^{2.18}\left(\frac{L}{D_J}\right)^{0.281} = 0.75(Fr)^{-0.447}(\mathrm{Re})^{2.18}\left(\frac{L}{D_J}\right)^{0.281} \quad (2.15)$$

De Frate and Ruch[58] give

$$\frac{\Phi_A}{\Phi_J} = 10^{-6}\left(\frac{\rho_A V_J^2 L}{\tau}\right) = 10^{-6} We \quad (2.16)$$

Szekely[59] proposes

$$\frac{\Phi_A}{\Phi_J} = \frac{4}{D_J^2}\left\{\frac{3\nu_g L}{V_J} + 1.73 D_J\left(\frac{\nu_g L}{V_J}\right)^{0.5}\right\} \quad (2.17)$$

Henderson *et al.*[60] derive

$$\frac{\Phi_A}{\Phi_J} = \left(\frac{D^*}{D_N}\right)^2 - 1 \quad (2.18)$$

Ciborowski and Bin[61] suggest

$$\frac{\Phi_A}{\Phi_J} = 5\times10^{-11} D_J^4\left[\left(\frac{V_J}{\sqrt{gL}}\right)\times\left(1-\frac{400}{We}\right)+A\right]^{0.00479 D_J - 1.603}\times\left(\frac{L}{D_J}\right)^{1.8}\times\left(\frac{\rho_W}{\rho_A}\right) \quad (2.19)$$

And Van de Sande and Smith[55] suggest for short jets

$$\frac{\Phi_A}{\Phi_J} = 0.027\, V_J\, \frac{V_J^{1/3}}{D_J^{1/2}} \quad (2.20)$$

and for long vertical jets

$$\frac{\Phi_A}{\Phi_J} = \frac{8.5\times10^{-6}}{\Phi_J} + 0.105\times10^{-3}\ \rho_W\, V_J^2 \quad (2.21)$$

with these, one may then estimate the ratio of air to liquid steel entrainment, Φ_A / Φ_J, using physical variables and conditions. Since the mechanisms of gas entrainment and its

amount, will probably depend on the individual processing operations, these correlations are so dissimilar that they cannot be combined into a single expression. Of the relations presented, Eq. (2.17) was derived on purely theoretical grounds, using boundary layer theory.[59] As it was claimed to be relevant to short coherent streams, its applicability and concepts in the case of extended dispersed streams would appear to be questionable.

More recently Choh *et al.*[62,63,64] have developed a new relationship using water, ethanol, glycerin aqua solution and liquid tin. And they confirmed that the rate of gas entrainment can be represented by a model assuming that the gas entrainment does not occur under the true cylindrical stream but arises by the cavity produced by the collision between the bath surface and the stream surface protuberances. They suggested

$$\frac{\Phi_A}{\Phi_J} = 0.02\left\{\frac{R_C - a}{a_o}\right\}^3 \qquad (2.22)$$

2.4.2 Shrouding of Liquid Metal

In continuous casting, the problem lies in transforming liquid metal to solid without reoxidation. Reoxidation may occur during the pouring of steel from the ladle to the tundish and then between the tundish and the solidifying strand. McLean *et al.*[65] studied factors affecting the reoxidation of molten steel during continuous casting. They concluded that the major ill effects of air teeming are: (1) oxidation of the stream and pool by direct contact with the air, (2) oxidation of metal within the pool by air entrained with the stream, (3) entrapment of nonmetallics, particularly oxide material from the pool surface, within the solidifying metal and (4) lack of control of flow patterns within the molten pool.

Based on the fact that the mass of oxygen available for reoxidation is only a function of the partial pressure of the oxygen in the surrounding gas,[59] inert gas (argon) was introduced to minimize the partial pressure of oxygen in the surrounding atmosphere.[66,67] Measuring the average oxygen, it was found that clean steel inert gas shrouding system (Figure 2.24) is effective on preventing reoxidation caused by pouring

liquid steel through air.[66,67] McPherson[68] measured nitrogen pick-up, as the extent of reoxidation between ladle and tundish, and found that reoxidation using physical (refractory) shrouds was higher than with inert gas shroud (argon), because of the difficulty in achieving a tight seal between the ladle nozzle and the inner neck of the physical shroud. He also found, however, that using the physical shroud and argon ring system (Figure 2.25) found to be the most effective way, among several systems he tried, to prevent reoxidation.

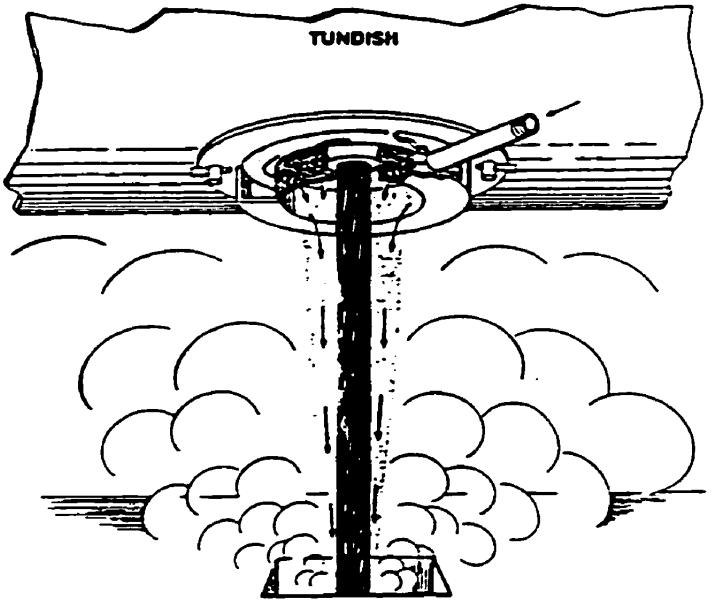

Fig. 2.24 Clean cast shrouding system[66]

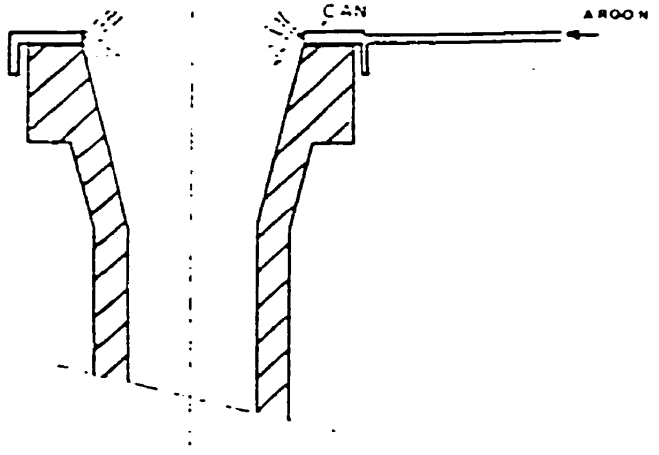

Fig. 2.25. Refractory shroud system[68]

The shrouding of the ladle stream found to be effective on reducing inclusion line severity and frequency in stainless flat rolled product[69,70] and surface quality of cold rolled steel product,[71,72] as well as preventing reoxidation.[66,67] Demasi and Hartmann[71] also observed that temperature loss from ladle to tundish reduced by as much as 10 to 15F by means of ladle shroud.

Since the height of the exposed section of ladle shroud is usually 0.8 to 1.2 meters above tundish-bath level, the static pressure at the shroud/collector-nozzle joint approaches a vacuum, as required by Bernoulli's equation for conservation of potential, kinetic and pressure energy. L. Wang *et al.*[73] studied about pressure distribution in ladle shroud applying water modeling and numerical simulation and concluded that sub-atmospheric pressures generated in the slide gate and shroud nozzle can lead to the ingress of a large quantity of air into the liquid during ladle teeming. M. Schmidt *et al.*[74] developed an "argon bayonet" design (Figure 2.26) for shielding joint between ladle to collector nozzle and ladle shroud to meet requirements: (1) Argon must be supplied to the shield in such a way that surrounding air cannot be entrained, (2) The argon supply to the shield must be sufficient to satisfy the maximum demand from a leak and (3) Argon gas must not be forced into the bore through overpressure.

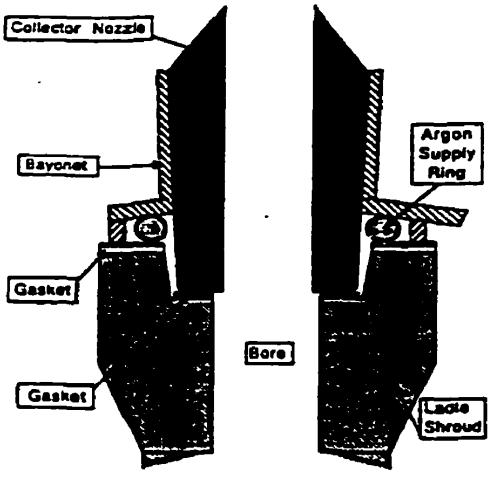

Fig. 2.26 Argon bayonet device for shielding joint between ladle collector nozzle and ladle shroud; Schmidt *et al.*[74]

CHAPTER
3

EXPERIMENTAL APPARATUS AND PROCEDURE

3.1 INTRODUCTION

As the title indicates, the experimental apparatus and the experimental procedures used in the present study are described in this chapter. There are three different subjects, *i.e.* (1) Slag Entrainment in Late Rotating Vortices, (2) Detection of early stage of Slag Entrainment applying AMEPA system and (3) Shroud Gas/Steel Flow Interactions. Various components of the experimental set-up for those three different subjects are discussed. Explanations for (1) ladle and nozzle fabrication, (2) ruler for determining radial position of surface marker and (3) inflow set-up will be given in experimental apparatus. The experimental procedures presented include those for three subjects along with the decay of tangential velocity distributions in the ladle.

3.2 EXPERIMENTAL APPARATUS

3.2.1 Ladle and Nozzle Fabrication

The ladle for the experiment of Detection of early stage of Slag Entrainment applying AMEPA system was made using a transparent sheet of Polycarbonate. The tubular section of the ladle was built by rolling up a rectangular sheet, of required dimensions, into a cylinder and joining together the two edges. The joint was either a continuous seam of glue, or a lap joint with a backing strip of Plexiglas and two rows of

bolts and nuts. A lap joint comprising a reinforcing strip of Plexiglas® on the outside, and two rows of bolts and nuts, was used in the fabrication of the 495-mm diameter ladle; 3.2-mm thick Polycarbonate sheets were used, and the ladle measured 620 mm in height.

Three rectangular sheets of 3.2 mm thick Polycarbonate, lap jointed together as before, were used to fabricate the 1160 mm ladle for the experiment of Slag Entrainment in Late Rotating Vortices. The height was 1500 mm.

The next step of the fabrication of the ladles for experiments was to cut a circular bottom plate to fit snugly within the rolled-up cylindrical tube, and glue it in place. The bottom plate of the ladle was made out of 6.4-mm thick sheet of Plexiglas®. The 1160-mm ladle was placed within an existing, square cross-sectioned, steel tank with a Plexiglas front-wall, and so was provided with a false bottom constructed from 38 × 89 mm and 19 mm thick plywood sheets.

By virtue of the circular shape of the bottom plate, the lower portion of the ladle was thus perfectly round. However, the upper portions of the ladle tended to become somewhat distorted. Thus the ladle, made from 3.2-mm thick walls, needed additional reinforcement in the form of a circular, spring-steel collar placed on their top rims. As for the 1160 mm, which was also made with the 3.2 mm thick walls, a sufficiently large collar could not be fabricated, and the ladle diameter was large enough to retain a reasonably well-rounded cross-section throughout.

Holes were then drilled in the bottom plates of the ladles, so that the nozzle holding adapters could be installed. The 1160-mm diameter ladles were also fitted with an additional, off-central nozzle holding adapter at roughly 2/3 radius. The axis of the off-central nozzle holding adapter was situated 402 mm away from the central axis (*i.e.*, eccentricity = 0.7). The ladle was fitted with a nozzle holding adapter on the central axis. A sketch of the nozzle assembly and the nozzle holding adapter on the floor of the ladle for the 1160-mm diameter ladle is shown in Figure 3.2. The nozzle was made from transparent Plexiglas.

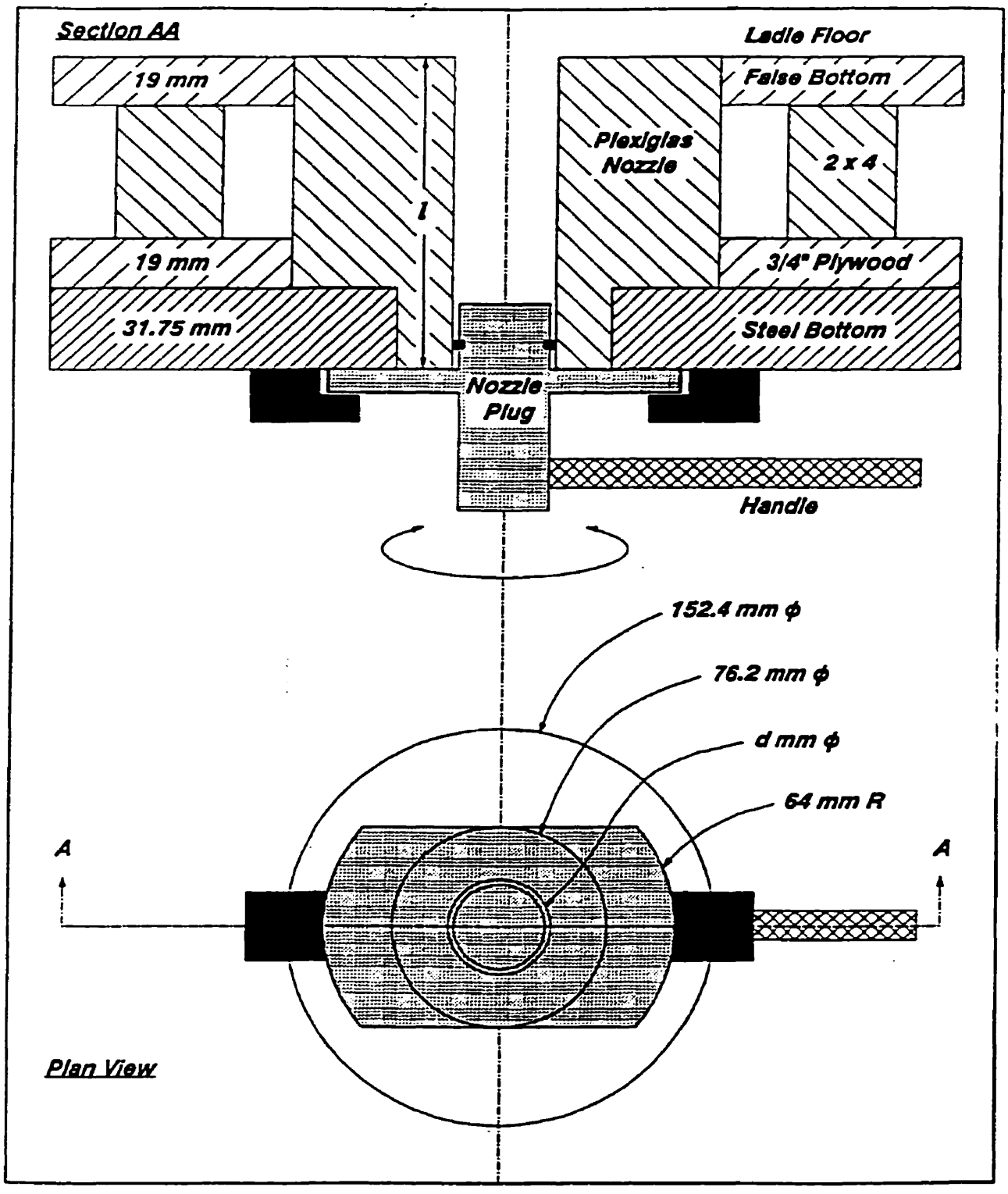

Fig. 3.1 A sketch of the nozzle, nozzle holding adaptor, and nozzle plug used in the 1160-mm diameter ladle[2]

For the experiment of Shroud Gas/Steel Flow Interactions, a 0.75 scale of shroud was fabricated. Two Polycarbonate pipes were connected to each other; the inner diameter of each Polycarbonate pipe was 53 mm and the length of each pipe was 600 mm so that the total length is 1200 mm. A PVC (Polyvinyl chloride) was attached around the top and bottom of the lower pipe and a PVC was attached around the bottom of the upper pipe so that these two pipes could be connected with each other using bolts and nuts. Using an O-ring between the PVC at the bottom of the upper pipe and the PVC at the top of the lower pipe, it was possible to prevent any air leaks through the joint.

A hole whose diameter was 4 mm was drilled in the upper part of the shroud with an angle of 46°, so as to render the length between the bottom of the shroud and the hole to 1150 mm. Then a transparent Plexiglas pipe of which inner diameter was same as that of hole was attached at the point of the hole with an angle of 46°, thereby rendering the angle of gas injection to 46°. A figure will be given in experimental procedure part.

One wished to simulate a typical liquid metal flowrate of about 4.0 tons per minute through an 80-mm diameter shroud, which corresponds to a linear velocity through the shroud of about 2 m/s. However, the maximum flowrate of water available in the laboratory was 265 liters per minute. In order to maintain an equivalent downflow velocity, the maximum diameter of tube was 53-mm instead of 80-mm, although the length of shroud nozzle used was typical of a full-scale system (1150-mm). The angle of gas injection was chosen as $\theta = 46°$ so as to correspond to the angle of gas entry that might be expected from any air leaks between the collector nozzle and the shroud.

The upper part of this shroud was connected to the water-flow meter that monitored water flow rate, then to a pressure gauge that monitored the absolute pressure and finally to a tap that controlled water flow. In order to monitor the air flowrate, a set of airflow meter was connected to a mercury manometer that was connected to the gas injection port and used to register the gas pressure at which air flowed into the ladle shroud.

3.2.2 Ruler for Determining Radial Position of Surface Markers.

The residual tangential velocity distribution in the ladle was deduced from the motion of Styrofoam markers on the surface of the water. Consider, for example, the case of a marker rotating around the axis of the ladle. If the radial position of a marker was known, its tangential velocity could be calculated from the time taken to traverse a known distance, say one-half or one-quarter of a circle. The time t corresponding to each such measurement was taken as the time at which the marker was mid-way through the arc under consideration, and all time was measured with reference to the end of filling as $t = 0$. Figure 3.2 shows the ruler devised to measure the radial position of markers. As seen, increasing radial distance was marked either side of a zero mark, which in turn was perfectly aligned with the central axis of the ladle. This radial position-measuring ruler was mounted on a Plexiglas strip and lowered to within 5 to 10 mm of the liquid surface in order to minimize parallax errors.

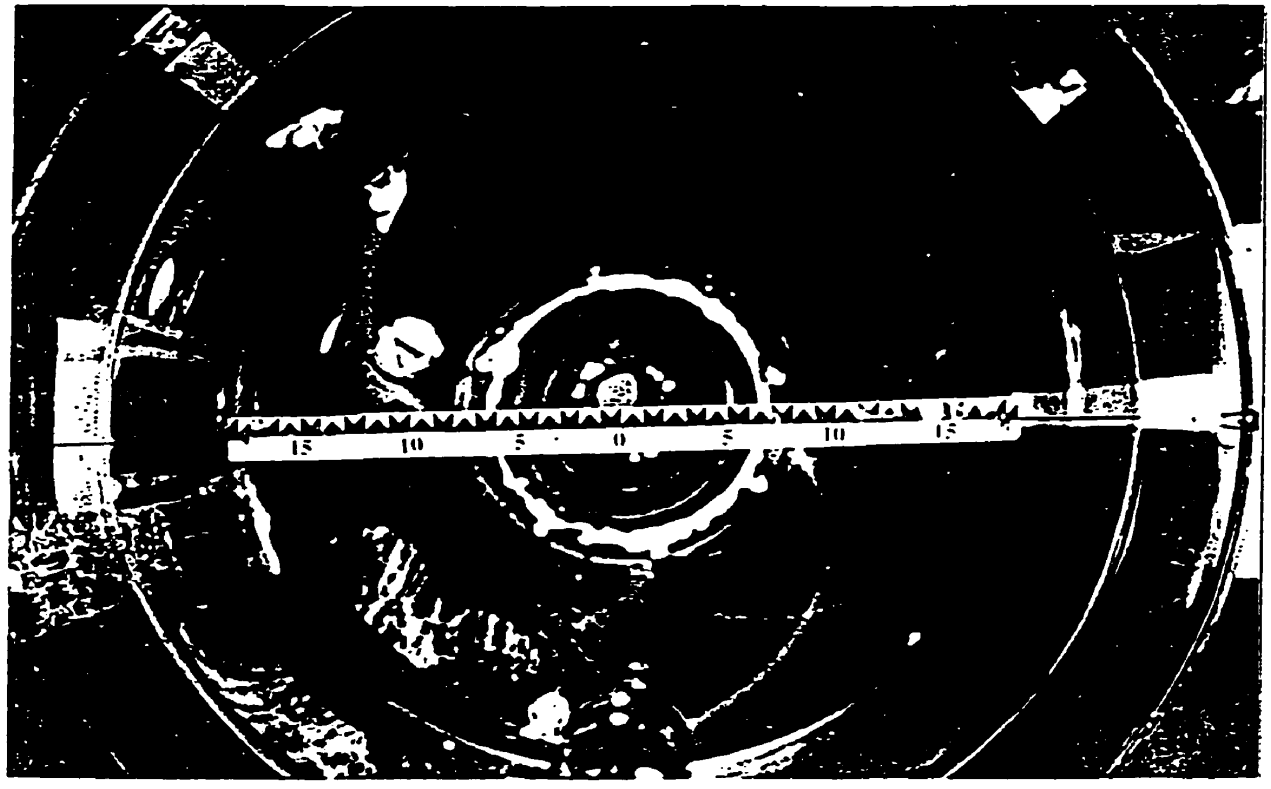

Fig. 3.2 Ruler to monitor the radial position of markers in the 495-mm ladle; Sankaranarayanan[2]

A cross-shaped ruler, with radial markings on two mutually perpendicular diameters, was used in the 1160-mm diameter ladle. Since the radial location of a marker could thus be measured four times during each of its revolutions around the ladle axis, the cross-shaped ruler was more suitable for the larger ladle than a ruler with markers on one diameter only.

3.2.3 Inflow Set-Up

The arrangement used to fill the ladles with water was probably the most critical component of the experimental vessel. A unique water inflow set-up was used that was capable of inducing tangential velocities that were nearly constant throughout the ladle, irrespective of the radial or axial location.

A copper tubing, of external diameter 13 mm was used to make the inflow tube. The tube was bent at an angle of 30° at a point 100-mm from the exit. The bent tube was clamped to the ladle wall so that the axis of its straight section was parallel to the ladle wall. The axis of the straight-section of the inlet tube was 90 mm closer to the central axis of the ladle than the ladle wall itself. The exit of the inlet tube was 460 mm above the bottom of the ladle.

Once installed in the ladle, the inlet tube was rotated 45° in the counter-clockwise direction about the vertical axis of its straight section, thereby imparting a clockwise directional motion to the water as it filled the ladle. Thus, the water jet issuing out of the filling inlet tube entered the ladle at an angle, and impinged upon the ladle wall at a point which was ahead of, and to the left of, the inlet tube's tip. The water would then follow the curvature of the ladle wall, and thus take on a clockwise sense of rotation. As the water level in the ladle increased above the initial jet impact point on the ladle wall, the radial and angular position of the jet impact point would shift.

As mentioned earlier, the residual tangential velocity distribution produced by this inflow arrangement was more or less independent of the axial, radial and azimuthal coordinates, *i.e.*,

$$V_{\theta,t} \neq f(r,z,\theta) \approx \text{Constant} \tag{3.1}$$

where $V_{\theta,t}$ denotes the residual tangential velocity at holding time t. The decay in the tangential velocity was of the following general form,

$$V_{\theta,t} = C_\theta t^{-n} \tag{3.2}$$

where C_θ and n were constants. The value of n was approximately equal to *one*. The magnitude of the tangential velocity at the end of filling (*i*.e., $t = 0$) was dependent on (1) the angle of entry of the inflow jet, (2) the relative position of the initial jet impact in the ladle, (3) the dimensions of the ladle, (4) the flow rate of filling, and (5) the level to which the ladle was filled. For each combination of the above parameters, the tangential velocity distribution, and its decay with increasing holding time, was determined as per the procedures.

A brief discussion of the reasons for choosing this filling arrangement is in order. First of all, this inflow arrangement is an exaggerated version of the BOF converter tapping stream, which when entering the ladle is neither perfectly vertical, nor perfectly aligned with the central axis of the ladle.

Secondly, the present filling arrangement permitted the deployment of a unique dimensionless tangential velocity number without having to resort to similarity with a potential vortex. While the tangential velocity distributions yielded by the present filling arrangement as well as the idealized tangential inlet arrangements used by several earlier workers can both be uniquely defined by a single value of initial tangential velocity, the present filling arrangement is less restrictive, and thus, more practical. Furthermore, the

present filling arrangement has the potential to yield some insights into the existence, or lack thereof, of a critical tangential velocity associated with the initiation of vortexing funnel formation.

Thirdly, purely radial and purely axial inlets cannot, in theory, produce any rotational motion. Since tangential velocities produced adventitiously by such inlets tended to be relatively weak, their usefulness to the fundamental objectives of the present study was limited.

3.3 EXPERIMENTAL PROCEDURES

3.3.1 Residual Tangential Velocity Distribution in the Ladle

The following was the step-wise experimental procedure adopted to determine the residual tangential velocity distribution in the ladle.

(1) Set up the experimental vessel.
(2) Install the radial position-measuring ruler in the ladle.
(3) Set up the video camera above the ladle.
(4) Switch the lighting fixtures on.
(5) Prepare about five Styrofoam markers (say, labeled A and B) and keep them handy.
(6) Start the video camera recording.
(7) Open the nozzle of the inflow set-up – continue filling the ladle until the desired initial depth was reached, and close the nozzle.
(8) As soon as the filling was completed, gently place two or three markers on the water surface, well separated from one another in terms of radial and azimuthal locations. In case of 1160-mm ladle, a small vertical tube was used to drop pieces of Styrofoam markers onto the surface of the filled, and rotating, body of water within the 1160-mm diameter ladle. Its time of transit between radially displaced lines corresponding to an angle of 63° at radial distances of 42-50 cm was measured for

each situation, so as to be sure that the same initial starting conditions were set up, prior to emptying the ladle through one of the two exit nozzles.

(9) Monitor the motion of the markers as a function of holding time. Thus, the radial and azimuthal positions of each marker, at all instants of time, became known. The markers did not always go around in exact circles; elliptical paths were not uncommon, probably due to the filling-induced eddies they not having been perfectly symmetrical about the ladle axis. Needless to say some disturbances were introduced by such relocation of markers, but as long as the disturbances were kept to a minimum, their effects on the overall flow patterns were negligible.

(10) Continue monitoring the markers, and the camera, *etc.*, until the rotational motion becomes almost imperceptible.

(11) Stop videotaping after all rotational motion had died down.

(12) Play back the videotape and note down the stopwatch time and the radial and azimuthal location of each marker as it crossed one of the leading edges of the radial position-measuring ruler. The distance traveled in a known time interval could be determined from successive readings of radial position, and angular position of a marker. Thus, it was possible to calculate an average value of tangential velocity for the time interval under consideration, which could then be assigned as the tangential velocity at the median time.

(13) Plot all the tangential velocity data (for all markers, for all radial positions, and all times) in one graph. Use regression analysis to establish the relationship between V_θ and the holding time.

3.3.2 Slag Entrainment in Late Rotating Vortices

The onset of a 'late' rotating vortex over an off-center drain nozzle at 2/3 radius was studied in an 1160-mm diameter tank. The critical height of water at which this late rotating vortex set in for a flat ladle bottom, was compared with the critical height of water for air (slag) entrainment with a bottom ladle surface, sloped at 3.5°. Identical starting conditions were used for the two conditions. Figure 3.6 provides an isometric drawing of the techniques used to study the onset of late rotating slag-entraining vortexes.

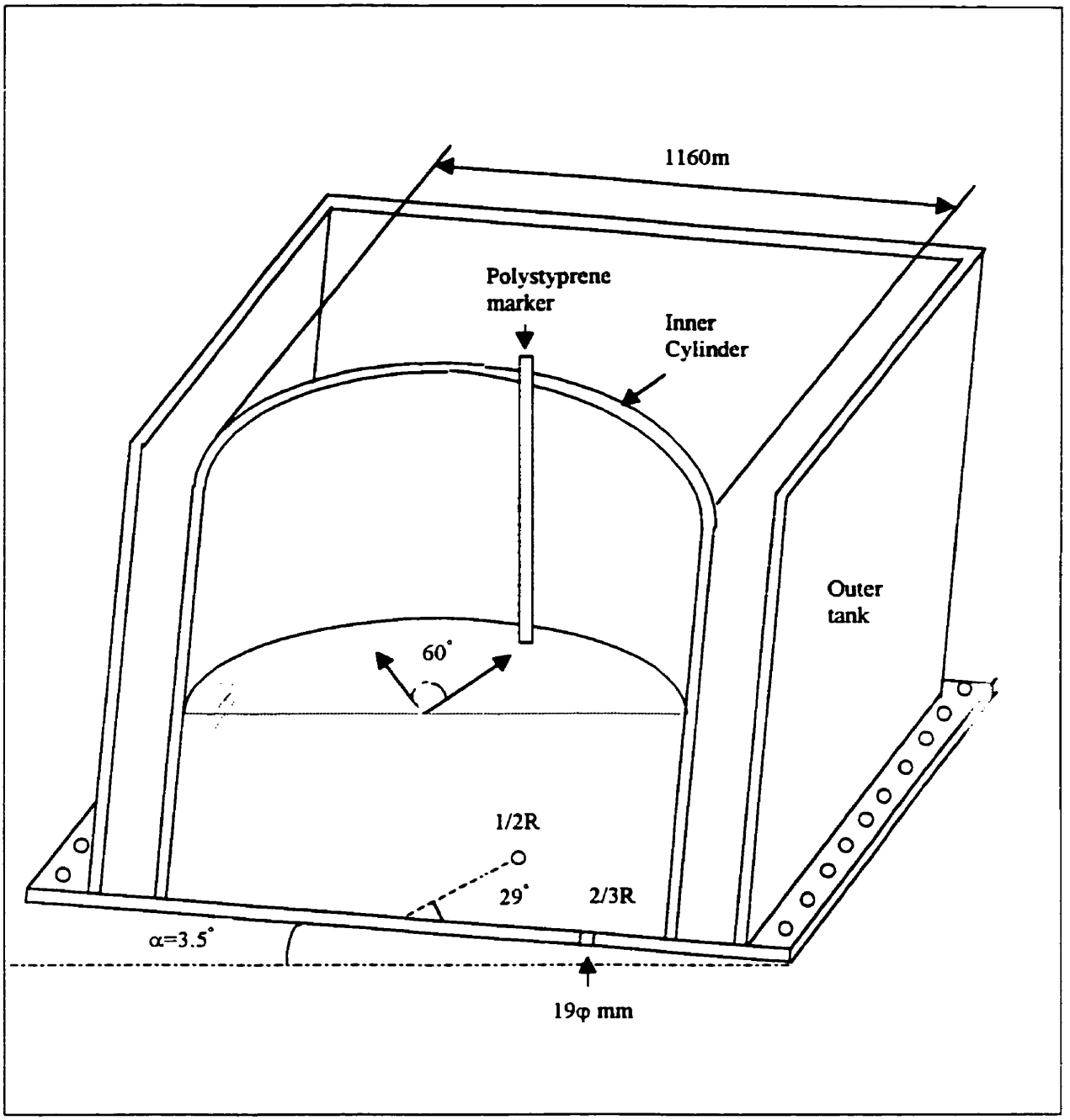

Fig. 3.3 Equipment used to study late rotating vortex formation

The following was the step-wise experimental procedure for the experiment of slag entrainment in late rotating vortices.

(1) Set up the experimental vessel – install the "centric ($\theta = 0^{\circ}$)" nozzle at 2/3R, and an off-set ($\theta = 29^{\circ}$) at 1/2R.
(2) Switch the lights on and ensure that the necessary background screens and reflectors were in place, and verify lighting conditions with a light meter.
(3) Prepare the cameras for shooting.
(4) Fill the ladle to the desired initial depth – open the water inflow (simultaneously starting the hand-held stopwatch), bring the level to required value. Note down the stopwatch time at the moment the inflow was closed completely.
(5) Do not start emptying the ladle until the chosen holding time had elapsed.
(6) Start the video camera recording.
(7) Start drainage by unplugging the nozzle and start visual observation.
(8) Note down the time at which the ladle became empty
(9) Review the videotape, and note down critical height of the vortexing funnel and set times.
(10) Repeat from (1) to (9) several times to make an average value of data.
(11) Tilt the ladle at an angle of 3.5° in order to simulate the effect of a sloped bottom, and its ability to improve steel yield prior to the establishment of a late rotating, slag-entraining, vortex.
(12) Repeat from (1) to (9) several times to get data for sloped bottomed ladle.

3.3.3 Detection of Early Stage of Slag Entrainment applying AMEPA System

As mentioned earlier in the Introduction, the purpose of the present work was to determine how the rotational core of a slag-entraining vortex could be displaced off the central vertical axis of the nozzle in a simple practicable way, so as to render the AMEPA system sensitive to early slag entrainment phenomena.

In order to divert the vortex funnel away from the central axis of the 45-mm diameter nozzle centrally placed in a 495-mm diameter cylindrical ladle, two methods were investigated.

The first concept involved putting a thin plate over a nozzle entrance, so as to partially block the nozzle's aperture, thereby creating a region of under pressure behind the nozzle plate (Figure 3.4). Due to the pressure difference across the cross section area of the shroud nozzle, lower pressure behind the plate and higher pressure in the opposite side of the shroud nozzle, it was probably possible to divert the vortex funnel to the lower pressure region of the shroud nozzle. The plate covered firstly 50% (i.e. a semi-circular area) of the nozzle, this coverage percentage was chosen arbitrary. Then 80% of the nozzle entrance was covered by blocking 3/4 of the nozzle with a thin square plate, hoping to divert the tip of the vortex funnel more abruptly to the nozzle's sidewall behind the plate.

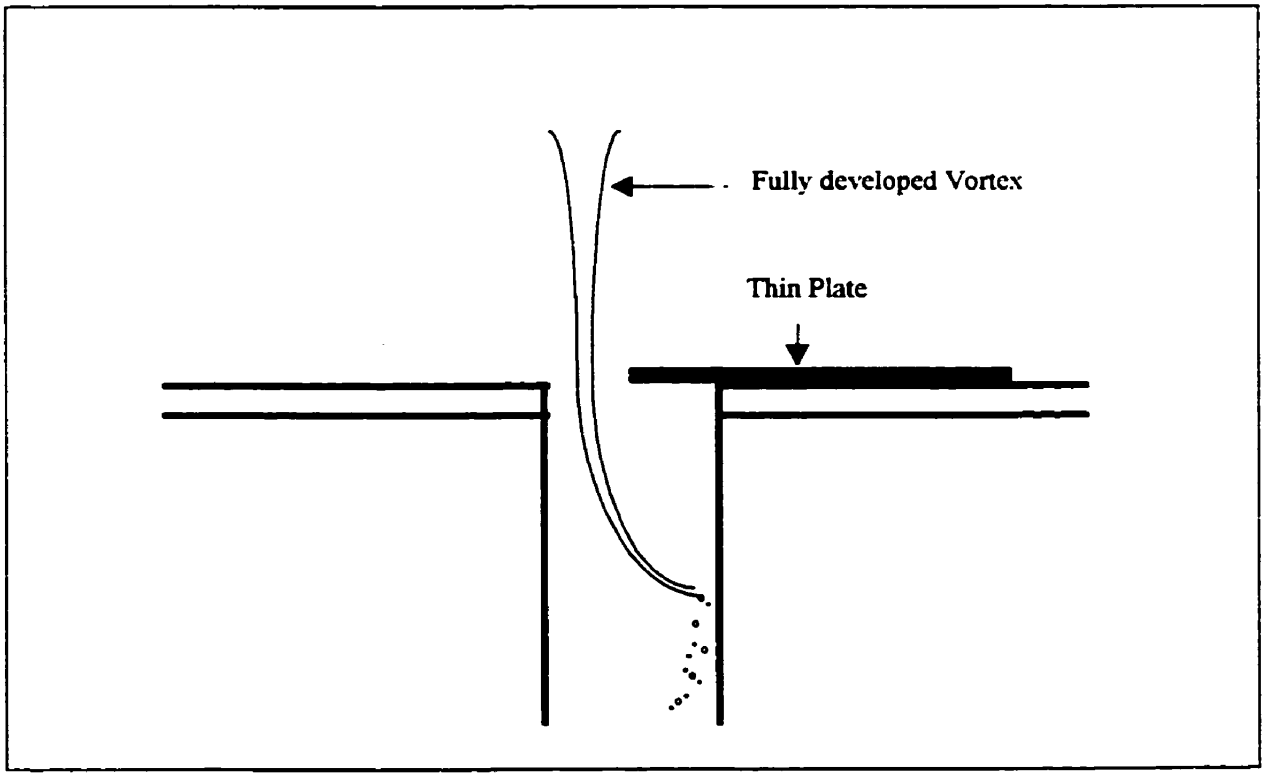

Fig. 3.4 Experimental apparatus of the first method

The thickness of the Plexiglas® can effect the velocity component of the liquid metal in the ladle, especially the tangential velocity component. This is discussed in detail in Chapter 4, along with other experimental observations from the present study. For the present work, it was decided not to disturb the velocity components as possible, and any other experimental parameters. In order to minimize this effect of the thickness of Plexiglas® on the tangential velocity of the liquid metal, the thickness of Plexiglas® should be thin enough.

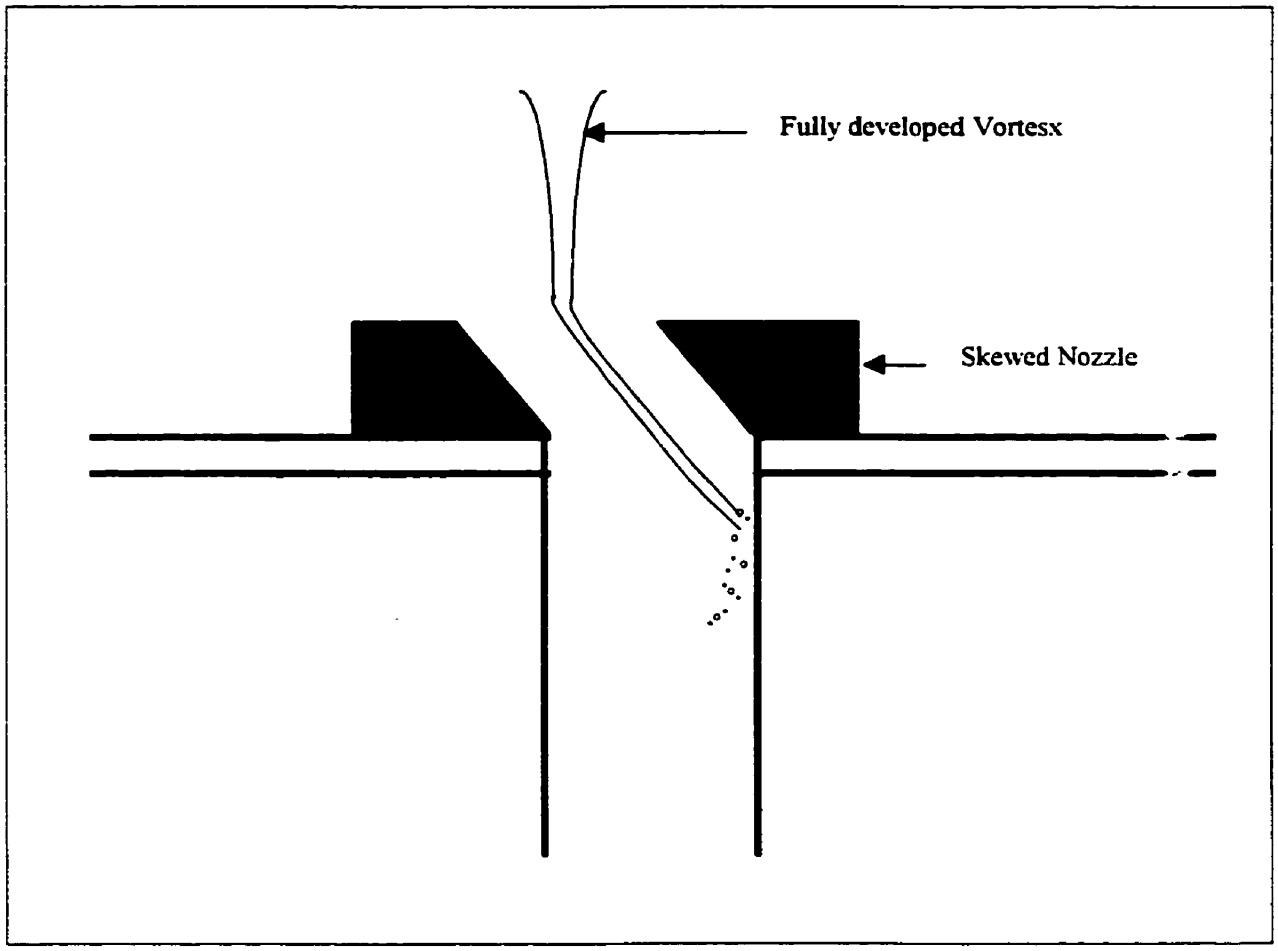

Fig. 3.5 Experimental apparatus for the second method (skewed nozzle)

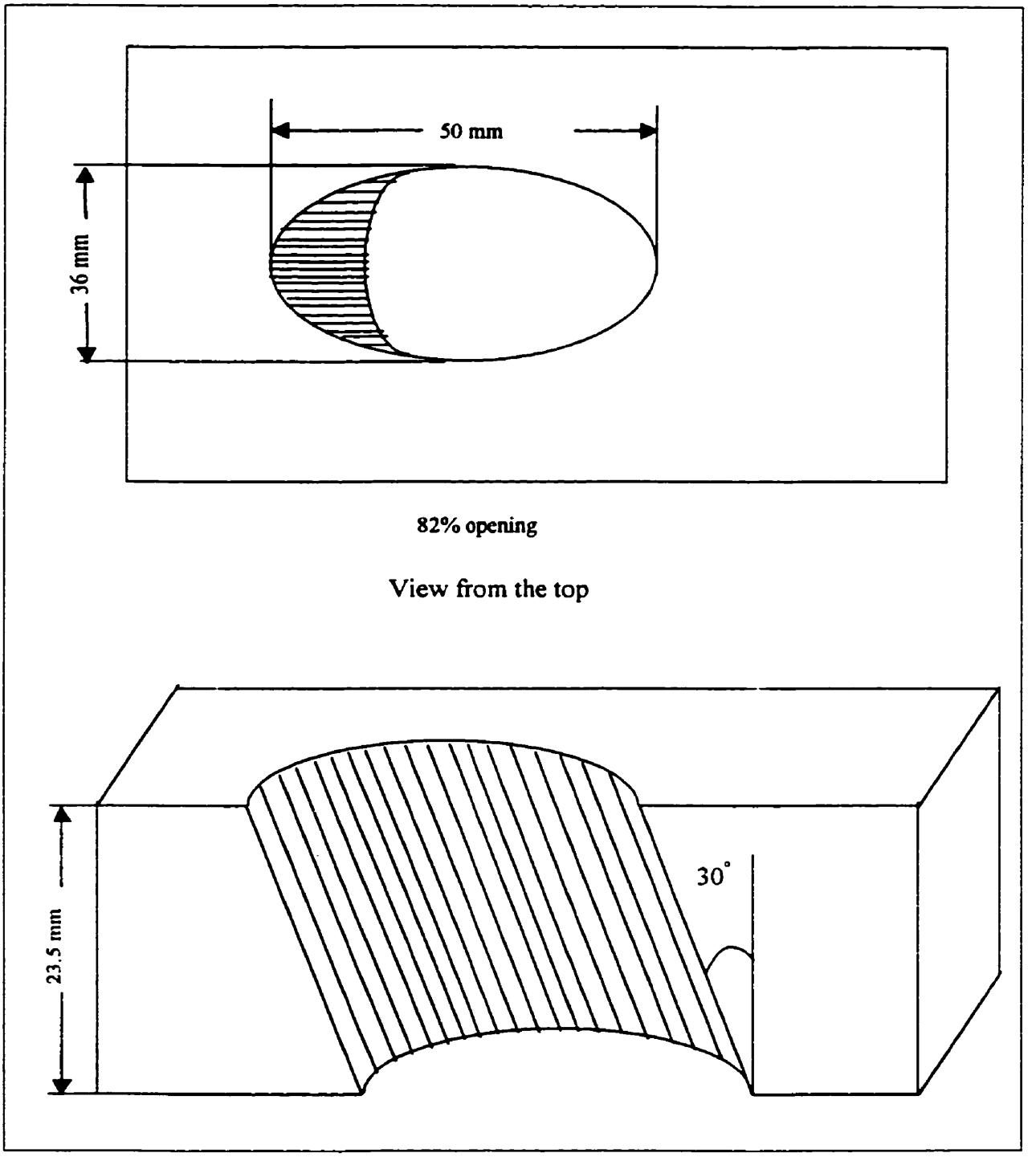

Fig. 3.6 A sketch of the skewed nozzle

The scale model water ladle was filled to an initial height of 430mm, with a kerosene (slag) layer 20mm thick on top. It should be noted that if the supernatant fluid was air, the core of the vortex funnel expanded abruptly as it entered the drainage nozzle, which happened whether or not the shroud nozzle is submerged in the water. But if the supernatant fluid was oil, this didn't happen, which is true in real system. Such outflow stream behavior has not been dealt with adequately in the published literature. It might be a function of the viscosity of the supernatant fluid and the pressure distribution.

It is a known fact that the critical height is inversely proportional to the size of the nozzle. So, the first method could result in a higher critical height than that without any treatment, which means lower yield of the liquid metal. Moreover, the flowrate of the liquid metal would decrease as the opening percent of the nozzle decrease, which means lower productivity of the liquid metal. Thus these two parameters, *i.e.*, critical height and flowrate, were the main drawbacks of the first method.

In order to overcome these difficulties and objections, the second approach involved redesigning the nozzle so as to generate a radial velocity component in liquid metal as it flows into shroud nozzle without changing the flowrate of the liquid metal. Figure 3.5 shows the experimental apparatus for this approach. A thick plate of Plexiglas® (23.5mm thick) was drilled at an angle of 30° to the vertical, so as to have an aperture area equivalent to that of the 45-mm diameter nozzle on which it was placed. It was calculated that the opening was around 82%. From this, it could be said that flowrate of the liquid metal would be less about 18% of the original flowrate. In this case, the re-designed nozzle could effect discharge coefficient in a bad manner. Figure 3.6 shows the re-designed nozzle for this experiment of the detection of the early stage of the slag entrainment. The thickness of the redesigned nozzle and the angle to the vertical were chosen arbitrary for the present work. However, it can be said that the thickness of the Plexiglas® will probably effect on the tangential velocity of the liquid metal near the nozzle, which results in lower critical height in hope. And the angle is probably related to the strength of the radial velocity component, then the length of the sidewall of impingement below the nozzle plate.

The following is a typical sequence of actions during diverting the tip of the vortexing funnel experiment:

(1) Setup the experimental vessel.

(2) Fill the ladle to the desired initial depth. Quickly place the thin plate or redesigned nozzle (skewed nozzle) on the marked position on the ladle bottom. Quickly transfer the oil from the bucket. Note down the end of filling time. Make sure that initial depth did not differ by more than ± 10 mm from the nominal value.

(3) Follow the procedure from (5) to (10) in section 3.3.2.

3.3.4 Shroud Gas/Steel Flow Interactions

In order to study the range of flow phenomena associated with the introduction of gases into the collar of the ladle shroud fitting around the collector nozzle of the slide gate nozzles, measurements of gas hold-up as a function of entry gas flowrate and water flowrate were carried out. Table 3.1 shows the experimental conditions for the present work.

Table 3.1 Experimental conditions for shroud gas/steel reaction

	Tube #	FLMR	Q_{air} (milliliters/min)	Q_{water} (liters/min)
1	FM082-03ST	15	262	265
2	FM082-03ST	25	384	265
3	FM082-03ST	90	1105	265
4	FM082-03ST	150	1682	265
5	N044-40T	25	8680	265
6	N044-40T	45	17305	265
7	N044-40T	47.5	18367	265
8	N044-40T	65	25025	265

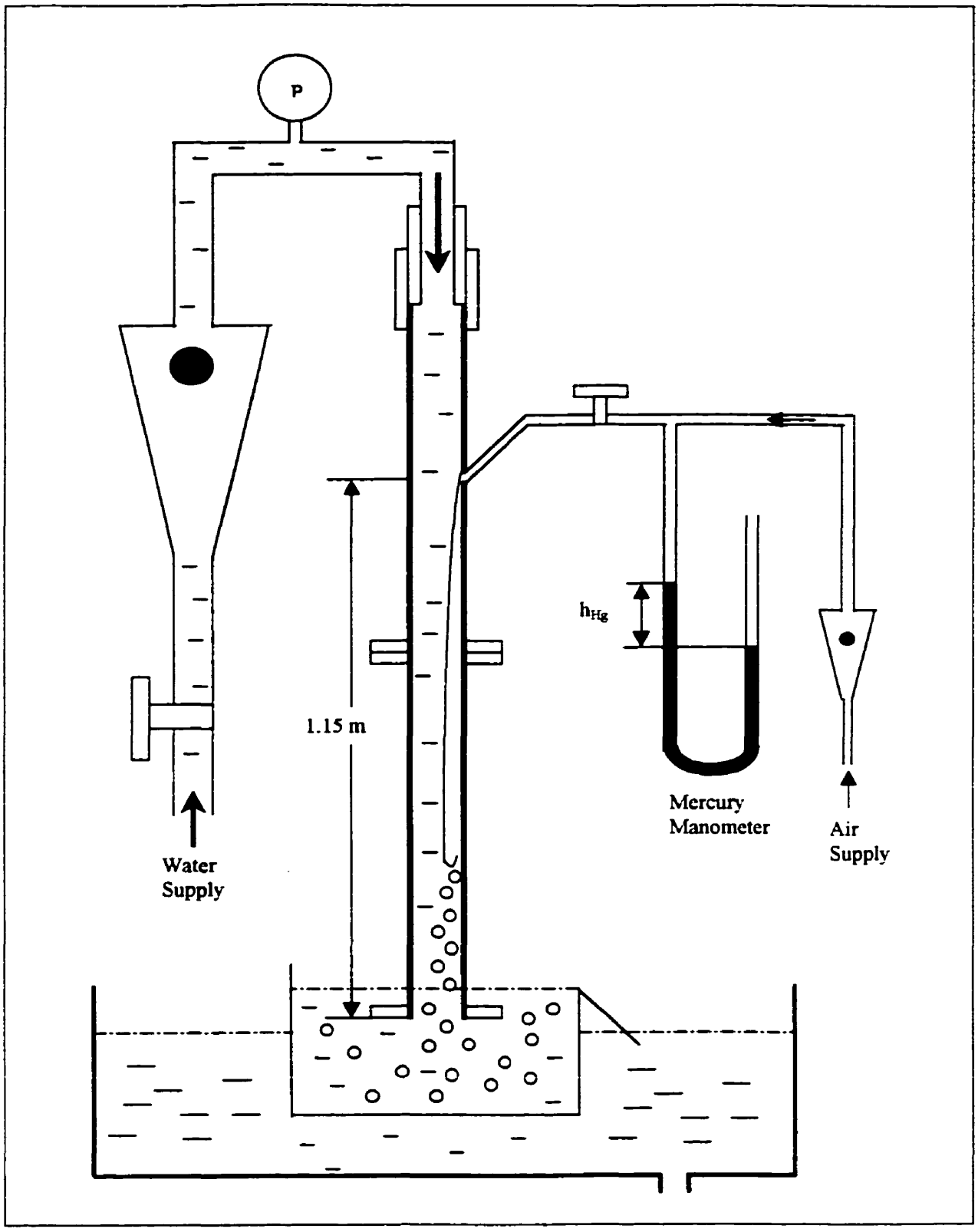

Fig. 3.7 Equipment used to study air infiltration into ladle shrouds

The condition of non-submerged nozzle was also compared to the submerged nozzle. A 0.75 scale water model was constructed to simulate the flow of liquid steel through a ladle shroud (53-mm ID, 1.15 m long) in the presence of gas infiltration with an angle of 46°. (Figure 3. 7). FLMR in Table 3.1 means Flowmeter Reading.

The following is an experimental procedure for the experiment of the shroud gas/steel interaction phenomena.

(1) Prepare the video camera for shooting.
(2) Open the water inflow with a chosen flowmeter reading.
(3) Note down the absolute pressure before introducing air into the shroud nozzle.
(4) Hit the record button on the video camera to start the videotaping at least five seconds before introducing air or helium into the shroud nozzle.
(5) Introduce air or helium into the shroud nozzle with a chosen flowrate.
(6) Note down the mercury manometer reading; to calibrate the exact air or helium flowrate.
(7) Measure the time-averaged length and width of gas hold up as a function of gas volume fraction.
(8) Terminate videotaping, and close the water inflow nozzle and air or helium nozzle.
(9) Prepare for the next experiment.

CHAPTER
4

EXPERIMENTAL OBSERVATIONS AND DISCUSSION

4.1 INTRODUCTION

In this chapter, several observations and data from the experiments are presented under the three subjects: Slag Entrainment in Late Rotating Vortices, Detection of Early Slag Vortexing Phenomena using AMEPA system and Shroud Gas/Steel Flow Interactions.

4.2 SLAG ENTRAINMENT IN LATE ROTATING VORTICES

4.2.1 Decay in the tangential velocity in 1160-mm ladle

The tangential velocity distributions in the ladle was determined according to the experimental procedures outlined in Section 3.2.1, from the motion of styrofoam markers on the water's free surface within the ladle. As mentioned earlier in chapter 2, the tangential velocity distribution was more or less constant across the entire surface (independent of radial position) and at all depths. The decay in the tangential velocity with holding time is shown in Figure 4.1, from which the appropriate time to begin draining, could be established. Data are plotted in Figure 4.1 along with a regression equation (Eq. (4.1)).

$$V_s = 47004 \cdot t^{-1.04} \qquad (4.1)$$

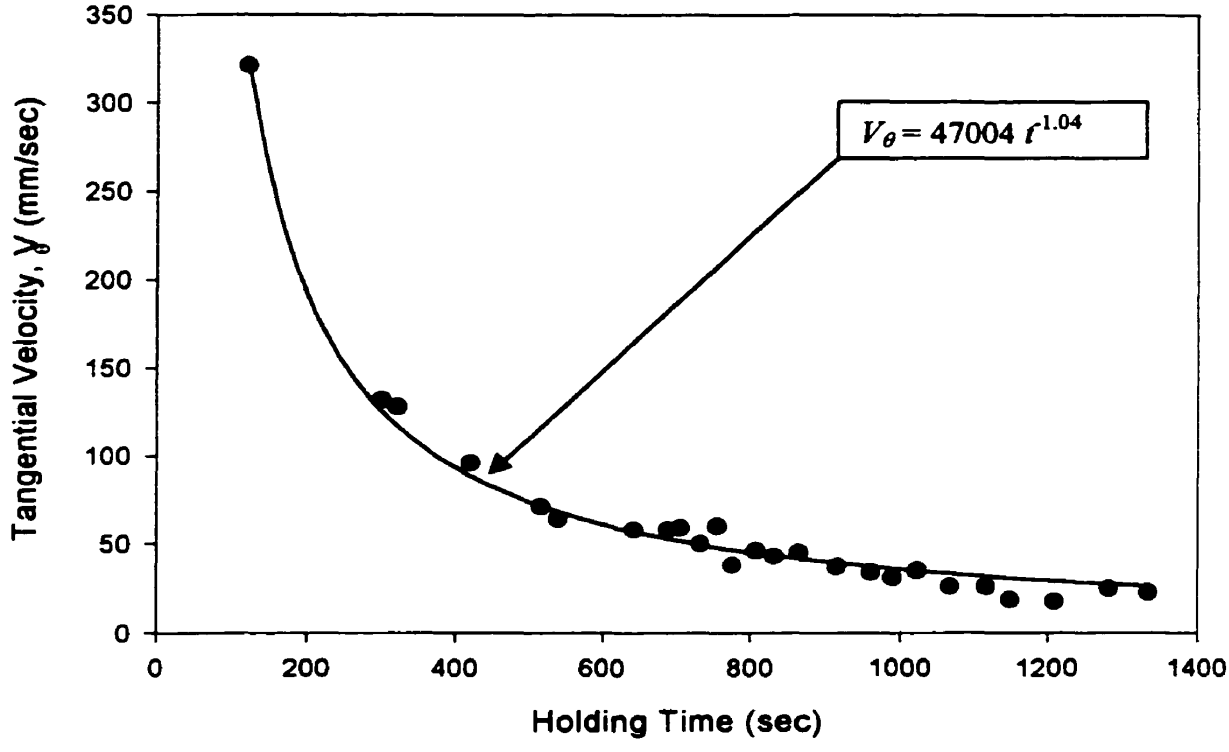

Fig. 4.1 Decay in the tangential velocity with holding time in the 1160-mm diameter ladle; Standard error of estimate = 6.6243

The paths taken by the markers were not entirely circular, particularly at shorter holding times when asymmetric eddies from the filling action were still in existence. The radial positions at the beginning and end of a known arc were used to calculate the average radial position of the marker, from which the distance traveled in a known time and the tangential velocity were determined. When the eccentricity of the loop, with respect to the central axis of the ladle, was high the distance traveled by the marker was sometimes underestimated, leading to an underestimation of the tangential velocity. All experiments began with an initial filled height of about 50 cm $\pm$ 1 cm, the ladle being filled with an angled pipe so as to impart rotational flows. Table 4.1 shows data from present work including residual water volume using Eq. (4.2).

$$V = \frac{\pi}{4} D^2 \cdot (H_{cr} / \cos\alpha - D\tan\alpha) + \frac{\pi}{8}\tan\alpha \cdot D^3 \qquad \textbf{(4.2)}$$

Table 4.1 Critical height data for late forming rotating vortexes

Slope (degree)	Nozzle	Location	Initial Tang'tl Velocity (m/sec)	Drain time (sec)	H_{init} (m)	H_{cr} (m)	Residual Volume (liters)
3.5	Offset	1/2R	0.0240	666	0.51	0.115	84
3.5	Offset	1/2R	0.0240	666	0.51	0.115	84
3.5	Offset	1/2R	0.0240	666	0.51	0.115	84
3.5	Centric	2/3R	0.0275	770	0.50	0.078	45
3.5	Centric	2/3R	0.0266	778	0.50	0.078	45
0	Centric	2/3R	0.0272	740	0.49	0.080	47
0	Centric	2/3R	0.0266	736	0.49	0.080	47
0	Offset	1/2R	0.0265	783	0.49	0.070	37
0	Offset	1/2R	0.0264	793	0.50	0.065	31

4.2.2 Change of the Critical Height

As seen from Table 4.1, initial tangential velocities at r = 40 cm corresponding to 2.6 $\pm$0.1 cm/s, were chosen for the four emptying situations modeled. Two sets corresponded to the ladle being tilted at an angle of 3.5°, in order to simulate the effect of a sloped bottom. The other two sets corresponded to situations, in which the ladle was flat, and the same "centric" nozzle at 2/3R, and an off-set (θ = 29°) at 1/2R, were used to compare the critical heights of water at which a late, slag-entraining, rotating vortex set in. All tests were carried out with a sharp-edged nozzle of 19-mm diameter. Typically, the nozzles were positioned at about 2/3-radius of the ladle.

As seen from Table 4.1, H_{cr} for the off-central nozzle was only slightly lower than the H_{cr} for central nozzles in the 1160-mm diameter ladle in case of flat bottom system. The axis of rotation that was initially aligned with the central axis of the ladle was found to move towards the axis of the eccentrically positioned nozzle, and as soon as the axis of

rotation approached the vicinity of the nozzle axis, the vortexing funnel was formed. Very often, a dimple was initiated away from the nozzle axis, and the growing tail of the vortexing funnel "bent in" towards the drainage nozzle; shortly after the onset of air entrainment, the vortexing funnel quickly aligned itself along the nozzle's axis. The worst situation corresponded to an off-set nozzle at r = 0.5 R, for a sloping surface in which air (slag) was entrained once the liquid level had dropped to 11.5 cm above the drain nozzle. However, for the nozzle at r = 2/3R and θ = 0°, and sloped ladle bottom, the late rotating vortex took more time to center in around the nozzle (~ 100 seconds longer), by which time the height of water above the nozzle had dropped to about 8 cm. This proved to be equivalent to the critical height above the same nozzle when the ladle bottom was flat. The result shows that in this case more steel can be drained from the nozzle with a sloping bottom surface.

A similar result was observed for the flat, off-set nozzle, located at r = 0.5 R, which suggested that a critical height of about 7 cm could be achieved before slag entrainment would be expected. The present data shows that a late rotating vortex produced by weak rotational flow velocities in the order of 2 cm/s can be established at critical heights as high as 11.5 cm for a sloped bottom fitted with an offset nozzle at half radius. This rotating vortex strengthens and would entrain increasing amounts of slag that would be entrained in a central core of slag surrounded by a rotating annular column of liquid steel. As the two-phase flow passed through the collector nozzle, the rapid acceleration of liquid oil (slag) into the nozzle elongates the entrained oil (slag) into a thin jet or thread. This thread of oil (slag), presumably as a result of Rayleigh instabilities, then breaks down into a fine dispersion of oil (slag) droplets in water, as the flow passed into the tundish. The action of a slide gate nozzle would be to disturb the central, or axial, flow of slag and to disperse slag droplets across the width of the shroud nozzle. However, once a draining funnel is established, the proportion of slag entrained rises practically instantaneously (~ milliseconds), to become a significant volume fraction of the liquid. Again, a partially closed slide gate nozzle would disrupt the central core of slag surrounded by the annular jet of steel issuing from the collector nozzle.

4.3 DETECTION OF EARLY SLAG VORTEXING PHENOMENA USING AMEPA SYSTEM

4.3.1 Decay in the Tangential Velocity in 495-mm ladle

The decay in the tangential velocity with holding time in the 495-mm ladle is shown in Figure 4.2 along with regression equation (Eq. (4.3)).

$$V_\theta = 33211 \cdot t^{-1.145} \tag{4.3}$$

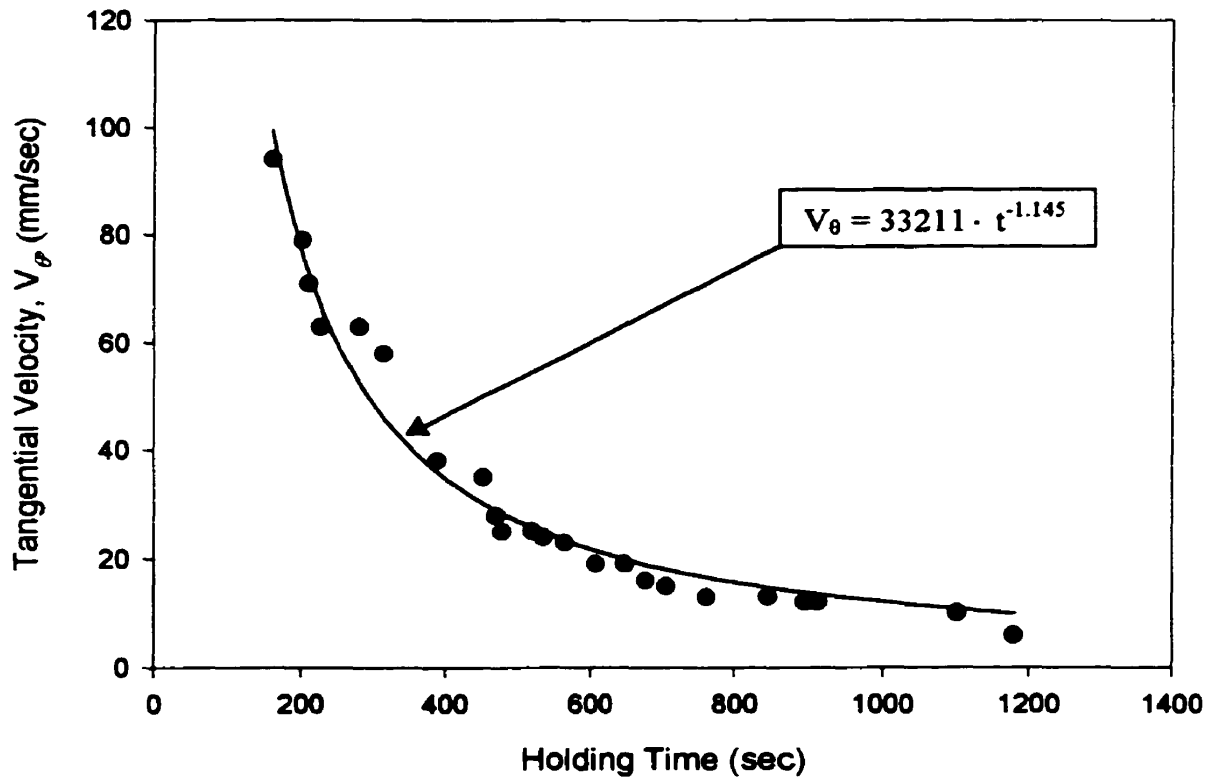

Fig. 4.2 Decay in the tangential velocity with holding time in the 495-mm ladle; Standard error of estimate = 4.4535

In experiments where there was a layer of oil atop the water, it was not possible to measure the decay in the tangential velocity within the water due to the difficulty in placing markers at the water-oil interface. Typically, the oil was poured from a plastic bucket immediately after the end of filling. As a first approximation, it was assumed that the oil layer did not affect the tangential velocity distribution too much, and that the decay in the tangential velocity within the water layer was identical to that measured in the absence of oil. As the top surface of the canola oil (viscosity = 50 mPa s) showed considerable rotation, the oil layer probably had a retarding influence on the tangential velocity at the water-oil interface (and hence in the bulk of the water) at any given holding time. Since a greater propensity for the formation of a vortexing funnel was observed in the presence of an oil layer, compared with the case where the filling conditions and the holding time were identical but the oil layer was absent, the result of assuming that the oil layer had no effect on the tangential velocity distribution only led to an underestimation of the role of the oil layer on the H_{cr} *versus* $V_{\theta,i}$ behavior. Thus, it was a reasonable first approximation to neglect the role of the oil layer in the tangential velocity distribution in the ladle as a function of holding time.

As the residual tangential velocity in the ladle is usually 30-40 mm/sec, 7 minutes with which tangential velocity in the ladle was 35 mm/sec was chosen as an appropriate holding time according to Eq. (4.3).

4.3.2 Diversion of the Slag Entraining into the Shroud Nozzle

As mentioned earlier, the purpose of the present work was to divert the vortex funnel away from the central axis of the nozzle, so as to make it possible to detect slag entraining in the early stage of slag entrainment. Figure 4.3 shows the situation without any treatment. Figure 4.4 and 4.5 show the diversion of the vortex funnel away from the central axis of the nozzle when the thin plate covered the entrance of the nozzle by 50% and 20%, respectively. The observation using the redesigned nozzle was shown in Figure 4.6.

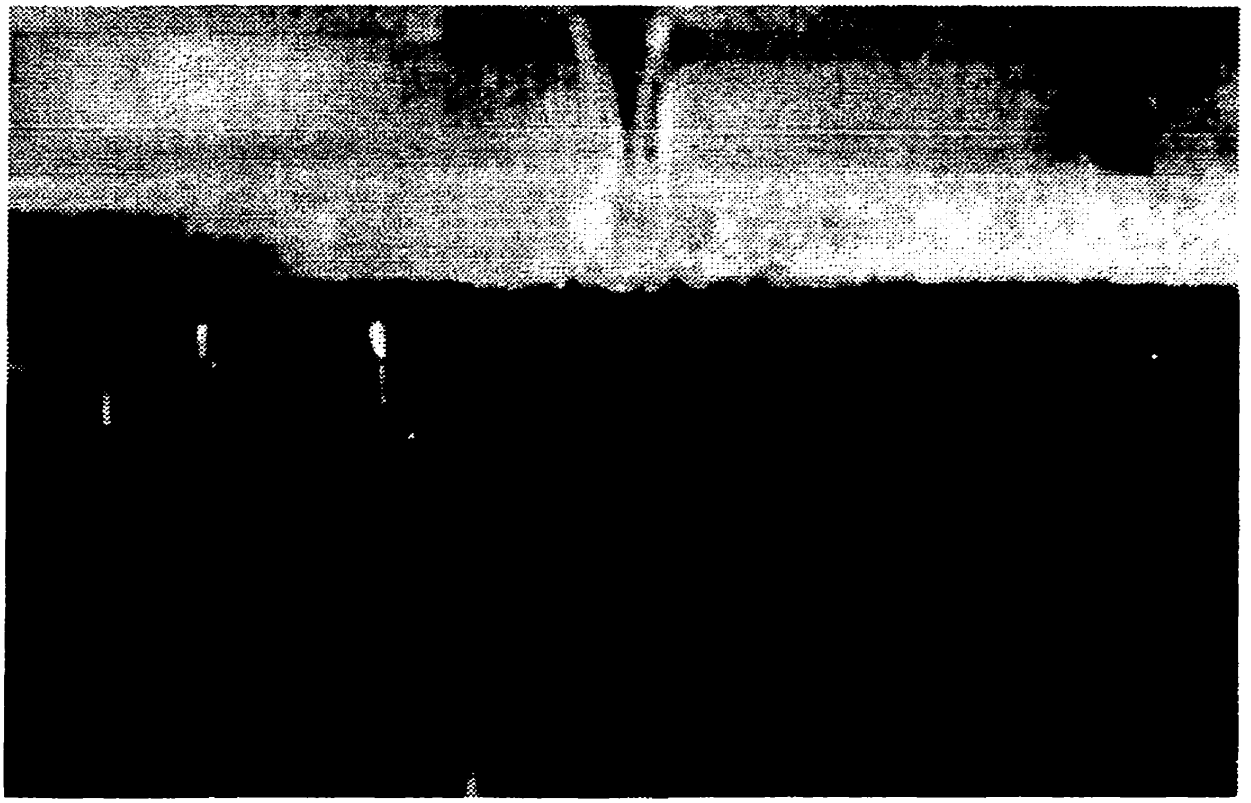

Fig. 4.3 Slag entraining into shroud nozzle with no treatment

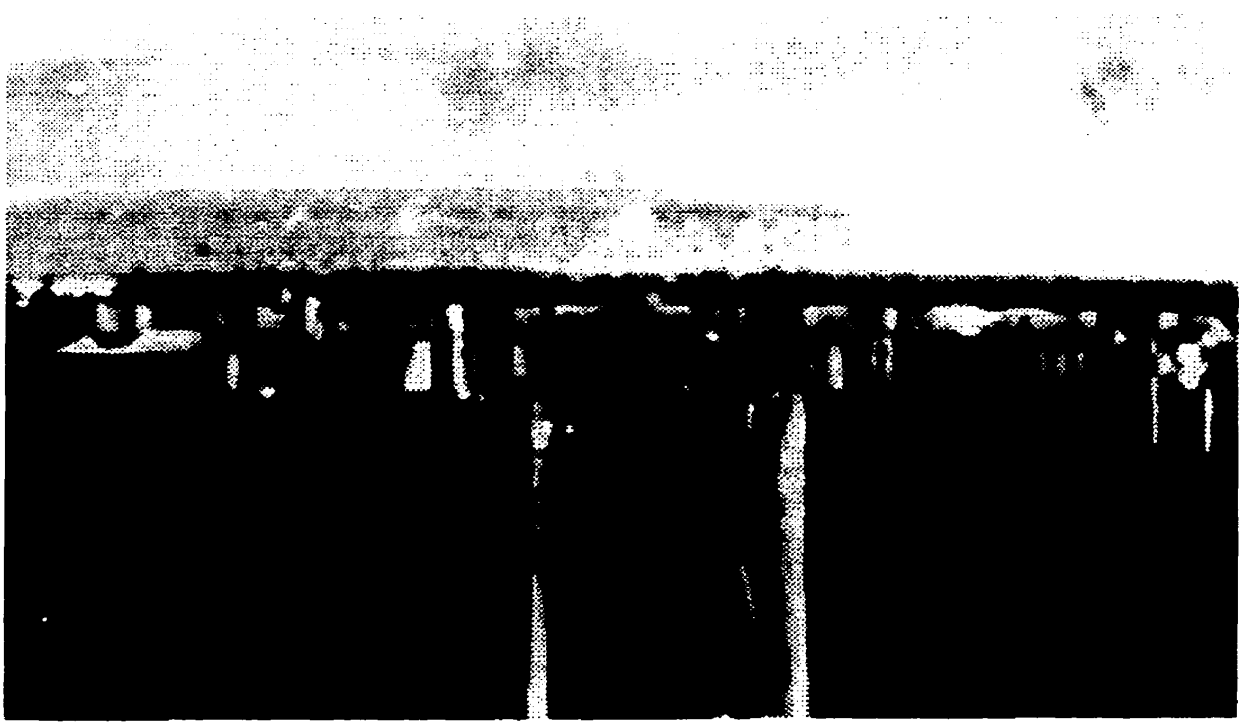

Fig. 4.4 Diversion of the slag entraining into shroud nozzle with 50 % opening

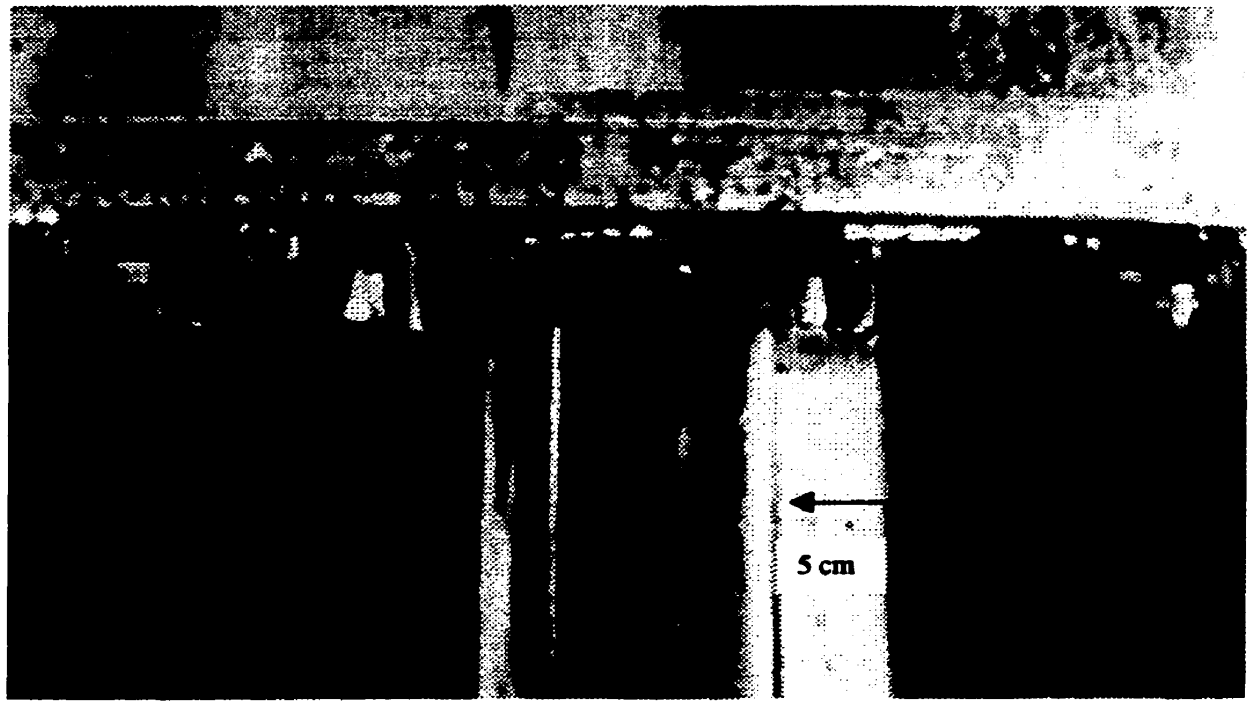

Fig. 4.5 Diversion of the slag entraining into shroud nozzle with 20 % opening

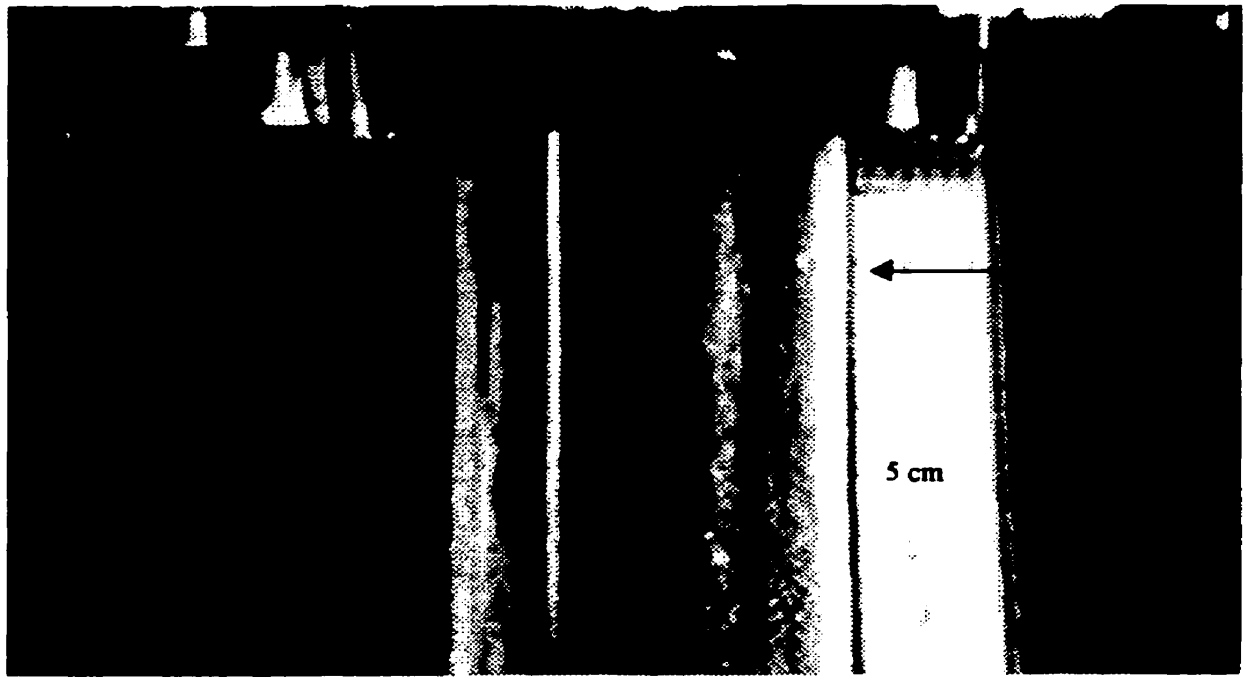

Fig. 4.6 Diversion of the slag entraining into shroud nozzle with redesigned nozzle

4.3.3 Length of the Sidewall Impingement below the Nozzle Plate

Without any treatment on the nozzle entrance, the core of slag entraining went through the center of the nozzle, while the core of slag entraining was displaced off the central axis of the nozzle and broken into many small droplets after impinging on the nozzle sidewall when two methods were applied.

Applying the first method involving putting a thin plate over the nozzle entrance, it was found that this simple method was effective in redirecting the vortex core of 'slag' (kerosene dyed red) away from the central axis of the nozzle. This can be thought as a similar case of the action of a slide gate nozzle that would be to disturb the central, or axial, flow of slag and to disperse slag droplets across the width of the shroud nozzle. The second approach using a redesigned nozzle (skewed nozzle) successfully created radial velocity component in the flowing fluid. Kerosene oil (slag) redirected its path from central axis to the wall of the nozzle at it flew out through the nozzle. As this rotating core of kerosene would impinge on the nozzle sidewall in both methods, the length of sidewall impingement below the nozzle plate was measured as a main parameter in this work. (Figure 4.7)

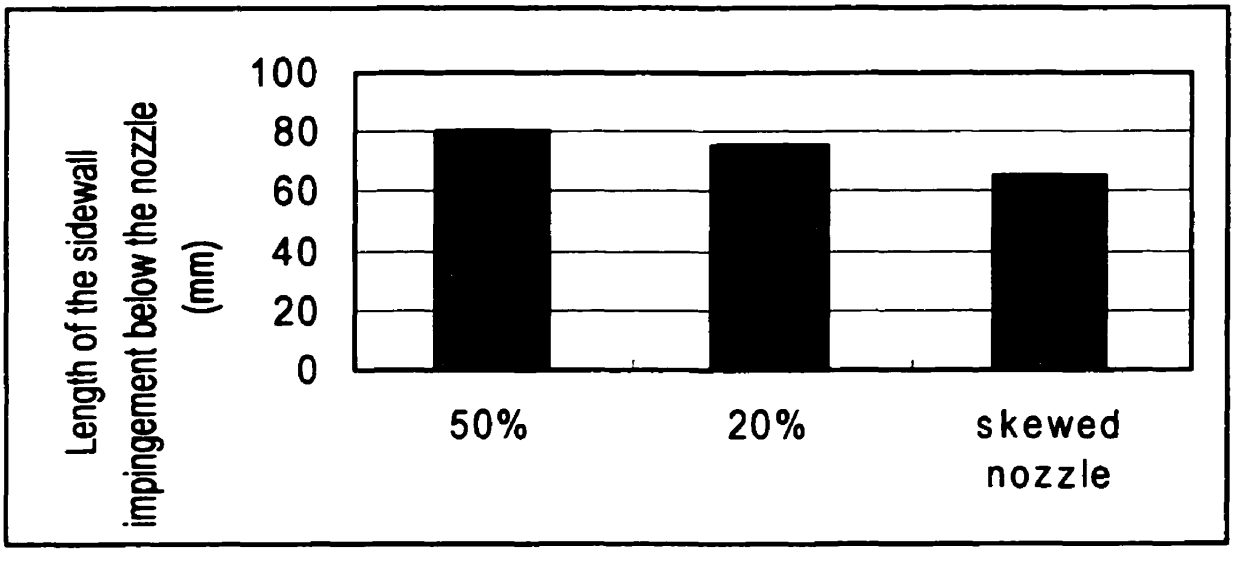

Fig. 4.7 Length of the sidewall impingement below the nozzle plate

In the first approach, the length of sidewall impingement below the nozzle plate was 78-83 mm when the plate covered 50% of the nozzle entrance (i.e. a semi-circular area), and 73-78 mm when the plate covered 80% of the opening. It is understandable from the point of Bernoulli's equation that 80% covering of the opening generated more pressure difference across the nozzle than 50% covering did, which resulted in shorter length of sidewall impingement below the nozzle plate when the covering was 80%.

As the path of slag entraining into the nozzle was found to be determined by the bulk flow in the second method using a skewed nozzle, the angle to the vertical of the skewed nozzle was important. Changing the angle to the vertical will probably change the length of sidewall impingement below the nozzle plate. In the present work, the angle was 30° and the length was 68-73 mm.

Since the thin concentric continuous stream of slag caused the insensitivity of the AMEPA system, first purpose of the present work was the diversion of the slag entrainment. However, the lengths of sidewall impingement below the nozzle plate were all short enough comparing the thickness of the ladle bottom, and small droplets resulted after the impingement of slag to the nozzle sidewall dispersed across the nozzle. Therefore, it can be stated that the less the length of sidewall impingement below the nozzle plate, the earlier detection of slag entraining is possible.

4.3.4 Change of the Flowrate

Clearly, the draw back to those two approaches is a lower flowrate of liquid metal, and also a higher critical height for slag entrainment, owing to increased energy losses in the entrance region of the nozzle caused by reduced nozzle opening. It is well known fact that the flowrate is proportional to the nozzle size. As the flowrate of the liquid metal is directly related to the productivity of the liquid metal, this parameter is very important in the process metallurgy and was measured. The change of the flowrate of liquid metal depending on two methods was shown in Figure 4.8. The prediction of the flowrate was also calculated using $Q_{Calculated} = C_D \cdot A_{Nozzle} \cdot \sqrt{2gh}$.

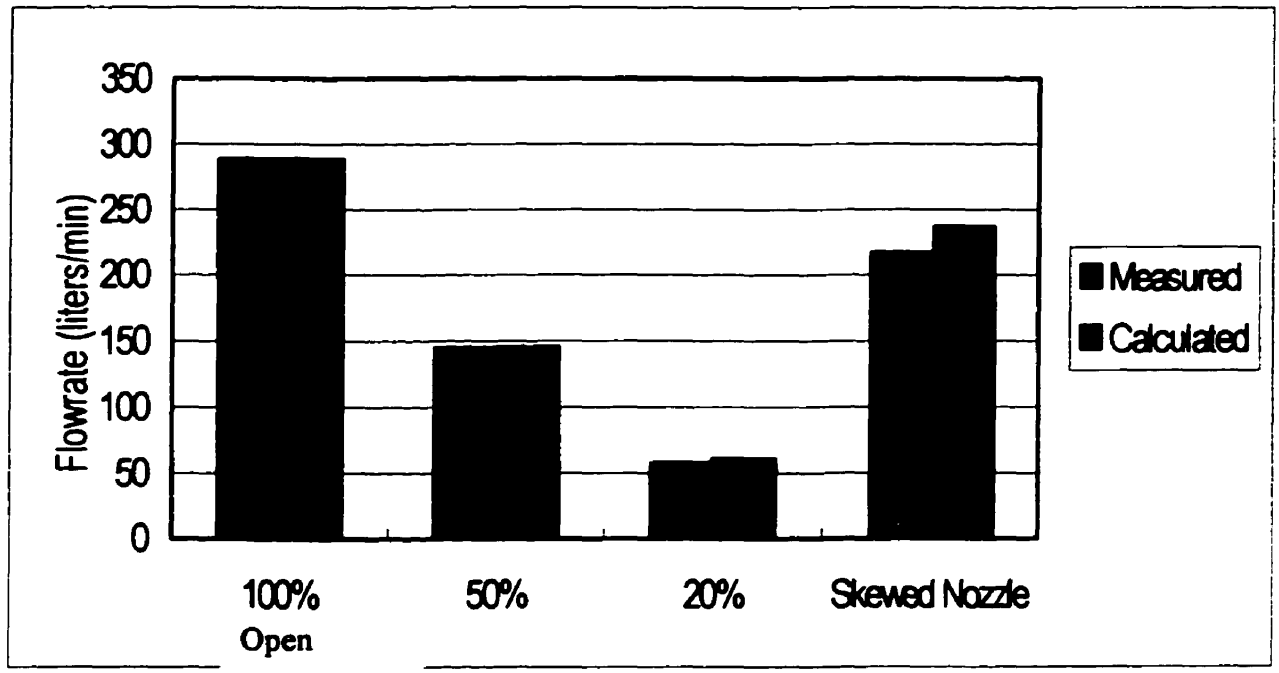

Fig. 4.8 Changes in Flowrate of liquid metal according to the nozzle opening and opening method.

A pre-determined height was used as a reference height for the measurement of the flowrate of liquid metal using Eq. (4.4) instead of measuring flowrate of whole liquid metal from the ladle, because the ladle would be closed with liquid metal left in the ladle.

$$Q_{measured} = \frac{\left(H_{init.} - H_{ref.}\right) \cdot A_{ladle}}{t_{ref.} - t_{init}} \tag{4.4}$$

Here, $H_{init.}$ and $H_{ref.}$ is a initial height and referential height, specifically and A_{ladle} is cross sectional area of the ladle. The drainage coefficient, C_D=*0.84*, for the theoretical flowrate of liquid metal determined by setting the theoretical flowrate be same as the practical flowrate when the opening was 100% was used for all cases.

The flowrate was decreased as the opening of the nozzle decreased. Moreover the measured flowrate was almost same as the calculated flowrate, when a thin plate was put on the nozzle entrance, independent of the opening percent in the present work. However, the measured flowrate from the second approach using a skewed nozzle was a little bit

lower than the calculated flowrate. Drainage coefficient was probably changed to just a little bit lower value, because of the increased energy losses in the entrance region of the skewed nozzle though it was not so much.

4.3.5 Change of Critical Height

Being directly related to the yield of the liquid metal from the ladle, critical height depending on the methods was also measured. It was shown in the Figure 4.9. As expected, the critical height increased as the opening of the nozzle decreased, when a thin plate was put on the nozzle entrance. As the increasing rate of the critical height was much greater than the decreasing rate of the opening, the exponential decay style relationship between two parameters might be deduced to the certain percent of the nozzle opening.

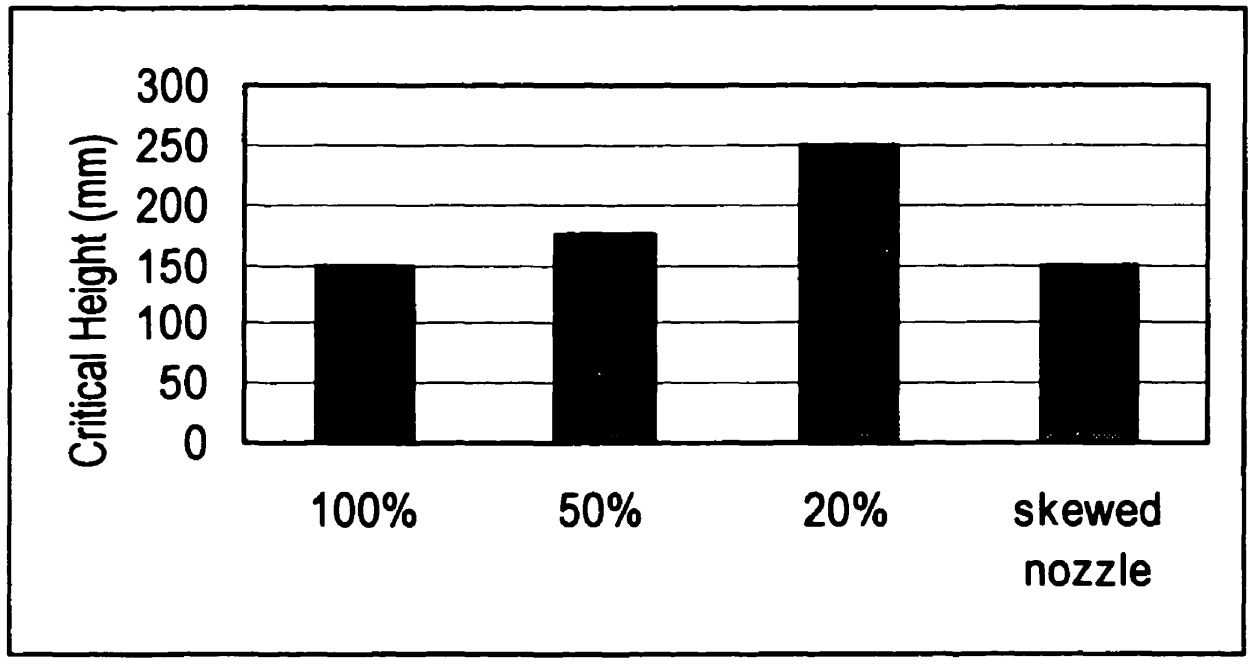

Fig. 4.9 Changes in critical height according to nozzle opening and opening method.

As the AMEPA is one of the detection-based ends of drainage methods, it cannot suppress the vortex formation by itself, which means that it merely address the effect of entrainment, rather than the cause itself. However, the use of a skewed nozzle reduced the critical height just a little bit, though the opening was reduced to 82% of the nozzle entrance. This phenomenon could be regarded that eccentricity of the nozzle entrance led to a reduced critical height by altering the rotational flow around the nozzle or hindering the flow flowing in the gravitational direction, against the increased energy loss in the entrance region of the nozzle caused by reduced nozzle entrance.

4.3.6 Size of the initial vortex funnel tip

The characteristic diameter of a vortexing funnel at the early stage of the slag entrainment was defined as the diameter along the interface between the primary liquid and the supernatant fluid at the very instant that the funnel first became fully-developed. This critical diameter increased in direct proportion with the nozzle diameter, as shown in Fig. 4.4, 4.5 and 4.6. Since the diameter of vortexing funnels was only of secondary importance to the overall objectives of the present study, no effort was made to measure the absolute values of the critical diameter.

4.3.7 Effect of the Thickness of the Plate over Nozzle Entrance

It was observed that the center of the vortex on the liquid surface was positioned over the extended radius perpendicular to the edge of the plate when it became fully developed vortex. There was no recognizable change to the end of the ladle drainage in the position with a thin plate over the nozzle. However, the initial position of the center moved around the center of the ladle in the counter-clockwise direction seen from the top, while the rotational direction of the liquid remained in the ladle was clockwise. When the center of the vortex on the liquid surface was over the extension of the plate edge, the fully developed vortex was disappeared. Therefore, there was no slag entrainment at all to the end of the ladle drainage. From this phenomenon, it is clear that the thickness of the

plate over the nozzle is related to the velocity components of the liquid left in the ladle though nothing was known about that relationship yet.

4.4 SHROUD GAS/STEEL FLOW INTERACTION

4.4.1 Two Phase Flow Regime with Fixed Water Flowrate

It was found that there was no noticeable change of reading from the pressure gauge monitoring the absolute pressure in the water flowing nozzle, whether or not there was an air introduction into the shroud nozzle. Therefore, the introduction of air into the shroud nozzle didn't change the pressure inside of the nozzle. The gauge pressure reading from mercury manometer decreased as the gas flowrate increased. The data of the gauge pressure reading from manometer was shown in the Table 4.2, along with the volume percent of air in the shroud nozzle. At low air infiltration rates, a negative gauge pressure of –7.65 cm Hg was measured, which is equivalent to (7.65 × 13.6) or 104 cm H_2O. This, as expected, closely corresponds to the height of the ladle shroud between its exit, (where P = atmospheric pressure) and the gas injection port. The gauge pressure was zero when there was about 7 volume percent of air introduction into the shroud nozzle, which means that no air infiltration would occur in this situation. An abrupt increase was found after this critical value by increasing the volume percent of air slightly. The real air flowrate was calculated from Eq. (4.5):

$$Q_{air} = K_{gas} \times Q_{std}$$
$$K_{gas} = \sqrt{\frac{T_{act}}{T_o} \times \frac{P_o}{P_{act}}} \qquad (4.5)$$

Where:

Q_{air} = Equivalent Air Flow Capacity at Standard Conditions

$Q_{std.}$ = Maximum Flow of Metered Gas

T_{act} = Absolute Temperature at Flow Conditions

Table 4.2 Air-Water flow data changing air flowrate

Tube #	FLMR	$Q_{std.}$ (l/min)	h_{Hg} (cm/Hg)	Q_{air} (l/min)	Q_{water} (l/min)	Volume % of Air
FM082-03ST	15	00.262	-7.7	00.276	265	0.10
FM082-03ST	25	00.384	-7.6	00.405	265	0.14
FM082-03ST	90	01.105	-7.5	01.163	265	0.42
FM082-03ST	150	01.682	-7.3	01.769	265	0.63
N044-40T	25	08.680	-5.5	09.012	265	3.17
N044-40T	45	17.305	-1.0	17.420	265	6.13
N044-40T	47.5	18.367	-0.5	18.428	265	6.48
N044-40T	65	25.025	8.1	23.789	265	8.63

T_o = Absolute Temperature at Standard Conditions

P_{act} = Pressure at Flow Conditions

P_o = Pressure at Standard Conditions

Vertically downward two-phase flow studied in the present work showed a different flow regime from the preceding experiments carried out by people in chemical process industry and petro-chemical technology. It was assumed that there would be a three different flow regime depending on the volume percent of air in the vertical pipe as the liquid flow down: bubbly flow, slug-bubbly flow and annular flow. However in the present work, no slug-bubbly flow appeared at all. Instead, a 'standing' jet of air at its point of entry into the water flow was observed. It was observed that air infiltration through a controlled leak lead to the formation of a small-submerged gas jet immediately below the air's point of entry. This standing jet broke up into smaller bubbles of about 1-5 mm equivalent diameter, that were carried downstream and became uniformly distributed across the shroud's cross-section, owing to the high flow velocity of the water (steel), (~ 2 m/s). Three pictures taken from the videotape corresponding to air volume percent of 1, 5 and 10 percent were shown in the Figure 4.10 to 4.12.

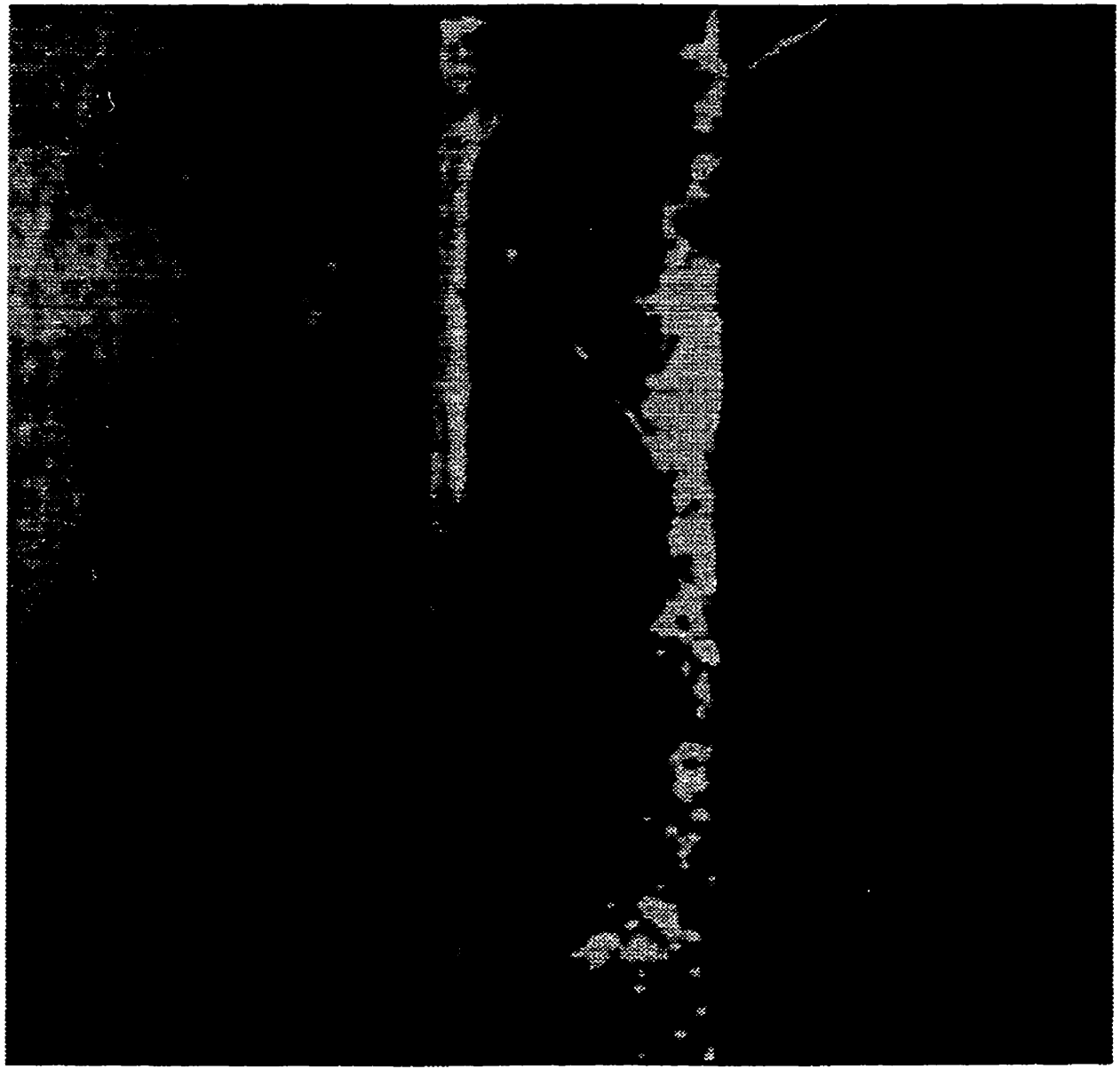

Fig. 4.10 Pictures taken from the videotape corresponding to air volume percent of 1%

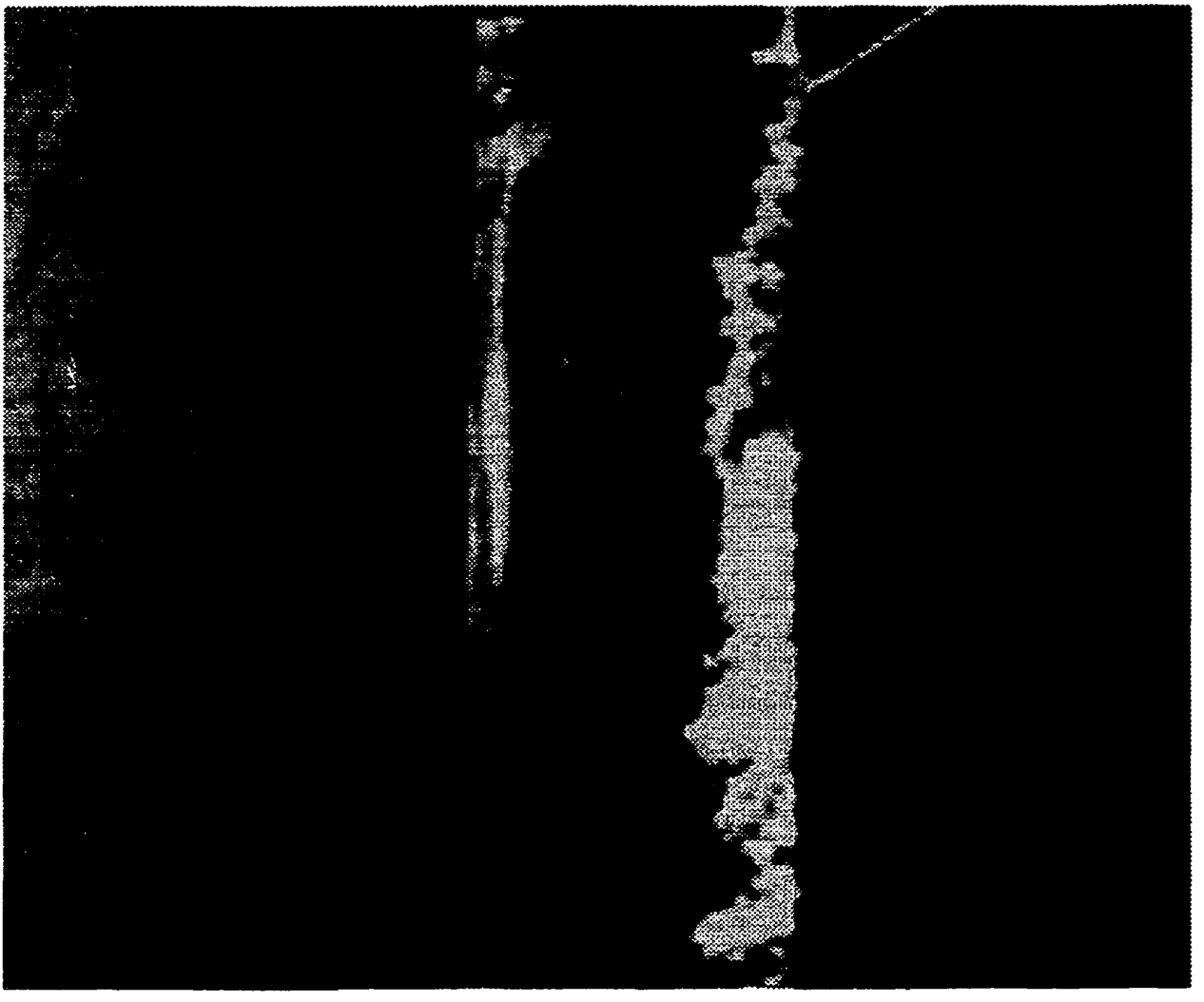

Fig. 4.11 Pictures taken from the videotape corresponding to air volume percent of 5%

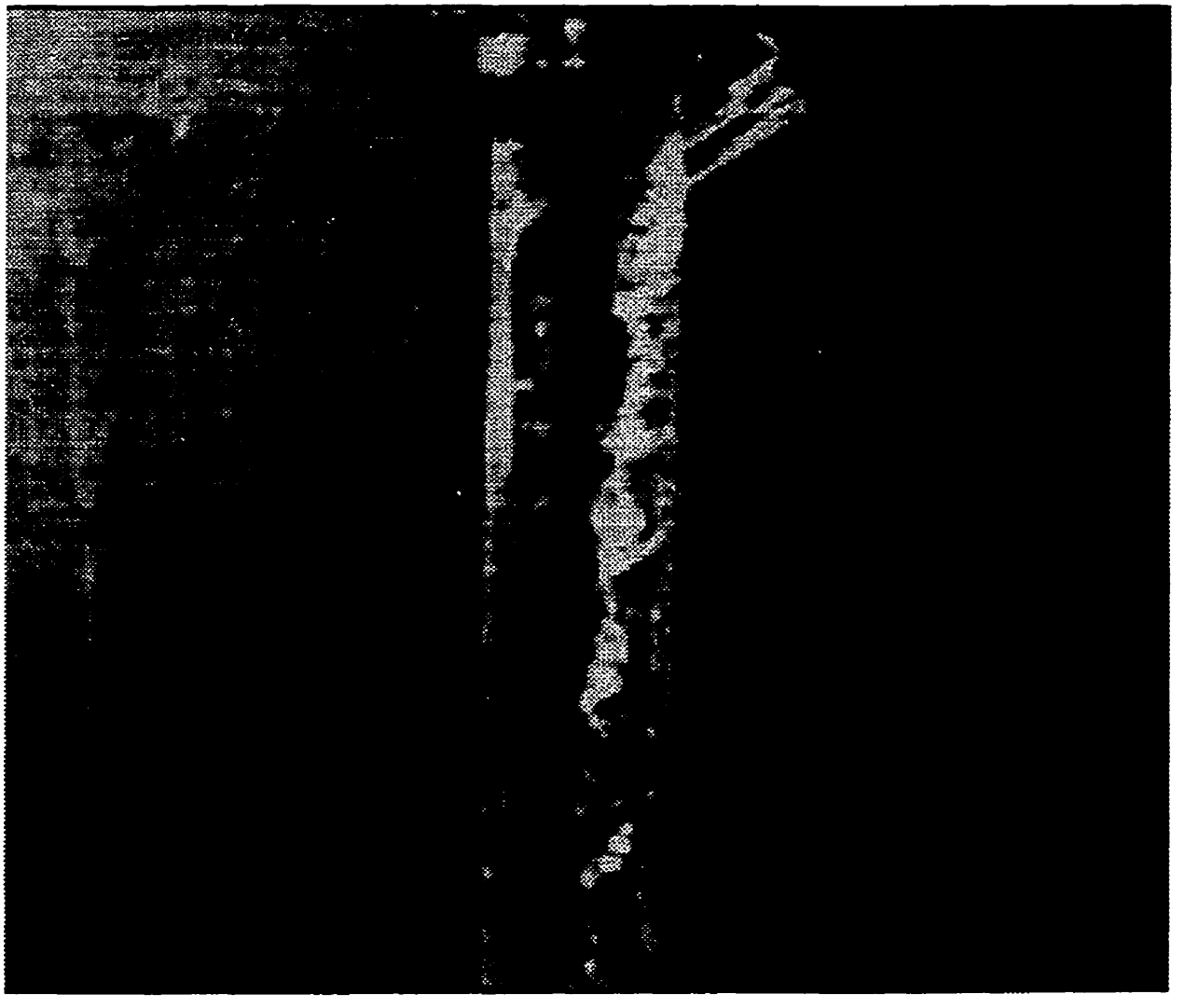

Fig. 4.12 Pictures taken from the videotape corresponding to air volume percent of 10%

These pictures demonstrate that small amount of gas infiltration lead to the entrainment of small gas bubbles which are dispersed across the cross section of the shroud nozzle, so as to become uniformly distributed about 0.5 m downstream from the point of injection of gases. Larger amounts of gas infiltration (5% volume ratio) then lead to a much larger envelope of gas extending downstream, together with its continuing break down into smaller bubbles. At very high gas infiltration/ blowing rates (9% volume ratio) the water flow tended to become annular with an air core hugging the sidewall, extending into the central axis of the shroud, and all the way to the shroud's exit.

As the volume percent of air entrainment rises towards the 9% maximum volume ratio studied in this work, the bubbles sheared from the submerged, 'standing jet of air at its point of entry into the water flow become larger. At the same time, the submerged jet extends further into the shroud, and further down the sidewall, such that parts of the sidewall are not contacted by the liquid steel jet. This could doubtlessly lead to a frozen jacket of steel and may account for the occasional loss in electrical contact between the electrode sensor and the steel stream in real shroud systems.

Similarly, at somewhat higher gas flowrates (~ 9%), a central air core tends to develop with water flowing in an annular fashion down the internal sidewall below its point of entry. Under these circumstances, massive amounts of gas entrainment would still blind the slag detection device. The question of gas hold-up in the column owing to the bubbles' rising velocities is ignored, since the downstream velocity of water, at 2 m/s, is significantly greater than the bubbles' rising velocities of perhaps 0.1- 0.2 m/s.

4.4.2 Submerged and Non-Submerged Shroud Nozzle

Four different water flowrates and eight different standard air flowrates were chosen to compare the results from submerged shroud nozzle with those from non-submerged nozzle. Table 4.3, 4.4, 4.5 and 4.6, corresponding to the water flowmeter reading 137, 100, 65 and 55 specifically, shows the results including standard air flowrates, real air flowrates using, pressure gauge readings, volume percent of air and the

size of the standing jet. Time-averaged width and length of the standing jet was used. When the water flow became annular with an air core, these parameters were not measured. As the data of the volume percent of air didn't make a noticeable difference, it was not shown.

Pressure gauge readings of the non-submerged shroud nozzle when air introduced into the nozzle generally showed less value than those of the submerged nozzle, except for the lowest water flowrate (Table 4.6) in this present work. When the water flow became annular with an air core hugging the sidewall, pressure gauge reading became positive, and no measurements was done for the width and length of the standing jet.

It could be stated from the Table 4.5 that it was less stable when a non-submerged nozzle was used. Finally, it could be stated that there was no big difference between submerged/non-submerged nozzle usage. Although there was a little bit difference in pressure gauge reading in both nozzle, the values of the real air flowrate, the width and length of the standing jet and the volume percent of air in both case was almost same.

Table 4.3 Air-water flow data when water flowrate is 184 liters/min

	$Q_{std.}$ (ml/min)	h_{Hg} (cm/Hg)		Q_{air} (ml/min)		Jet width (cm)		Jet length (cm)	
		Non	Sub.	Non	Sub.	Non	Sub.	Non	Sub.
1	385	-7.8	-6.2	406	402	0.5	0.0	1	0
2	1105	-7.6	-5.9	1164	1150	1.8	1.8	5	5
3	1682	-7.4	-5.7	1770	1749	2.5	2.1	7	8
4	2744	-7.0	-5.5	2880	2848	2.5	3.3	9	10
5	5734	-6.2	-4.6	5983	5914	4.4	4.0	15	18
6	8937	-5.1	-3.6	9253	9156	4.5	4.8	22	23
7	13153	-3.7	-2.0	13485	13330	5.0	4.8	30	30
8	20247	-0.1	1.4	20260	20063	5.5	5.3	45	45

Table 4.4 Air-water data when water flowrate is 133 liters/min

	$Q_{std.}$ (ml/min)	h_{Hg} (cm/Hg)		Q_{air} (ml/min)		Jet width (cm)		Jet length (cm)	
		Non	Sub.	Non	Sub.	Non	Sub.	Non	Sub.
1	385	-7.8	-6.3	406	402	1.5	1.5	3	3
2	1105	-7.6	-6.1	1165	1152	2.8	2.5	6	6
3	1682	-7.4	-5.9	1770	1751	3.5	3.0	7	8
4	2744	-7.0	-5.5	2880	2849	4.0	4.0	11	11
5	5734	-6.1	-4.6	5977	5916	5.0	5.0	19	20
6	8937	-4.8	-3.3	9233	9134	5.5	5.2	30	30
7	13153	-2.7	-1.3	13393	13264	5.6	5.3	50	45
8	20247	3.5	6.0	19803	19498	N.A	N.A	N.A	N.A

Table 4.5 Air-water data when water flowrate is 83 liters/min

	$Q_{std.}$ (ml/min)	h_{Hg} (cm/Hg)		Q_{air} (ml/min)		Jet width (cm)		Jet length (cm)	
		Non	Sub.	Non	Sub.	Non	Sub.	Non	Sub.
1	385	-7.9	-6.5	407	402	2.0	2.2	2	2
2	1105	-7.6	-6.1	1164	1152	3.5	3.3	6	6
3	1682	-7.4	-5.9	1770	1751	3.7	3.8	10	9
4	2744	0.1	-5.3	2743	2845	N.A	4.3	N.A	15
5	5734	0.5	-4.0	5715	5889	N.A	5.5	N.A	27
6	8937	1.3	-2.4	8862	9082	N.A	5.6	N.A	40
7	13153	-1.6	-0.2	13289	13170	5.6	5.7	50	60
8	20247	3.5	6.0	19796	19498	N.A	N.A	N.A	N.A

Table 4.6 Air-water data when water flowrate is 68 liters/min.

	Q_{std} (ml/min)	h_{Hg} (cm/Hg)		Q_{air} (ml/min)		Jet width (cm)		Jet length (cm)	
		Non	Sub.	Non	Sub.	Non	Sub.	Non	Sub.
1	385	-0.4	-6.5	386	402	N.A	3.0	N.A	2
2	1105	-0.2	-6.1	1106	1152	N.A	4.0	N.A	7
3	1682	0.0	-5.8	1682	1749	N.A	4.5	N.A	9
4	2744	0.2	-4.9	2740	2837	N.A	5.0	N.A	17
5	5734	0.9	-3.5	5702	5869	N.A	5.2	N.A	35
6	8937	1.6	-1.5	8847	9027	N.A	5.6	N.A	45
7	13153	2.3	0.7	12963	13093	N.A	5.7	N.A	60
8	20247	3.6	6.1	19790	19480	N.A	N.A	N.A	N.A

4.4.3 Helium-Water Flow Data

Helium was also used to study the helium-water flow phenomena with a same water and gas flowrates. As the density of helium is less than that of air, the difference caused by density change could be studied. Data was shown in Table 4.7, 4.8, 4.9 and 4.10 changing the water flowrate. Standard flowrates of helium were chosen as same amount of air, in order to compare the results from using helium with those from using air. Real helium flowrate was calculated using Eq (4.5). Here again, the volume percent of helium of non-submerged nozzle was almost same that of submerged nozzle. As the helium flowrate increased, the pressure gauge reading was also increased in both submerged and non-submerged shroud nozzle, and the size of standing jet became wider and longer. The width of standing jet could be greater than the inner diameter of the shroud nozzle because it was measured from the outside wall of the nozzle whose wall thickness is thick enough. No big difference in the size of standing jet was measured between submerged and non-submerged nozzle because of the error in measuring time- average value of width and length. The pressure gauge reading of using submerged nozzle was a little bit greater than that of using non-submerged nozzle.

Table 4.7 Helium-water flow data when water flowrate is 184 liters/min

	$Q_{std.}$ (ml/min)	h_{Hg} (cm/Hg)		Q_{helium} (ml/min)		Jet width (cm)		Jet length (cm)	
		Non	Sub.	Non	Sub.	Non	Sub.	Non	Sub.
1	390	-7.7	-6.1	411	407	0.5	1.0	1	2
2	1090	-7.5	-6.1	1148	1136	2.5	1.6	6	6
3	1650	-7.4	-5.5	1737	1713	2.8	3.0	8	8
4	2800	-6.8	-5.0	2934	2897	4.5	4.3	15	13
5	5700	-6.2	-4.8	5948	5889	5.0	4.5	22	20
6	8800	-5.4	-3.2	9130	8991	5.0	5.5	30	43
7	13200	-4.4	2.0	13600	13030	5.5	N.A	50	N.A
8	20300	1.6	2.9	20090	19923	N.A	N.A	N.A	N.A

Table 4.8 Helium-water data when water flowrate is 133 liters/min

	$Q_{std.}$ (ml/min)	h_{Hg} (cm/Hg)		Q_{helium} (ml/min)		Jet width (cm)		Jet length (cm)	
		Non	Sub.	Non	Sub.	Non	Sub.	Non	Sub.
1	390	-7.8	-6.3	412	407	1.5	1.5	3	3
2	1090	-7.7	-6.2	1149	1137	3.0	2.0	6	4
3	1650	-7.5	-6.0	1738	1719	3.5	3.0	7	8
4	2800	-6.6	-5.3	2930	2902	5.0	4.7	18	15
5	5700	-6.4	-4.7	5956	5885	5.0	5.2	25	24
6	8800	-4.6	-3.2	9079	8991	5.5	5.5	45	45
7	13200	0.8	2.0	13131	13034	N.A	N.A	N.A	N.A
8	20300	1.6	2.9	20090	19923	N.A	N.A	N.A	N.A

Table 4.9 Helium-water data when water flowrate is 83 liters/min

	$Q_{std.}$ (ml/min)	h_{Hg} (cm/Hg)		Q_{helium} (ml/min)		Jet width (cm)		Jet length (cm)	
		Non	Sub.	Non	Sub.	Non	Sub.	Non	Sub.
1	390	-7.9	-6.5	412	408	2.8	2.2	4	2
2	1090	-7.6	-6.4	1139	1139	3.5	3.0	6	3
3	1650	-7.5	-6.0	1738	1719	4.0	4.0	9	8
4	2800	-6.5	-5.0	2928	2896	4.5	5.0	20	20
5	5700	-5.1	-3.9	5901	5852	5.5	5.6	35	35
6	8800	-3.7	-2.5	9022	8948	5.6	5.6	50	50
7	13200	0.9	2.1	13123	13021	N.A	N.A	N.A	N.A
8	20300	1.7	3.0	20077	19917	N.A	N.A	N.A	N.A

Table 4.10 Helium-water data when water flowrate is 68 liters/min

	$Q_{std.}$ (ml/min)	h_{Hg} (cm/Hg)		Q_{helium} (ml/min)		Jet width (cm)		Jet length (cm)	
		Non	Sub.	Non	Sub.	Non	Sub.	Non	Sub.
1	390	-0.4	-6.5	391	408	N.A	3.0	N.A	3
2	1090	-0.3	-6.4	1092	1139	N.A	3.5	N.A	4
3	1650	-0.2	-5.9	1652	1718	N.A	4.5	N.A	10
4	2800	0.0	-3.9	2800	2875	N.A	5.6	N.A	40
5	5700	0.2	-2.9	5693	5812	N.A	5.6	N.A	45
6	8800	0.5	-1.5	8771	8888	N.A	5.6	N.A	70
7	13200	1.4	2.2	13080	13013	N.A	N.A	N.A	N.A
8	20300	2.3	3.2	20000	19886	N.A	N.A	N.A	N.A

Considering the error measuring time-averaged value, it could be stated that the size of the standing jet was not a function of the gas density. Moreover, the pressure gauge reading of using helium was almost same that of using air. Therefore, two-phase flows in the shroud nozzle are independent of whether the gas is air or helium, owing to the highly turbulent flow.

CHAPTER
5

CONCLUSIONS

5.1 INTRODUCTION

A general summary and conclusion of the thesis is presented in this chapter under the three subjects: Slag Entrainment in Late Rotating Vortices, Detection of Early Slag Vortexing Phenomena using AMEPA system and Shroud Gas/Steel Flow Interactions.

5.2 SLAG ENTRAINMENT IN LATE ROTATING VORTICES

The onset of a late rotating vortex over an off-center drain nozzle at 2/3 radius was studied in an 1160-mm diameter tank. The critical height of water at which this late rotating vortex set in for a flat ladle bottom, was compared with the critical height of water for air (slag) entrainment with a bottom ladle surface, sloped at 3.5°. Identical starting conditions were used for the two conditions. It was found that the critical height of liquid before air (slag) entrainment took place was about the same for the sloped bottom situation, and that this translated into an increased yield of clean steel, thanks to the sloped bottom. However, the opposite observations were observed for an off-centered nozzle, located at 1/2R, and off set- to the sloping central axis of the bottom surface, at an angle of 29° from the sloping axis. Much lower critical heights of water were obtained when the bottom of ladle was flat rather than sloped, thereby residual volume was also lower.

The results suggest that there is a benefit to be gained in terms of steel yield by using a sloped ladle bottom, provided the exit nozzle is located other than 1/2R, on the center line of the sloping axis. However, if the maximum slope of the bottom does not coincide with the position of the (offset) nozzle, then it becomes easier for a rotating column of liquid to 'set in' over such a nozzle, thereby compromising possible steel yield and rendering a sloped ladle bottom counter-productive. Furthermore, a sloped bottom ladle could also lead to an intensification of residual tangential velocities during steel tapping and argon stirring.

5.3 DETECTION OF EARLY SLAG VORTEXING PHENOMENA USING AMEPA SYSTEM

In order to render the AMEPA system sensitive to early slag entrainment phenomena by diverting the rotational core of a slag entraining away from the central vertical axis of the nozzle, two methods were investigated. The length of sidewall impingement below the nozzle plate, the critical height and the water flowrate were measured to compare the results from both methods.

The first concept involved putting a thin plate over the nozzle entrance, so as to partially block the nozzle's aperture, thereby creating a region of under pressure behind the plate. The scale model water ladle was filled to an initial height of 430mm, with a kerosene (slag) layer 20mm thick on top. The same initial tangential velocity was used for two methods. Once draining began, the liquid level would descend until a critical height was reached for the generation of a rotating funnel vortex. The 'slag' would then be entrained in this funnel. It was found that this simple method was effective in redirecting the vortex core of 'slag' (kerosene dyed red) away from the central axis of the nozzle. Opening percentage was related to the length of sidewall impingement below the nozzle plate, as required by Bernoulli's equation. However, as the opening of the nozzle entrance decreased, the critical height increased exponentially and the water flowrate decreased proportionally.

The second approach overcame these difficulties and objections, and involved redesigning the nozzle so as to generate a radial velocity component. A thick plate of Plexiglas® (23.5mm thick) was drilled at an angle of 30° to the vertical, so as to have an aperture area equivalent to that of the 45mm diameter nozzle on which it was placed. It was found that following the generation of a rotating funnel vortex, and subsequent entrainment of 'slag', this rotating core of kerosene would impinge on the nozzle sidewall, and then be broken into many small droplets. The angle to the vertical seems to be related to the length of sidewall impingement below the nozzle plate; higher the angle, lower the length. As the critical height decreased with this redesigned nozzle (skewed nozzle), the yield of liquid metal would improve. Moreover, as long as the opening of the nozzle entrance was maintained to the 100%, the flowrate, directly related to the productivity of the liquid metal, would not decrease significantly. Therefore, minor modification of the nozzle and well block to impart a radial component of velocity to the spinning vortex core, should allow the AMEPA system to detect the resulting field of fragmented drops of slag, following sidewall impingement. Unfortunately, such a modification would cause enhanced erosion, but this should be of similar magnitude to that created in the ladle shroud by the slidegate nozzle system in the partially open mode of operation.

5.4 SHROUD GAS/STEEL FLOW INTERACTION

A 0.75 scale water model was constructed to simulate the flow of liquid steel through a ladle shroud (53-mm ID, 1.15-m long) in the presence of gas infiltration. Helium was introduced into the shroud nozzle for the present work as well as air. Finally, the effect of submerged and non-submerged shroud nozzle into the tundish was also investigated.

It was observed that air infiltration through a controlled leak lead to the formation of a small-submerged gas jet immediately below the air's point of entry. This standing jet

broke up into smaller bubbles of about 1-5 mm equivalent diameter, that were carried downstream and became uniformly distributed across the shroud's cross-section, owing to the high flow velocity of the water (steel), (~ 2 m/s). Larger amount of gas infiltration (5% volume ratio) then lead to a much larger envelope of gas extending downstream, together with its continuing break down into smaller bubbles. As very high gas infiltration/ blowing rates (9% volume ratio) the water flow tended to become annular with an air core hugging the sidewall, extending into the central axis of the shroud, and all the way to the shroud's exit. As the dye tests indicated that the air jet did not disengage entirely from the sidewall below its point of entry, massive amounts of gas entrainment would still blind the ladle shroud slag detection device under these circumstances.

No big difference was observed, whether it was a submerged or non-submerged nozzle used for the experiment, though the use of non-submerged nozzle showed less stability. However, owing to the highly turbulent flow, the size of the standing jet seems to be independent of the nozzle situation and the gas introduced into the shroud nozzle.

REFERENCES

1. K. Haindl, "Contribution to air entrainment by a vortex," International Association for Hydraulic Research, 8th Congress, Montreal, 1959, Paper 16-D, pp. 1-17
2. R. Sankaranarayanan, "Modeling of Slag Entraining Funnel Formation ('Vortex') During Liquid Metal Transfer Operations," Ph.D Thesis, McGill Univ. 1994
3. P. Hammerschmid, K.-H. Tacke, H. Popper, L.Weber, M.Dubke and K. Schwerdtfeger, "Vortex formation during drainage of metallurgical vessels," Ironmaking and Steelmaking, 11, N° 6, 1984, pp. 332-339
4. D. Sucker, J.Reinecke and H. Hage-Jewasinski, Stahl und Eisen, 105, N° 14/15, 1985, pp. 765-769
5. L.L. Daggett, G.H. Keulegan, "Similitude in free-surface vortex formations," Proceedings of the ASCE, Journal of the Hydraulics division, 100, HY11, November 1974, pp. 1565-1568
6. H. Ichikawa, I.Yamazaki, and Y. Tozaki, "Progress of Quality Steel Slab Casting at Kashima Steel Works," Proceedings of the Open Hearth and BOF Conference, Steelmaking Conference of AIME, 1977, pp.243-256
7. P.H. Dauby, D.F. Havel, P.A. Medve, H.D. Baker, A.J. Rumler and C.E. Tomazin, "A Steel Quality Leapfrog – Detection and Elimination of Ladle-to Tundish Slag Carry-over," Iron & Steel Maker, 17, N° 7 July 1990, pp. 27-32
8. J.S. Powers, W.H. Emling and C.E. Tomazin, "Refinement of Casting Parameters for Improved Surface Quality of Cold Rolled AKDQ sheet," Steelmaking Conference Proceedings, ISS-AIME, 72, 1989, pp. 29-37
9. M. Byrne, A.W. Cramb and T.W. Fenicle, "The Sources of Exogenous inclusions in Continuous Cast, Al-Killed Steels," Steelmaking Conference Proceedings, ISS-AIME, 68, 1985, pp. 451-461
10. A.W. Cramb and M. Byrne, "Tundish Slag Entrainment at Bethlehem's Burns Harbor (Indiana) Slab Caster," Steelmaking Conference Proceedings, ISS-AIME, 67, 1984, pp. 5-13

11. D. Schauwinhold, W. Haumann, R. Krumpholz, B. Müsgen and W. Zimnik, "Demands of Materials Technology on Metallurgy for the Improvement of the Service Properties of Steels," Proceedings of the International Conference Secondary Metallurgy, Aachen, West Germany, Sept. 1987, Preprints, pp. 3-18
12. A.W. Cramb and M. Byrne, "Chemical Interactions in Ladle, Tundish and Mould Slags," Steelmaking Conference Proceedings, ISS-AIME, 69, 1986, pp. 719-735
13. H.-J. Engell, D. Janke and P. Hammerschmid, "Kinetics of Metal-Slag Reactions in Secondary Steelmaking", Proceedings of the International Conference Secondary Metallurgy, Aachen, West Germany, September 1987, Preprints, pp. 19-53
14. E. Hüffken, H.-D. Pflipsen and W. Florin, "Measure taken to avoid the entrainment of converter slag during tapping and their effect on rephosphorization; Al melting loss; and the degree of purity of the steel," Proceedings of the International Conference Secondary Metallurgy, Aachen, West Germany, September 1987, Preprints, pp. 124-136
15. G. Poferl and M. Eysn, "Automated Tapping and Reduction of the slag carryover with tapping of LD/BOF converters," Proceedings of the International Conference Secondary Metallurgy, Aachen, West Germany, September 1987, Preprints, pp. 137-148
16. W. Bading, E. Hees, H. Lax and H. Richter, "Processes and Equipment used for Secondary Metallurgy in the Beeckerwerth BOF Steelmaking shop at Thyssen Stahl AG," Procedings of the International Conference Secondary Metallurgy, Aachen, West Germay, September 1987, Preprints, pp. 367-379
17. M. Saiguasa, A. Nanbe, K. Emoto and Y. Iida, " New method for limiting slag carryover into steel ladle," Ironmaking and Steelmaking, N° 1, 1981, pp. 39-42
18. A. Nicholson, G.K. Notman and D.S. Harvey, "The influence of Secondary Steelmaking Facilities on Steel Process Routes", Proceedings of the International Conference Secondary Metallurgy, Aachen, West Germany, September 1987, Preprints, pp. 565-580
19. Y. Miyashita and Y. Kikuchi, "recent Developments in Vacuum Treatment of Steel in Japan," Proceedings of the International conference Secondary Metallurgy, Aachen, West Germany, September 1987, Preprints, pp. 195-207

20. H. Ohmori, H. Yamada, T. Fujiyama, T. Shibayana, K. Nakanishi and K. Saito, "Development of Slag Separation Technique by Siphon Tapping Hole in LD Converter," Transactions ISIJ, 21, April 1981, B-477

21. D.J. Harris and J.D. Young, "Water Modeling – A Viable Production Tool," Steelmaking Conference Proceedings, ISS-AIME, 65, 1982, pp. 3-16

22. M. Byrne and A. W. Cramb: "Operating Experiences with Large Tundishes", Transactions of ISS, Vol 10, (1989), p 91 - 100.

23. E. Julius, W. Theissen, and F.R. Block, "Function and application of an electromagnetic slag detection system," Fachberichte Hüttenpraxis Metallweiterverarbeitung, 24, N° 10, 1986, pp. 906-913 (Also see World Steel and Metal Working, 8, 1986/87, pp. 51-56

24. D. Bolger, R.I.L. Guthrie, D.H.M. Kings, R.A. Sommers & J.D. Usher, "Ladle Shroud Slag Detector", Steelmaking Conference Proceedings, 1996, pp. 481-484

25. E.N. Da C. Andrade, "Whirlpools and Vortices," Proceedings of the Royal Institute of London, 29, 1936, pp.320

26. F.M. White, "Fluid Mechanins," McGraw-Hill, 1979

27. R.I.L. Guthrie, "Engineering in Process Metallurgy," Clarendon Press, Oxford, 1989

28. T. Toyokura and S. Akaike, " Vortex Phenomena in a Water Tank," Bulletin of the JSME, 13, N° 57, 1970, pp. 373-381

29. L.L. Daggett, G.H. Keulegan, "Similitude in free-surface vortex formations," Proceedings of the ASCE, Journal of the Hydraulics division, 100, HY11, November 1974, pp. 1565-1568

30. H.A. Einstein and H. Li, "Steady vortex flow in a real fluid," La Houille Blanche, August-September 1955, N° 4, pp. 483-496

31. H.O. Anwar, "Flow in a Free Vortex," Water Power, 17, N° 4, April 1965, pp. 153-161

32. K. Kimura and S. Hasimoto, "Velocity distribution in water circulating uniformly about a central axis," Journal of the Faculty of Science, Imperial Univ. of Tokyo, Sec I, 1, 1929, pp. 439-463

33. H.O. Anwar, "Formation of a Weak Vortex," Journal of Hydraulic Research, International Association for Hydraulic Research, 4, N° 1, 1966, pp. 1-16

34. M.C. Quick, "Scale Relationships between geometrically similar Free Spiral Vortices (Part I)," Civil Engineering and Public Works Review, 57, September 1962, 674, pp. 1135-1138

35. M.C. Quick, "Scale Relationships between geometrically similar Free Spiral Vortices (Part II)," Civil Engineering and Public Works Review, 57, October 1962, 675, pp. 1319-1320

36. M.Y.M. Kamel, "The Effect of Swirl on the Flow of Liquids Through Bottom Outlets," Fluids Engineering conference, New York, N.Y., ASME Paper 64WA/FE-37,1964, pp. 1-9

37. J.C. Stevens and R.C. Kolf, "Vortex Flow through Horizontal Orifices," Transactions of the ASCE, 124, 1959, Paper 3004, pp. 871-893

38. H. Ohmori, T. Fujiyama, S. Tamada, K. Hirayama, M. Ohnishi and R. Tachibana, "Plant Experiment of Siphon Tapping Hole," Transactions ISIJ, 21, April 1981, B-478

39. P.-O. Melberg and S. Linder, " Automatic metal level control in metal processing," 4th Symposium on Automation inMining, Mineral and Metal Processing, International Federation of Automatic Control, Helsinki, Finland, August 1983, pp. 291-296

40. P.-O. Melberg and S. Linder, "Principles and Applications of Electromagnetic Sensor Techniques in Liquid Metal Processing," Proceedings of the 5th Process Technology Conference, ISS-AIME, 1985, pp. 79-84

41. P.-O. Melberg, "Automatic metal level and slag transfer control in continuous casting," Continuous Casting '85, Proceedings of the International conference, May 1985, The institute of Metals, Paper 55, pp. 55.1-55.6

42. S. Dawson, D. Walker, N. Mountford, I.D. Sommervill and A. Maclean, "The Application of Ultrasonics to Steel Ladle Metallurgy," Proceedings International Symposium on Ladle Steelmaking and Furnaces, 27th Annual Conference of metallurgists, CIM, Montreal, August 1988, pp. 80-91

43. N.D.G. Mountford, L.J. Heaslip, E. Bednarek, and A.N. Sinclair, "The development of an ultrasonic sensor for metal quality in steel casting tundishes," Steelmaking Proceedings, ISS-AIME, 69, Washington DC, 1986, pp. 699-704

44. T. Itoh, T. Koshikawa, T. Imai, and A. Takahashi, "Development of Ladle Slag Detector in CC Machine," Transactions of the ISIJ, 21, 1981, B-90

45. Sumitomo Metal Industries, Ltd., "Detection system of Slag Entrained to Teeming Stream in Continuous Casting," Transaction of the Iron and Steel Institute of Japan, 26, N° 6, 1986, p. 590

46. "Verfahren und Vorrichtung zur Erkennung des Gießendes beim Vergießen von Metallen aus Gießgefäßen," Patent DE 28 14 699, April 1978

47. H.-J. Ehrenberg, J. Glaser, H. Jacobi and K. Wünnenberg, "Slag carry-over in sequence casting of steel – early detection and metallurgical results," Proceedings of the International Conference Secondary Metallurgy, Aachen, West Germany, September 1987, Preprints, pp. 149-159

48. P. Andrzejewski, A. Diener and W. Pluschkell, "Model Investigations of slag flow during last stages of ladle teeming," Steel Research, 58, N° 12, 1987, pp. 547-552

49. H. Gruner, H.-J. Ehrenberg, H. Schrewe and K. Wünnenberg, "Low-head strand casting machines for slagb – the concept for the future," Ironmaking and Steelmaking, 14, N° 3, 1987, pp. 122-128

50. E.Julius, "Elecktromagnetiche Schlackenerkennung an metallurgischen Gefäßen," Stahl und Eisen, 107, 1987, pp. 397-402

51. M. Dubke and K. Schwerdtfeger, "Phenomena occurring during drainage of metallurgical vessels: Effect of stopper rod on vortex formation and development of surface waves," Ironmaking and Steelmaking, 17, N° 3, 1990, pp. 184-192

52. H. H-Jewasinski and D. Sucker, "Strömungs- und Modelluntersuchungen zum Schlackemitlaufen aus Gießpfannen mit Bodenausguß," Stahl and Eisen, 107, 1987, N° 23, pp. 1099-1104

53. R. Steffen, "Fluid Flow Phenomena of Metal and Slag during drainage of Metallurgical Vessels," Proceedings of the International Conference Secondary Metallurgy, Aachen, West Germany, September 1987, Preprints, pp. 97-118

54. T.J. Lin and H.G. Donnely, A.I.Ch.E.J. 1966, 12, pp.563-571

55. E. Van de Sande and John M. Smith, "Jet Break-up And Air Entrainment by Low Velocity Turbulent Water Jets," Chemical Engineering Science, 1976, 31, pp. 219-224

56. R. Burley and B.S. Kennedy, "An Experimental Study of Air Entrainment as a solid/liquid/gas interface," Chemical Engineering Science, 1976, 31, pp. 901-911

57. Ohyama Y., Takashima Y. and Idemura H., *Kagaku Kenkyusho Hokoku*, 1993, 19, 344

58. De Frate L. and Rush F., Selected Papers Symposium – Part II, 64th National Meeting A.I.Ch.E. New Orleans, Louisiana, March, 1969

59. J. Szekely, "On the Estimation of Oxygen Absorption by Continuous Molten Metal Streams," Transactions of The Metallurgical Society of AIME, February 1969, 245, pp. 341-344

60. M.J. McCarthy, W.G. Kirchner, N.A. Molloy and J.B. Henderson, "Mechanism of gas bubble entrainment by plunging liquid jets," Proc. Chemeca. 1970 (Australia), Sec. 2, pp. 86-100, Butterworths, London

61. J. Ciborowski and A. Bin, *Inzymera Chemiczna* II, 1972, 4, 557

62. Takao CHOH and Michio INOUYE, "The Rate of Oxygen Absorption of Liquid Iron," Transactions ISIJ, 20, 1980, pp. 768-775

63. Katsuyoshi IWATA, Takao CHOH and Michio INOUYE, "A Model Experiment on the Gas Entrainment with Pouring Liquid Steel Stream," Transactions ISIJ, 23, 1983, pp. 218-227

64. Takao CHOH, Katsuyoshi IWATA and Michio INOUYE, "Estimation of Air Oxidation of Teeming Molten Steel," Transactions ISIJ, 23, 1983, pp. 598-607

65. J. Little, M. Van Oosten and A. McLean, "Factors affecting the reoxydation of molten steel during continuous casting," Canadian Metallurgical Quarterly, 7, November 4, pp. 235-246

66. Frank A. Vonesh and Robert F. Schmehl, "Inert Gas Shrouding of Molten Metal Streams," Iron and Steel Engineer, July, 1987, pp. 35-39

67. B. Bowman and J. Deluca, "Assessing the Efficiency of Tundish to Mold Inert Gas Shrouds," I&SM, August, 1985, pp. 17-18

68. N.A. McPherson, "Continuously Cast Clean Steel," Steelmaking Proceedings, Detroit, Mich., ISS-AIME, 68, April 14-17, 1985, pp. 13-25

69. T.W. Scamman and S.J. Miller, " The Effect of Argon Shrouding of Stainless Ingots on Inclusion Lines," "The shrouding of steel flow for casting and teeming," Iron and Steel Society, Inc., 1986, pp. 95-100

70. Allan R. Obman, W. Terry Germanoski, and Richard C. Sussman, "Surface and Subsurface Defects on Stainless Steel First slabs," "The shrouding of steel flow for casting and teeming," Iron and Steel Society, Inc., 1986, pp. 55-59

71. G.A. Demasi and R.F. Hartmann, "Development of the Ladle Shroud Mechanism and Its Metallurgical Benefits," "The shrouding of steel flow for casting and teeming," Iron and Steel Society, Inc., 1986, pp. 3-11

72. Frank J. Nahlik and Eric C. Knorr, "Effect of 85% Ladle to Tundish Shrouding at Inland's No. 1 Slab Caster on Slab and Cold Rolled Steel Quality," "The shrouding of steel flow for casting and teeming," Iron and Steel Society, Inc., 1986, pp. 13-20

73. Laihua Wang, Hae-Geon Lee and Peter Hayes, "Modelling of Air Ingress and Pressure Distribution in Ladle Shroud System for Continuous Casting of Steel," Steel Research, 1995, 66, pp. 279-286

74. Manfred Schmidt, Thomas J. Russo and Daniel J. Bederka, "Steel Shrouding and Tundish Flow Control to Improve Cleanliness and Reduce Plugging," Steelmaking Conference Proceeding, 1990, pp. 451-460